Chem Soc Rev

TUTORIAL REVIEW

View Article Online
View Journal | View Issue

Cite this: *Chem. Soc. Rev.*, 2021, **50**, 9391

Small-molecule fluorescence-based probes for interrogating major organ diseases

Hai-Hao Han, [a] He Tian Jr., [a] Yi Zang, [b] Adam C. Sedgwick, [c] Jia Li, *[b] Jonathan L. Sessler, *[c] Xiao-Peng He *[a] and Tony D. James *[de]

Chemical tools that allow the real-time monitoring of organ function and the visualisation of organ-related processes at the cellular level are of great importance in biological research. The upregulation/downregulation of specific biomarkers is often associated with the development of organ related diseases. Small-molecule fluorescent probes have the potential to create advances in our understanding of these disorders. Viable probes should be endowed with a number of key features that include high biomarker sensitivity, low limit of detection, fast response times and appropriate *in vitro* and *in vivo* biocompatibility. In this tutorial review, we discuss the development of probes that allow the targeting of organ related processes *in vitro* and *in vivo*. We highlight the design strategy that underlies the preparation of various promising probes, their optical response to key biomarkers, and proof-of-concept biological studies. The inherent drawbacks and limitations are discussed as are the current challenges and opportunities in the field. The hope is that this tutorial review will inspire the further development of small-molecule fluorescent probes that could aid the study of pathogenic conditions that contribute to organ-related diseases.

Received 25th March 2021

DOI: 10.1039/d0cs01183e

rsc.li/chem-soc-rev

Key learning points

(1) Codifies the design strategies used to develop small molecule fluorescent probes for biomarker detection.
(2) Stresses the importance of biomarker detection for the study of organ dysfunction and other organ-related diseases.
(3) Details the use of small molecular fluorescent probes for monitoring various pathogenic processes *in vitro* and *in vivo*.
(4) Highlights recent advances and the current limitations of small molecule-based fluorescent probes that have been developed for targeting organ specific diseases.
(5) Outlines opportunities in the field that could be tackled through the design of new effective fluorescent probes.

1. Introduction

The human body contains multiple major organs (*cf.* Scheme 1a), all of which are crucial to maintaining healthy function. Each major organ plays a specific role in the body; however, synergy between various major organs is required for optimal health. Aberrant organ function can affect these connections and result in catastrophic consequences. Over the years, advances in diagnostic technologies have led to the identification of several biomarkers that are correlated with disease development and organ dysfunction. These biomarkers underlie a number of analytical methods, including enzyme-linked immunosorbent assay (ELISA), gel electrophoresis, immunohistochemistry (IHC), immunofluorescence (IF) and western blotting. Most of these analytical methods are based on traditional immunoassays, which are time-consuming and require large quantities of expensive antibodies. Moreover, these techniques typically cannot be used to achieve the real-time detection and tracing of biomarkers *in situ*.[1] Developing alternative methods that are non-invasive and able to visualize disease-based biomarkers at a specific organ in real time, would improve our ability to study the pathological changes

[a] *Key Laboratory for Advanced Materials and Joint International Research Laboratory of Precision Chemistry and Molecular Engineering, Feringa Nobel Prize Scientist Joint Research Center, Frontiers Center for Materiobiology and Dynamic Chemistry, School of Chemistry and Molecular Engineering, East China University of Science and Technology, 130 Meilong Rd, Shanghai 200237, China. E-mail: xphe@ecust.edu.cn*
[b] *National Center for Drug Screening, State Key Laboratory of Drug Research, Shanghai Institute of Materia Medica, Chinese Academy of Sciences, 189 Guo Shoujing Rd, Shanghai 201203, P. R. China. E-mail: jli@simm.ac.cn*
[c] *Department of Chemistry, University of Texas at Austin, 105 E 24th Street, A5300, Austin, USA. E-mail: sessler@cm.utexas.edu*
[d] *Department of Chemistry, University of Bath, Bath, BA2 7AY, UK. E-mail: t.d.james@bath.ac.uk*
[e] *School of Chemistry and Chemical Engineering, Henan Normal University, Xinxiang 453007, China*

of a specific organ, improve disease diagnosis and aid the development of effective therapeutics.

In recent years, optical imaging modalities have shown promise in the context of a number of health-related applications, including disease diagnosis and optical-guided surgery. Compared to traditional methods, fluorescence-based imaging has enabled the non-invasive detection of biomarkers *in vitro* and *in vivo* with high sensitivity, fast response times and excellent spatio-temporal resolution.[2,3] Fluorescence-based imaging often relies on the use of chemical tools known as small molecule fluorescent probes,

Hai-Hao Han

Hai-Hao Han is a postdoctoral research fellow working under the supervision of Prof. Xiao-Peng He at School of Chemistry and Molecular Engineering, ECUST. His research interests in the development of new fluorescent probes for disease diagnosis and active analyte detection.

He Tian Jr.

He Tian Jr. is a PhD student in Applied Chemistry under the supervision of Prof. Xiao-Peng He from East China University of Science and Technology. His research interests include synthesis and biological studies of novel fluorescent probes.

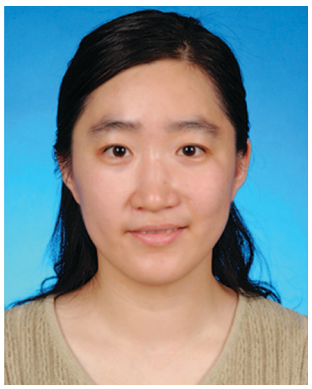

Yi Zang

Yi Zang is professor at SIMM (CAS). Her research mainly focuses on the biological research of AMPK and development of new chemical probes.

Adam C. Sedgwick

Adam C. Sedgwick is a postdoctoral research fellow working under the supervision of Prof. Jonathan L. Sessler at The University of Texas in Austin. His research interests are in the realms of stimuli-responsive materials, molecular imaging agents, and theranostic agents.

Jia Li

Jia Li received his PhD from SIMM in 2000 and was promoted to professor in 2005. He stayed at the University of Cambridge (UK, February 2003–August 2003) and Garvan Institute of Medical Research (Australia, August 2004–February 2005) as a visiting scholar. He received the China National Fund for Distinguished Young Scientists in 2011. From 2019 he has served as the director of SIMM.

Jonathan L. Sessler

Jonathan L. Sessler received a BSc degree in chemistry in 1977 from the University of California, Berkeley. He obtained his PhD from Stanford University in 1982. After postdoctoral stays in Strasbourg and Kyoto, he accepted a position at the University of Texas at Austin, where he is currently the Doherty-Welch Chair. He was also a WCU Professor at Yonsei University and from 2016–2020 held a part-time laboratory directorate at Shanghai University. He was a co-founder of Pharmacyclics, Inc. His latest technology is the basis for a new company, Oncotex, Inc.

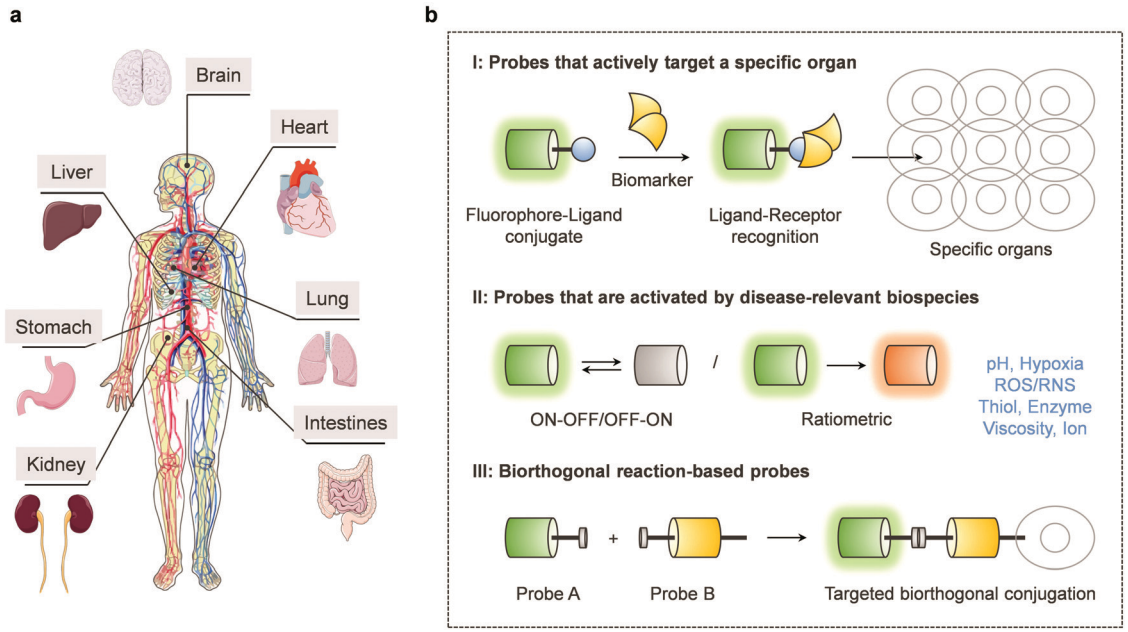

Scheme 1 (a) Schematic diagram of the major organs in the human body considered in the context of the present review (graphic elements of major organs were taken from Smart Servier Medical Art (https://smart.servier.com/). (b) Schematic diagram of the three main design strategies that have been used to create small molecule-based fluorescent probes capable of tracking major organ disease.

which are designed to bind/react with a target disease-based biomarker and provide a measurable change to the fluorescence signal. In general, these small molecule-based fluorescent probes should have high sensitivity and specificity for their target analyte to ensure its accurate detection within a biological system. For *in vivo* applications, fluorescent probes with near-infrared (NIR)[4] fluorescence emission or two-photon (TP)[5] excitation are desired for deep tissue imaging. The minimal autofluorescence (background interference) and the deep tissue penetration produced from NIR light allows the major organs to be directly imaged *via* whole-body imaging. However, to visualize dynamic cellular processes in live animals requires the use of intravital imaging as this technique offers higher imaging resolution compared to whole-body imaging. Unfortunately, before intravital imaging can be performed, surgery is required to implant an imaging window.[6] Whereas, whole-body imaging is relatively easy and allows the animal to be placed directly into the imaging system without complex manipulation. As such, small molecule-based fluorescent probes with the previously mentioned properties could provide useful tools for studying organ-related diseases. However, while progress has been made, there remains an urgent need to develop a wide variety of fluorescent probes for targeting individual organs and diagnosing their associated disease states. This is likely to require different design strategies.

In this review, we will discuss recent advances involving small molecule fluorescent probes designed to aid in the study of major organ diseases. We will focus on probes that allow the detection of disease-based biomarkers that show promise in monitoring disease progression in various organs. We will discuss the current limitations and present our own perspective on how to overcome these shortcomings. We anticipate this review will provide guidance for the development of new fluorescent probes useful in studying various facets of organ disease.

Xiao-Peng He

Xiao-Peng He is a professor at the Feringa Nobel Prize Scientists Joint Research Center, School of Chemistry and Molecular Engineering, ECUST. He obtained his BSc (2006) and PhD (2011) from ECUST. He completed a co-tutored doctoral program at ENS Cachan (France) (2008 to 2009) and postdoctoral research with Kaixian Chen (SIMM, CAS) from 2011 to 2013 at ECUST.

Tony D. James

Tony D James is a Professor at The University of Bath and Fellow of the Royal Society of Chemistry. He was awarded the Daiwa-Adrian Prize (2013), Inaugural CASE Prize (2015), MSMLG Czarnik Award (2018) and currently holds a prestigious Royal Society Wolfson Research Merit Award (2017–2022).

2. Design strategies for small molecule-based fluorescent probes for major organ disease

The design of effective small molecule-based fluorescent probes for interrogating and evaluating the development of major organ disease should meet the following requirements: significant signal change before and after biomarker recognition, fluorophore with good photostability, high fluorescence quantum yield, adequate water solubility, cell permeability and acceptable biocompatibility. Historically, three limiting approaches have been taken in an effort to meet these design needs. They will be seen throughout this review. A common approach for the targeted imaging of abnormal organs is the covalent attachment of a fluorophore to a ligand (*e.g.*, drugs, peptide sequences, aptamers and other easily modified molecules) that can selectively target a receptor that is overexpressed at in or near a diseased organ. Unfortunately, this strategy is labour intensive as it requires screening numerous ligands to identify a ligand with high affinity for the corresponding receptor. An alternative approach is based on the detection of biomarkers that are upregulated within the organ microenvironment (*e.g.*, pH, viscosity, hypoxia, reactive oxygen species (ROS)) during or after the onset of organ disease. This strategy requires the modification and ''masking'' of a fluorophore with a biomarker reactive group, which results in its change to the fluorescent signal. Subsequently, in the presence of the target biomarker, the fluorophore is ''unmasked'' and the fluorescent signal of the original fluorophore is restored. The third approach is the use of bioorthogonal chemistry. The selective introduction of a biorthogonal functional group (*e.g.*, an azide group) on a target biomolecule, enables its attachment to a fluorophore that is functionalized with a complementary functional group. This enables the fluorescent labelling of target molecules (Scheme 1b). Due to their disparate nature, different organ diseases may require the use of fluorescent probes with different mechanisms of action. In favourable cases, more than one strategy may be employed; in others, the design of effective probes remains an unmet need that would benefit from further research and development efforts.

3. Small molecule-based fluorescent probes for brain diseases

The brain is central to human life, enabling the day-to-day function of seemingly simple, but fundamentally complex tasks such as movement control and producing sensations. People often compare the brain to the headquarters of the whole body – ''the command centre''. The activities of the various major organs and parts of the human body are connected to the brain using nerves through which the brain sends out signalling information. Therefore, when the brain is damaged, the consequences are often apparent throughout the whole human body. The development of small molecule-based fluorescent probes with rapid response and high selectivity for biomarkers responsible for brain disorders has the potential for guiding physiological function research and disease diagnosis.[7] Many small molecule-based fluorescent probes have been developed for visualizing biomarkers specific to the brain. In this section, we will discuss some representative small molecule-based fluorescent probes for brain disease.

3.1 Small molecule-based fluorescent probes for Alzheimer's disease

Alzheimer's disease (AD) is a neurodegenerative disease with irreversible characteristics (*i.e.*, memory loss) that progressively affect an individual's quality of life. Extracellular amyloid-β (Aβ) peptide plaques and intracellular neurofibrillary tangles of hyperphosphorylated tau (NFTs) are the main pathological characteristics of AD. These are key biomarkers for studying AD development and progression. As such, a variety of fluorescent probes using differing design strategies have been reported for detecting these AD biomarkers.

Zhu *et al.* designed and synthesized a NIR aggregation-induced emission (AIE)-based probe **QM-FN-SO$_3$** for Aβ plaques in AD models (Fig. 1).[8] The probe was developed using a ''step-by-step'' rational molecular design strategy with NIR emission and activatable fluorescence properties upon binding to Aβ plaques. The staining of Aβ plaques in the brain slices and *in vivo* imaging of an AD mice model further demonstrated that the probe **QM-FN-SO$_3$** can achieve accurate binding and NIR fluorescent labelling of Aβ plaques and effective blood–brain barrier (BBB) penetration. The use of probe **QM-FN-SO$_3$** was also found to overcome problems associated with the commercial dyes, thioflavin T (ThT) and thioflavin S (ThS), including their short emission wavelengths, distortion of their inherent fluorescence signals due to aggregation quenching, ''always-on'' background interference, and difficulty in penetrating the BBB. As a result of these limitations, ThT and ThS are not appropriate for ultra-sensitive and high-fidelity *in situ* imaging of Aβ plaques. In contrast, probe **QM-FN-SO$_3$** appears highly promising in this regard.

Tang and co-workers reported a series of push–pull (donor–acceptor) AIE-active fluorescent probes (**DM-BZ**, **PD-BZ**, **PD-NA** and **PD-NA-TEG**) for the super-resolution imaging of Aβ plaques (Fig. 2).[9] Piperidine and dimethylamino functionalities were introduced to serve as the donor units and to facilitate binding to Aβ plaques. All four probes exhibited AIE features in solution owing to the gradual restriction of intramolecular rotation (RIR). In 30% EtOH/H_2O solution, **DM-BZ**, **PD-BZ**, **PD-NA** and **PD-NA-TEG** displayed an AIE response in the presence of Hen egg white lysozyme (HEWL, a model protein for Aβ studies). A strong correlation was seen between fluorescence enhancement and the increase in concentration of fibrillar HEWL. Subsequent colocalization experiments with a reported Aβ fluorescent probe, **8C**, indicated that **PD-NA** and **PD-NA-TEG** could effectively bind to Aβ plaques in brain slices of a transgenic (Tg) mouse (Tg6799, 9-month old, male). Remarkably, **PD-NA** and **PD-NA-TEG** were established as super-resolution imaging agents to visualize Aβ deposits with 30 nm optical resolution in Tg mouse brain slices.

Recent studies have indicated that lipid droplets increase the intracellular production of Aβ peptides. Thus, the correlation between lipid droplets and Aβ is an important relationship to investigate in order to understand the development and progression

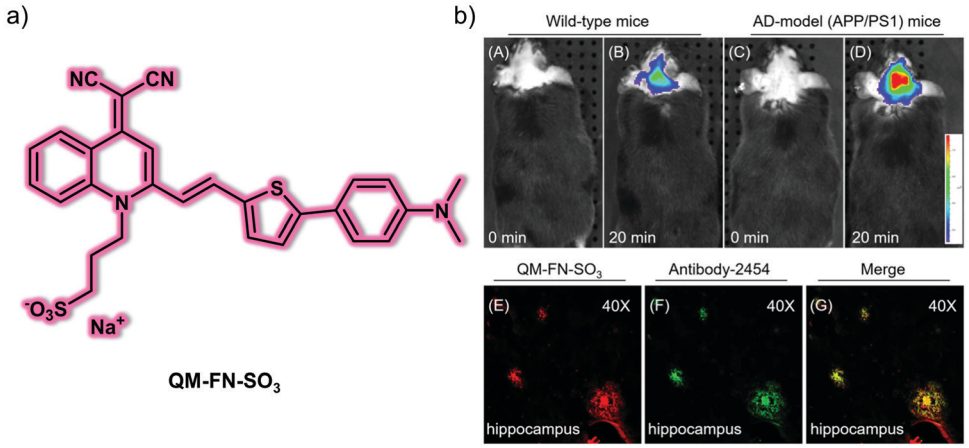

Fig. 1 (a) Small molecule-based NIR AIE-active fluorescent probe **QM-FN-SO_3** designed to permit the detection of Aβ plaques. (b) *In vivo* fluorescence imaging of the brains of (A and B) wild-type mice and (C and D) AD-model mice at different times recorded after treatment with probe **QM-FN-SO_3**. *Ex vivo* fluorescence images of brain slices from APP/PS1 mice with (E) probe **QM-FN-SO_3** and (F) antibody-2454. (G) Merged image of (E) and (F). Reproduced with permission from ref. 8. Copyright (2019) American Chemical Society.

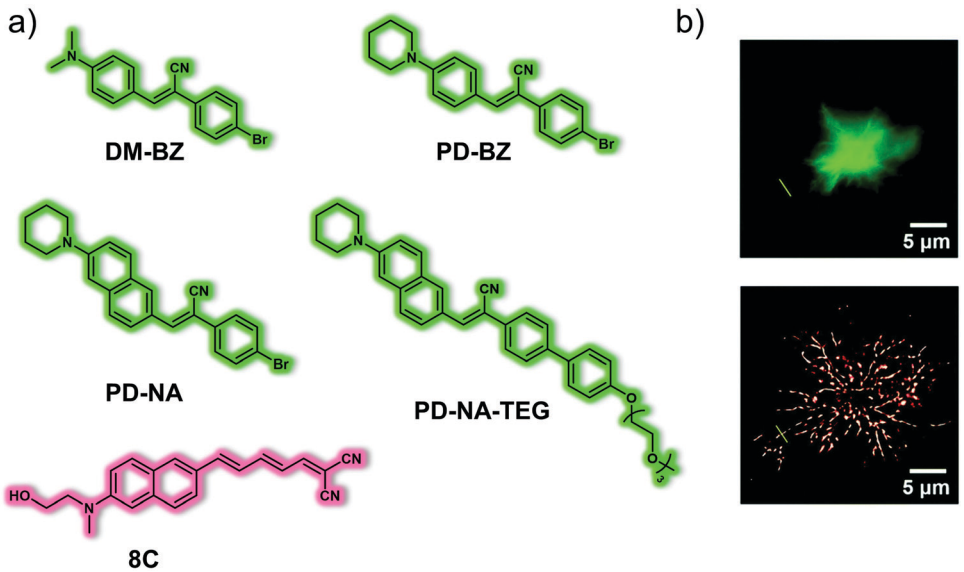

Fig. 2 (a) Small molecule-based AIE-active fluorescent probes **DM-BZ**, **PD-BZ**, **PD-NA**, **PD-NA-TEG** and reported Aβ fluorescent probe **8C** developed for the detection and super-resolution imaging of Aβ plaques. (b) Conventional (top) and super-resolution (bottom) fluorescence imaging of Aβ deposits in the brain slices of a Tg mouse (Tg6799, 9-month old, male). λ_{ex} = 405 nm, λ_{em} = 525 ± 50 nm. Reproduced with permission from ref. 9. Copyright (2018) The Royal Society of Chemistry.

of AD. For these reasons, Yan *et al.* developed the AIE-based fluorescent probe, **FB**, for the dual detection of Aβ plaques and lipid droplets in brain sections of AD mice (Fig. 3).[10] **FB** consists of a donor (dimethylamine group)–π–acceptor (cyano group) structure for targeting Aβ plaques and a hydroxyethyl structure to adjust the lipophilicity and to enhance the binding affinity for Aβ plaques. Due to the hydrophobic (lipophilic) nature of this probe, lipid droplets can be targeted by the principle of "like dissolves like". **FB** exhibited typical AIE behaviour in THF/H_2O solution when the water fraction reached 70%. In the presence of Aβ aggregates, **FB** was shown to produce a 20-fold fluorescence enhancement at 570 nm with excellent sensitivity (limit of detection: 26.9 nM). In addition, a 533-fold fluorescence enhancement at 588 nm was seen with increasing viscosity. **FB** was able to detect Aβ aggregates in transfected PC12 cells (PC12-EGFP-Aβ cells) and viscosity changes in monensin or nystatin treated SH-SY5Y cells, respectively. Notably, **FB** could be used for the precise imaging of Aβ aggregates and lipid droplets in brain sections of APP/PS1 transgenic AD mice. This study provides a potential imaging tool for improved AD diagnosis.

Li *et al.* reported a versatile oligomer-specific small molecule-based NIR fluorescent probe **PTO-41** for the detection of Aβ oligomers (AβOs) (Fig. 4).[11] The hydroxyethyl group was incorporated into the design so as to increase the affinity toward the AβO, optimize the lipophilicity, and improve *in vivo* pharmacokinetics. Probe **PTO-41** displayed an emission wavelength maximum at

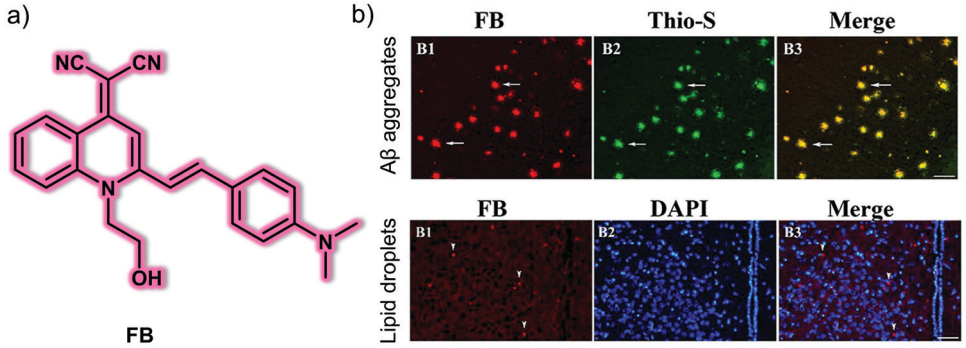

Fig. 3 (a) Small molecule-based AIE fluorescent probe **FB** developed for the detection of Aβ plaques and lipid droplets. (b) *Ex vivo* fluorescence images of brain slices from APP/PS1 transgenic mice with (B1) probe **FB** and (B2) Thio-S, DAPI. (B3) Merged image of (B1) and (B2). Thio-S: thioflavin-S, which could be used for detecting Aβ plaques. DAPI counterstaining was used to expose the tissue structure better. Scale bar: 100 μm. Reproduced with permission from ref. 10. Copyright (2020) Elsevier B.V.

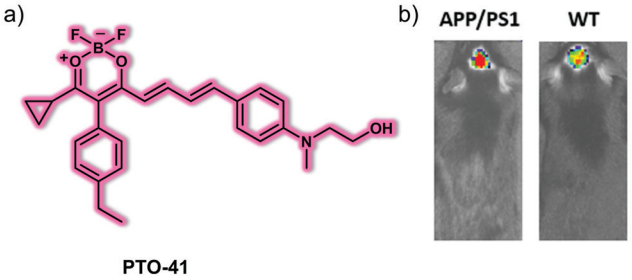

Fig. 4 (a) Small molecule NIR fluorescent probe **PTO-41** used for the detection of Aβ oligomers. (b) *In vivo* fluorescence imaging of the brains of AD-APP/PS1 model mice and wild-type (WT) mice. λ_{ex} = 570 nm, λ_{em} = 680 nm. Reproduced with permission from ref. 11. Copyright (2020) Elsevier B.V.

695 nm in PBS with low fluorescence intensity. However, when allowed to interact with Aβ42 oligomers, **PTO-41** displayed a significant 15.0-fold fluorescence intensity increase. This probe also exhibited high sensitivity, high selectivity, and strong affinity toward a specific set of AβOs, namely Aβ42 oligomers, in solution as determined from spectroscopic analyses and associated binding studies. **PTO-41** was used to successfully detect AβOs *in vivo* using an IVIS® Spectrum animal imaging system, wherein monitoring the NIRF signal was used to differentiate APP/PS1 mice from age matched wild-type mice. These favourable findings were ascribed to the NIR emission and BBB penetrating characteristics of **PTO-41**. The ability to target the Aβ oligomers produced at onset of AD means **PTO-41** could be useful in effecting early AD diagnosis compared with Aβ plaque-targeting probes.

In addition to Aβ plaques and oligomers, novel AD biomarkers are constantly being sought. Monoamine oxidases (MAO-A and MAO-B) are of interest in this regard. MAOs comprise a family of flavin adenine dinucleotide (FAD)-dependent enzymes found in the outer mitochondrial membrane of neuronal and glial cells. The activity of MAOs is significantly up-regulated in age-related neurological diseases, especially in AD. Ahn *et al.* reported a fluorescent probe for the detection of MAOs, namely the two-photon excitation probe, **MAO Probe1**.[12] **MAO Probe1** could be used to monitor simultaneously the activity of Aβ plaques in an AD mouse model using a sequential response mechanism, which permitted the first *in vivo* correlation between Aβ plaques and MAOs to be established. As prepared, **MAO Probe1** is nonfluorescent; however, it produces a highly fluorescent product, **IBC 2**, when allowed to react with MAOs (Fig. 5). This product, **IBC 2**, acts as a flat and elongated dipolar dye. As such, its fluorescence intensity at 600 nm is enhanced by *ca.* 5-fold in the presence of Aβ plaques. It also displays a reasonable two-photon absorption cross section (TPACS) of 180 GM. The net result is that both MAOs and Aβ plaques can be selectively and sequentially detected using **MAO Probe1**. Based on the excellent photophysical properties of **IBC 2**, the endogenous changes in MAOs activity and Aβ plaque number and size could be tracked using the **MAO Probe1** in healthy and 5XFAD AD mice at a depth of up to 600 μm. The associated imaging results revealed a distinctive age-dependent fluorescence enhancement for both amyloid-β plaques and MAOs activity, leading the authors to suggest that **MAO Probe1** might find use in exploring the role of, and correlation between, MAOs and Aβ plaques in biological systems.

3.2 Small molecule-based fluorescent probes for Parkinson's disease

Parkinson's disease (PD) is another serious and progressive neurodegenerative disease, which is characterized by degeneration and necrosis of dopamine neurons and the striatal pathway in substantia nigra. Overproduced reactive oxygen/nitrogen species (ROS/RNS) are thought to cause a dopaminergic deficit. Therefore, the development of appropriate chemical tools to monitor the dynamic changes of biological-related ROS/RNS concentrations may be helpful in exploring the pathogenic determinants of PD.

Peroxynitrite ($ONOO^-$) is a RNS with a high oxidizing and nitrating capacity. It is typically formed in biological milieu by the diffusion-limited reaction of nitric oxide ($NO^\bullet$) with the superoxide radical anion ($O_2^{\bullet -}$). Overproduction of $ONOO^-$ is regarded as a key neurotoxic factor in oxidative stress and neurodegeneration associated with PD. Liu *et al.* reported a NIR-based fluorescent probe **NIR-PN1** for the detection and imaging of $ONOO^-$.[13] **NIR-PN1** was constructed using dicyanoisophorone containing a donor (D)–π–acceptor (A) structure as the NIR fluorescent

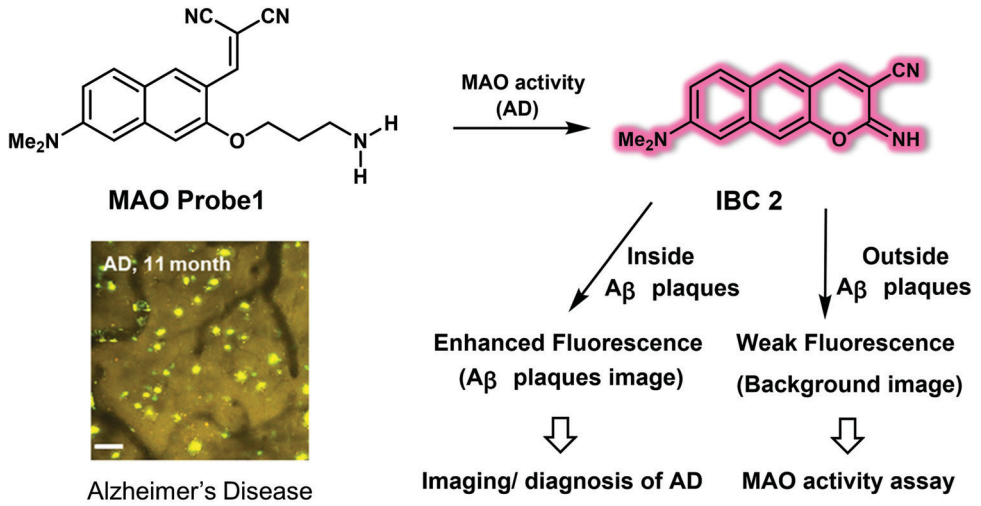

Fig. 5 Small molecule-based two-photon fluorescent probe **MAO Probe 1** developed to allow the detection of MAO activity and Aβ plaques in an AD mice model. Scale bar: 60 μm. Reproduced with permission from ref. 12. Copyright (2016) American Chemical Society.

reporter group. A *p*-aminophenol group was coupled to the donor group of the fluorophore as the $ONOO^-$ reactive site (Fig. 6). In the absence of $ONOO^-$, the **NIR-PN1** emission is quenched because of photoinduced electron transfer (PeT). Addition of $ONOO^-$ to **NIR-PN1** induces cleavage of the *p*-aminophenol group, leading to a strong fluorescence recovery centred at 670 nm when excited at 511 nm. The response of **NIR-PN1** towards $ONOO^-$ in PBS buffer (10 mM, pH 7.4, containing 0.4% Tween 80 and 3% DMSO) could be observed within seconds, providing support for the contention that **NIR-PN1** is capable of ultrafast sensing and that it may be used to detect $ONOO^-$ with high sensitivity. In addition, **NIR-PN1** permitted the selective sensing of $ONOO^-$ over other ROS or RNS. **NIR-PN1** was subsequently used to monitor changes in endogenous $ONOO^-$ concentrations in live PC12 and SH-SY5Y cells. It also proved effective for the same purpose *in vivo* as evidenced by studies of PD models that included Parkin-null drosophila, mice brain slices, and WLZ3 *C. elegans*.

Hydrogen peroxide (H_2O_2) is a physiologically-relevant ROS that plays a role in cell signalling processes. However, accumulation of H_2O_2 leads to intracellular oxidative stress, which is closely related to the pathogenesis of PD. Li *et al.* developed the NIR probe **NIR-HP1** to permit the ratiometric detection of H_2O_2 in PD models.[14] **NIR-HP1** contains a boronic ester group that serves as an H_2O_2 reporter and a NIR excited-state intramolecular proton transfer (ESIPT) fluorophore as the reporter group (Fig. 7). Excitation of **NIR-HP1** gives rise to a green fluorescence at 500 nm, which gradually disappears upon the addition of H_2O_2 while an emission band centred at 650 nm grows in. These spectral changes were interpreted in terms of an ESIPT mechanism, triggered by the removal of the boronic ester and liberation of the masked phenol group in **NIR-HP1**. A linear relationship between the fluorescence

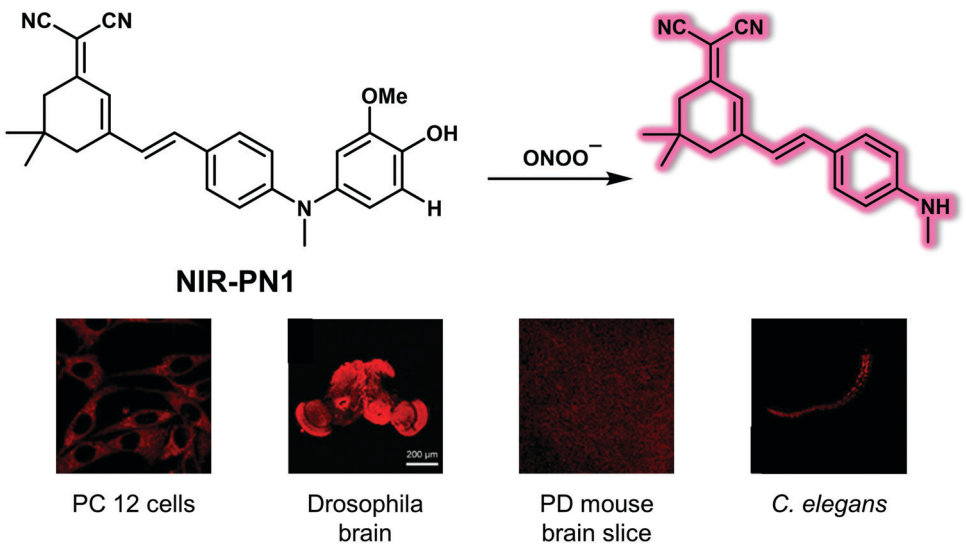

Fig. 6 Structure of the small molecule-based NIR fluorescent probe **NIR-PN1** designed to permit the reaction-based detection and imaging of $ONOO^-$, as evidenced by images involving different PD models. Reproduced with permission from ref. 13. Copyright (2020) American Chemical Society.

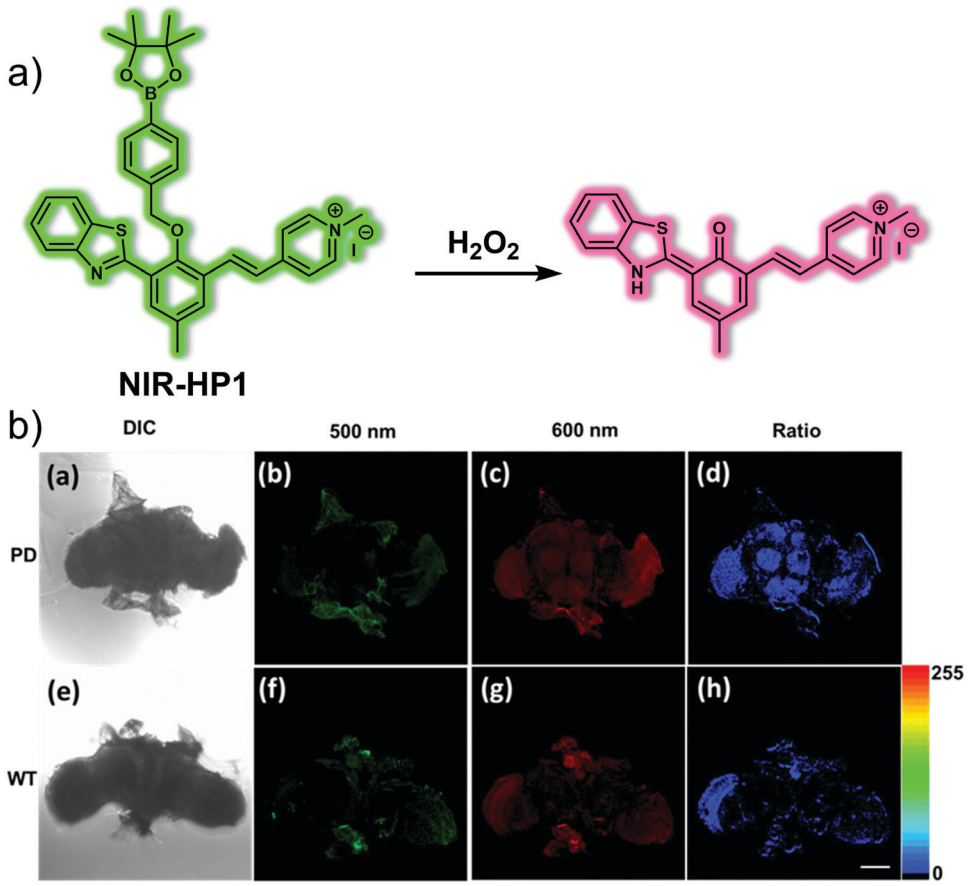

Fig. 7 (a) Small molecule-based NIR fluorescent probe **NIR-HP1** designed to permit the ratiometric detection of H_2O_2 in PD models. (b) Fluorescence images of brain of Parkinson's disease (PD) and WT drosophila incubated with **NIR-HP1** (10 μM). (a) DIC: drosophila brain of WT. (b) PMT range was 470–520 nm (green). (c) PMT range was 620–670 nm (red). (d) The ratio of (c)/(b). (e) DIC: drosophila brain of Parkinson's disease (PD). (f) PMT range was 470–520 nm (green). (g) PMT range was 620–670 nm (red). (h) The ratio of (g)/(f). Scale bar = 100 μm. Reproduced with permission from ref. 14. Copyright (2019) Elsevier B.V.

intensity ratio (F_{650}/F_{500}) and H_2O_2 concentration (0–10 equiv.) was observed. The calculated k_{obs} value for **NIR-HP1** with H_2O_2 proved larger than those for most reported H_2O_2 probes, leading to the inference that **NIR-HP1** constitutes a highly sensitive probe. Changes in the endogenous H_2O_2 production induced by rotenone (RO) in HeLa cells could be tracked using **NIR-HP1**. In addition, **NIR-HP1** was found to localize in the mitochondria of HeLa cells, a finding ascribed to its heterocyclic cationic nature. Due to its favourable properties, including low toxicity, high sensitivity and selectivity, **NIR-HP1** could be used to successfully image H_2O_2 ratiometrically *in vivo* using PD models that included zebrafish and Parkin-null drosophila brains.

In addition to oxidative stress, mitochondrial dysfunction is strongly associated with PD. Mitochondrial viscosity is an important parameter that can be used to assess whether mitochondrial function is normal. It is often linked to hydrogen sulphide (H_2S), a critical signalling gasotransmitter. In order to create a more effective system to study the putative link between mitochondrial viscosity and the progression of PD, Li *et al.* designed a two-photon dual-channel fluorogenic probe (**Mito-HS**) (Fig. 8).[15] **Mito-HS** is non-fluorescent as the result of a proposed twisted intramolecular charge transfer (TICT) that dominates in the absence of a substrate. Upon reacting with H_2S, **pre-Mito** (a "donor–π–acceptor" fluorescent molecule) is produced. This leads to a strong green fluorescence at 585 nm. At higher viscosity, the rotation of **Mito-HS** is restricted, and **Mito-HS** produces an intense red fluorescence emission at 750 nm. Previously reported H_2S probes that are functionalised with mitochondrial targeting groups, cannot distinguish whether reaction with H_2S occurs in the cytoplasm or in the mitochondria. In contrast, **Mito-HS** reacts only with H_2S in the mitochondria because its rate of reaction with H_2S is less than the rate at which it targets the mitochondria. Both **pre-Mito** and **Mito-HS** proved suitable for two-photon imaging. This allowed cell-based imaging studies to be carried out. Per the design expectations, **Mito-HS** proved non-fluorescent in low viscosity HepG2 cells. However, when the viscosity was increased *via* the exogenous addition of nystatin (an ionophore used to regulate mitochondrial viscosity), **Mito-HS** exhibited fluorescence (700–750 nm) under excitation at 800 nm using a two-photon fluorescence microscope (TPFM). It also displayed a good localisation coefficient (Pearson's r value = 0.81) with Mito Tracker® Red. Similarly, when the exogenous H_2S inducer (Cysteine, Cys) was added, a green fluorescence (550–600 nm)

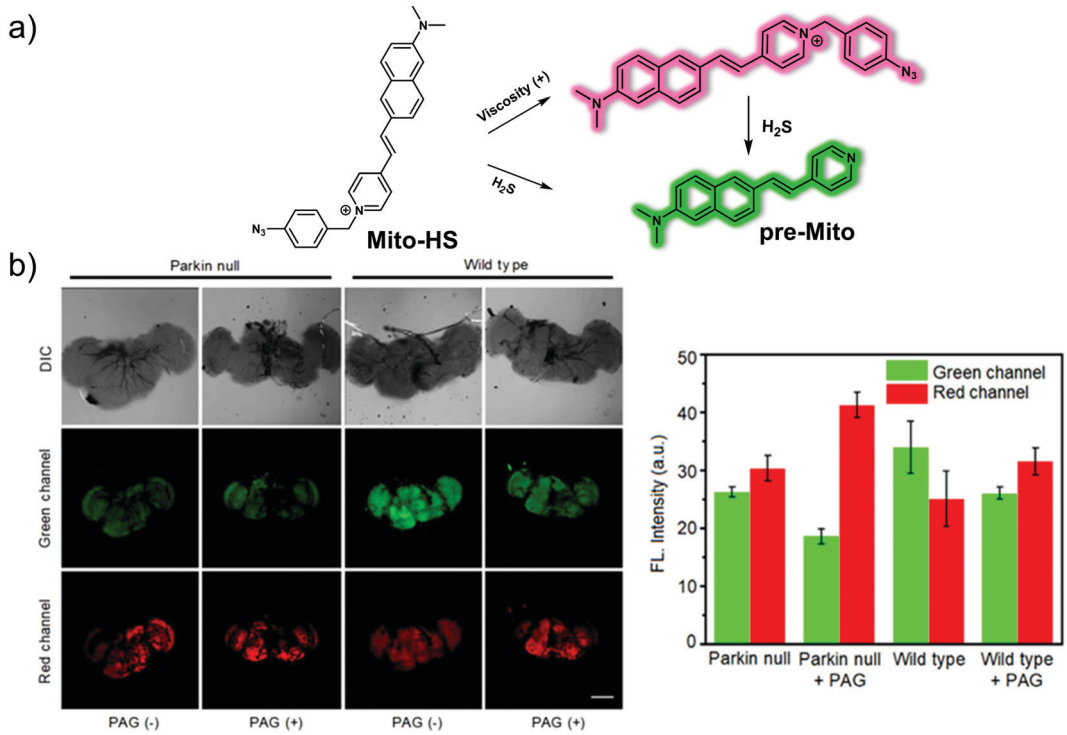

Fig. 8 (a) Small molecule-based two-photon fluorescent probe **Mito-HS** developed to permit detection of viscosity and H_2S. (b) Two-photon fluorescence images and quantification of insect PD and wild-type drosophila models treated with **Mito-HS** (50 μM, 1 h) with or without added PAG (1 mM, 1 h). The excitation and emission wavelengths for the green channel are 760 nm and 550–600 nm, respectively. The excitation and emission wavelengths for the red channel are 800 nm and 700–750 nm, respectively. Reproduced with permission from ref. 15. Copyright (2020) Elsevier B.V.

was observed. In addition, **Mito-HS** could be used to monitor a PD cell-based model induced by Rotenone (ROT) and regulated by Brillian-VB3 (VB3) reflecting the close relationship between endogenous H_2S levels and viscosity. Importantly, **Mito-HS** was used for the *in situ* imaging of mitochondrial H_2S/viscosity in the brain of a drosophila Parkinson's disease model. In wild-type Drosophila brains, the green fluorescence intensity is high, while the red fluorescence intensity is low. In Parkin-null (PD) drosophila brains, the fluorescence intensity is the opposite of that in the wild-type specimens, *i.e.*, the green fluorescence intensity is low while the red fluorescence intensity is high. On this basis, it was concluded that the viscosity in PD Drosophila increases and the H_2S levels decrease. The presence of H_2S was further confirmed with the addition of DL-propargylglycine (PAG), a specific inhibitor of cystathionine-γ-lyase that serves to reduce the H_2S levels.

3.3 Small molecule-based fluorescent probes for epilepsy

Epilepsy is a chronic neurodegenerative disease characterised by recurrent unpredictable convulsions. Oxidative stress and dysfunction of mitochondria are not only correlated with the onset of epileptic seizures, they are also thought to promote initial development of the disease. In particular, overexpression of $ONOO^-$, a factor considered to be critically neurotoxic, is believed to play an important role in the pathogenesis of epilepsy. As such, it could serve as a potential biomarker to study this still-mysterious neurological disorder.

In 2019, Qian *et al.* reported a NIR fluorescent probe **ONP** and demonstrated that it could be used to trace endogenous $ONOO^-$ signals in kainate (KA)-induced epileptic seizures while providing a means for screening antiepileptic inhibitors.[16] **ONP** was developed using methylene blue (MB) as the reporter agent with a boronic ester serving as a selective reactive moiety for $ONOO^-$ (Fig. 9). Initially, no fluorescence response was observed. However, when **ONP** reacts with $ONOO^-$, the boronic ester moiety is removed producing the colourless leuco form of MB, which is then further oxidized to MB. The net result is the generation of strong NIR fluorescence signal at 692 nm under conditions of 665 nm excitation. **ONP** displayed high specificity and selectivity toward $ONOO^-$, and exhibited minimal interference towards biologically relevant metal ions, anions, ROS and other RNS species in solution. **ONP** was used to track exogenous and endogenous $ONOO^-$ overproduction regulated by SIN-1 and lipopolysaccharide (LPS), respectively, as well as suppression by FeTMPyP (5,10,15,20-tetrakis(*N*-methyl-4′-pyridyl)porphinato iron(III)) and *N*-acetyl cysteine, respectively, at the cellular level. **ONP** exhibited excellent photostability, low cytotoxicity and good cell-membrane permeability. It was also found to possess other desirable features, such as BBB permeability and NIR excitation and emission wavelengths. By combining **ONP** with high-content analysis technology, a fluorescence-based *in situ* cellular screening method was developed for the screening of $ONOO^-$ inducers and inhibitors. **ONP** was also used to image endogenous $ONOO^-$ levels in epileptic brains using a KA-induced

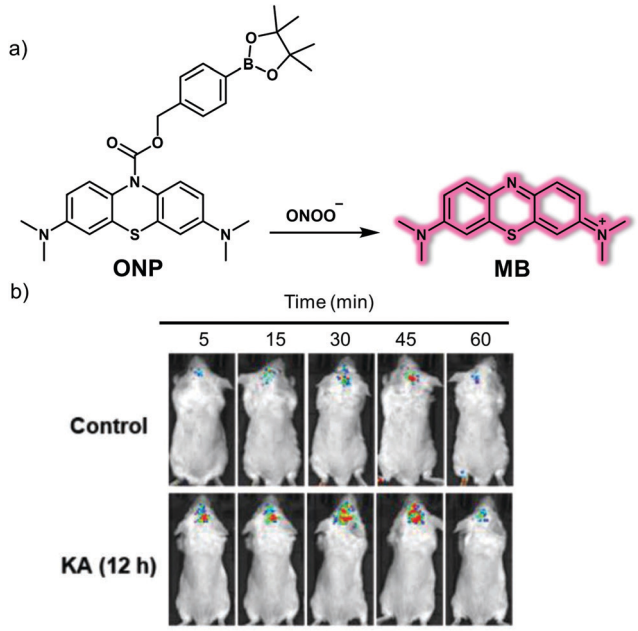

Fig. 9 (a) Small molecule-based NIR fluorescent probe **ONP** for the detection of $ONOO^-$ that produces a NIR emission after release of methylene blue (MB). (b) Time-dependent fluorescence images of the brains of normal and kainate (KA)-induced epileptic seizure mice injected with **ONP** (1.5 mg Kg^{-1}). λ_{ex} = 640 nm, λ_{em} = 650–750 nm. Reproduced with permission from ref. 16. Copyright (2019) by the authors J.-S. Hu, C. Shao, X. Wang, X. Di, X. Xue, Z. Su, J. Zhao, H.-L. Zhu, H.-K. Liu and Y. Qian, Published by Wiley-VCH Verlag GmbH & Co. KGaA.

BALB/c mouse model. Based on the results obtained, the authors concluded that the concentration of $ONOO^-$ in the brain is increased significantly 12 hours after KA injection as compared with the 24 hour group.

Myeloperoxidase (MPO) is a peroxidase enzyme that mediates a series of oxidative stress-related biological processes. A close relationship exists between elevated MPO and epilepsy, leading to the inference that MPO may be a promising biomarker for understanding epilepsy and could provide a potential therapeutic target. In 2020, the Qian research team reported a two-photon fluorescent probe, **HCP**, prepared using a simple condensation between 6-(dimethylamino)quinoline-2-carbaldehyde and diaminomaleonitrile (Fig. 10).[17] As prepared, **HCP** exhibited weak yellow fluorescence emission. However, upon the addition of HClO, a 138-fold enhancement in the emission at 495 nm was observed (excitation wavelength 396 nm). The limit of detection (LOD) for HClO using **HCP** was 104 nM. **HCP** was then used to visualize intracellular MPO-mediated HClO production under different oxidative stress conditions. It was also applied as a fluorescence-based high-throughput screening platform for potential natural product-based HClO regulators. In addition, **HCP** was successfully used to monitor endogenous HClO levels *in vivo* in epileptic brains slices using an IVIS Spectrum imaging system with an imaging depth of 150 μm using a two-photon microscope. Finally, by using the **HCP** fluorescent screening platform, a lead compound for the prevention and treatment of epilepsy, apigenin, was found that exhibited promising preliminary results.

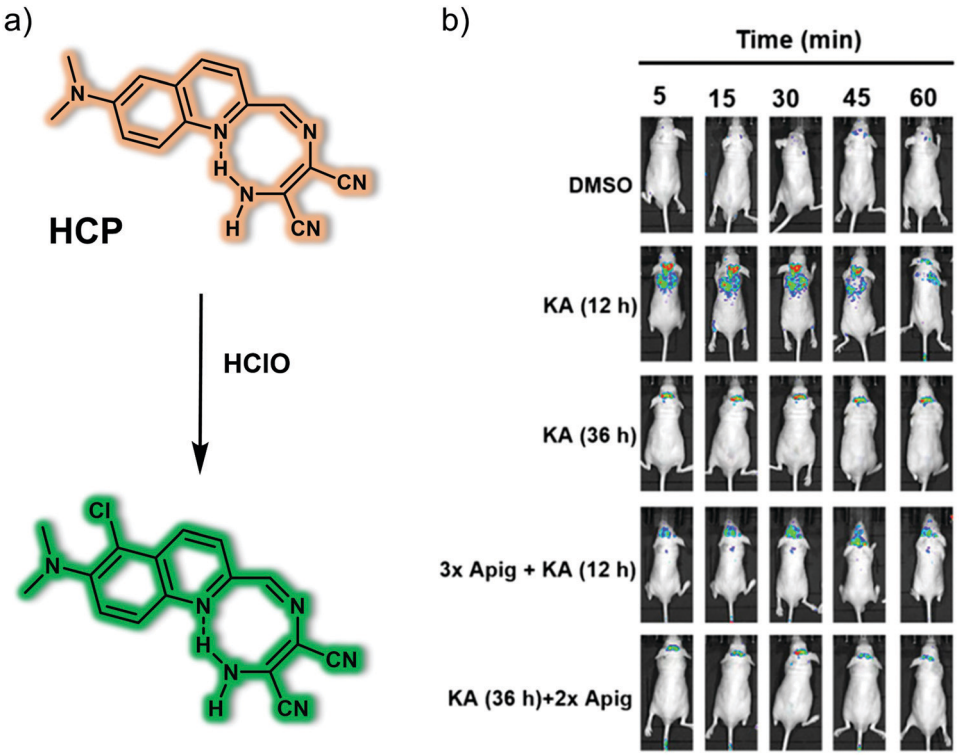

Fig. 10 (a) Small molecule-based two-photon fluorescent probe **HCP** that allows the detection of HClO. (b) Time-dependent fluorescence images of the brains of normal, kainate (KA)-induced epileptic seizure mice and apigenin/KA co-treated mice following injection of **HCP**. λ_{ex} = 430 nm, λ_{em} = 500–600 nm. Reproduced with permission from ref. 17. Copyright (2020) Published by National Academy of Sciences.

As mentioned above, a hallmark of epilepsy is a continuous level of oxidative stress within the brain. Cysteine (Cys) is a recognized reducing metabolite that plays a cytoprotective role against oxidative damage. Liu and colleagues reported a new mitochondria-targeting NIR fluorescent probe, **Mito-CP**, for the selective detection of Cys *in situ* in the epileptic brain (Fig. 11).[18] In **Mito-CP**, Mito-Q serves as the fluorophore reporter, while acrylate acts as the recognition site for Cys. The positive charge of the quinoline cation within Mito-Q was expected to promote localisation of **Mito-CP** within the mitochondria of living cells. **Mito-CP** exhibited a large Stokes shift ascribed to the intramolecular charge transfer (ICT) effect of an electron push–pull system (*N*,*N*-dimethylamino moiety and quinoline cation, respectively). A major advantage of **Mito-CP** is its ability to emit in the NIR region. This makes it well-suited for *in vivo* imaging applications. The NIR capability helps address the issue of background noise when used in the context of biological samples; however, it also reduces photodamage and alleviates concerns associated with poor photo-transmittance. As expected, generation of endogenous Cys by stimulation with dithiothreitol (DTT) and quenching of Cys by external H_2O_2 and the associated oxidative stress in PC12 cells could be tracked using **Mito-CP**. Additionally, changes of endogenous Cys levels in pentylenetetrazole (PTZ)-induced epileptic mice and epileptic mice brain treated with the antiepileptic drug curcumin could be imaged using **Mito-CP**.

3.4 Small molecule-based fluorescent probes for depression

Depression, also known as depressive disorder, is one of the primary mood disorders. The pathogenesis of depression is still unclear; however, mainstream hypotheses attribute its pathogenesis to various mechanisms, including oxidative stress, ion channel changes, and inflammation.

The hydroxyl radical (•OH) is one of the more reactive and oxidizing ROS overproduced during oxidative stress. Excessive production of •OH can cause irreversible damage to nerve cells. Tang and co-workers developed a two-photon •OH-response fluorescent probe, **MD-B**, that relies on an intramolecular charge transfer (ICT) mechanism.[19] In constructing **MD-B**, a 3-methyl-pyrazolon moiety was selected as the •OH recognition site and coumarin (Cou151) bearing a trifluoromethyl group was chosen as the fluorophore (Fig. 12). Due to the push–pull effect caused by the carbonyl and nitrogen atoms, **MD-B** exhibits almost no fluorescence in its native state. However, when exposed to •OH, one-electron oxidation of 3-methyl-pyrazolone occurs. This results in the formation of **MD-B-OH**, a species that gives rise to a strong green fluorescence emission. The fluorescence quantum yield Φ_f increased from 0.037 to 0.25 upon treatment with •OH. The •OH detection limit for **MD-B** was 2.4 nM. Moreover, **MD-B** displayed good selectivity for •OH, excellent photostability and low cytotoxicity, leading to the suggestion that **MD-B** could be used for biological imaging. Endogenous •OH was detected using **MD-B** as a two-photon probe in living neural cells (PC12) and mouse macrophage cells (RAW 264.7). It was found to display good tissue penetration while the trifluoromethyl group was thought to allow **MD-B** to cross the BBB. As a result, exogenous •OH fluctuations in the brain of depression-like mice could be monitored using **MD-B**. A correlation between •OH levels and depression-like behaviour was found with the authors discovering that silent information regulator 1 (SIRT1) inactivation by •OH is responsible for an observable depression phenotype.

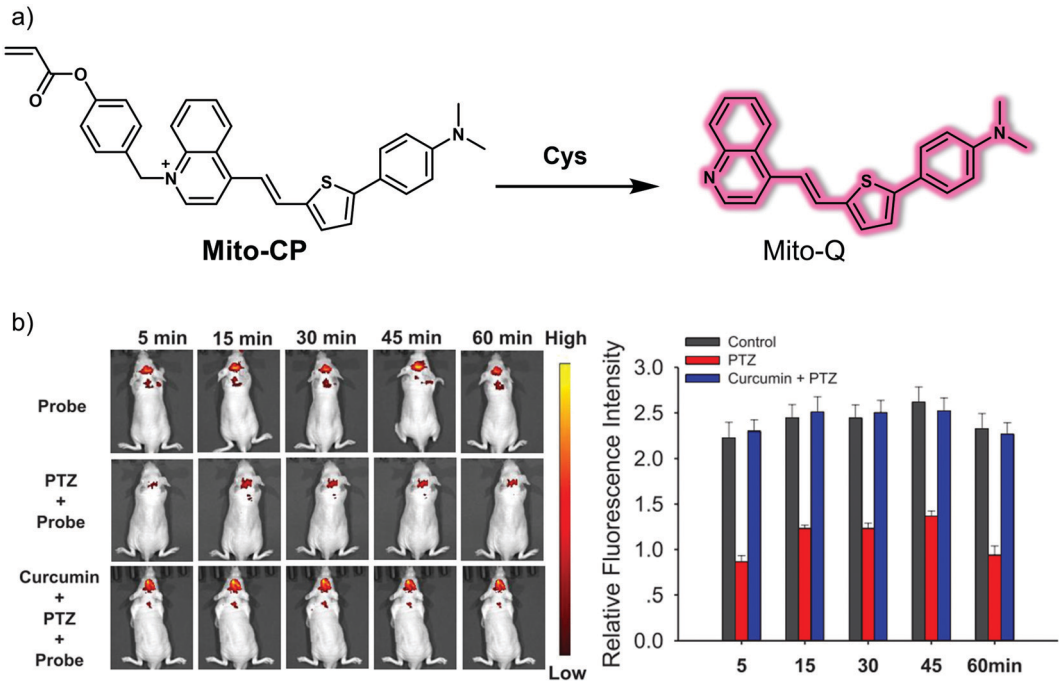

Fig. 11 (a) Small molecule-based NIR fluorescent probe **Mito-CP** developed for the detection of Cys. (b) Time-dependent fluorescence images and quantification of normal, PTZ-induced epileptic seizure mice, and PTZ/curcumin co-treated mice injected with **Mito-CP**. λ_{ex} = 430 nm, λ_{em} = 700 nm. Reproduced with permission from ref. 18. Copyright (2020) American Chemical Society.

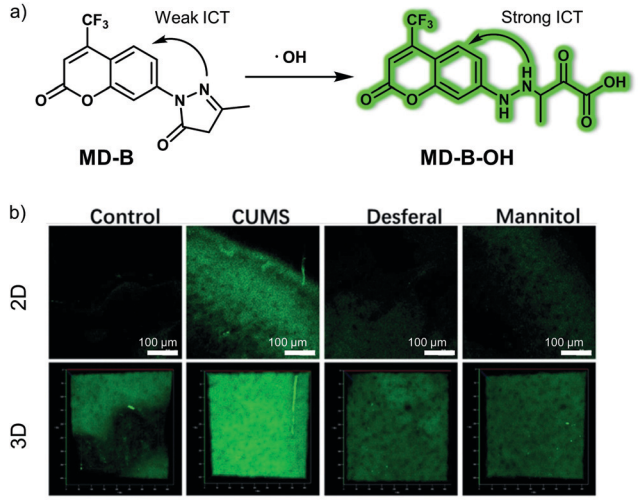

Fig. 12 (a) Small molecule-based two-photon fluorescent probe **MD-B** that was developed to allow detection of •OH *in vivo*. (b) 2D and 3D fluorescence images of the brain of normal, CUMS (chronic unpredictable mild stress) mice demonstrating depression-like behaviour and desferal- or mannitol-treated CUMS mice with **MD-B**. λ_{ex} = 800 nm, λ_{em} = 400–650 nm. Reproduced with permission from ref. 19. Copyright (2019) Wiley-VCH Verlag GmbH & Co. KGaA, Weinheim.

Dysfunctional brain neurotransmitter metabolism is closely related to oxidative stress. Acetylcholinesterase (AChE) is an important hydrolytic enzyme that cleaves and inactivates acetylcholine (Ach, a neurotransmitter). Abnormal expression of AChE can affect the metabolism of neurotransmitters, disrupt neurotransmission to the brain, and even lead to depression. The Tang group developed a small-molecule two-photon fluorescent probe **MCYN**, for detecting AChE activity in the brain of depression-like mice. This probe relies on merocyanine as the fluorescent platform and a dimethyl carbamate moiety as an AChE responsive unit, (Fig. 13).[20] Initially, a weak fluorescence signal corresponding to the merocyanine dye was observed due to a weak push–pull electronic effect. However, after exposure to AChE, which leads to cleavage of the dimethyl carbamate unit, the push–pull electronic effect was enhanced, leading to a strong fluorescence signal being observed. The associated fluorescence signal enhancement endowed **MCYN** with the ability to detect AChE activity in aqueous media. **MCYN** exhibited characteristics desirable in an AChE probe, including a fast response time, good performance at physiological pH (6.5–8.5), a low detection limit (0.36 U mL^{-1}), and minimal cytotoxicity. This research team then showed that AChE activity in PC12 cells could be monitored using **MCYN** under conditions of two-photon excitation. The resulting two-photon fluorescent images provided support for the notion that **MCYN** could be used monitor endogenous AChE activity changes *in situ* during apoptosis and oxidative stress. Moreover, due to its ability to permeate the BBB, **MCYN** allowed the AChE activity level in the brains of live chronic stress-induced depressive animals to be determined using two-photon excitation.

The nature of ion channels also change during oxidative stress and depression. Therefore, fluorescent probes that allow the monitoring of ion channel changes could have a role to play in visualizing depression. The *N*-methyl-D-aspartic acid (NMDA) receptor is a subtype of the ionotropic glutamate receptor and is a ligand-gated ion channel whose over-activation is thought to play an important role in the pathogenesis of depression. Thus, visualizing the levels of Zn^{2+} and H^{+}, the regulatory binding partners of the NMDA receptor, during depression could contribute to a better understanding of the mechanism

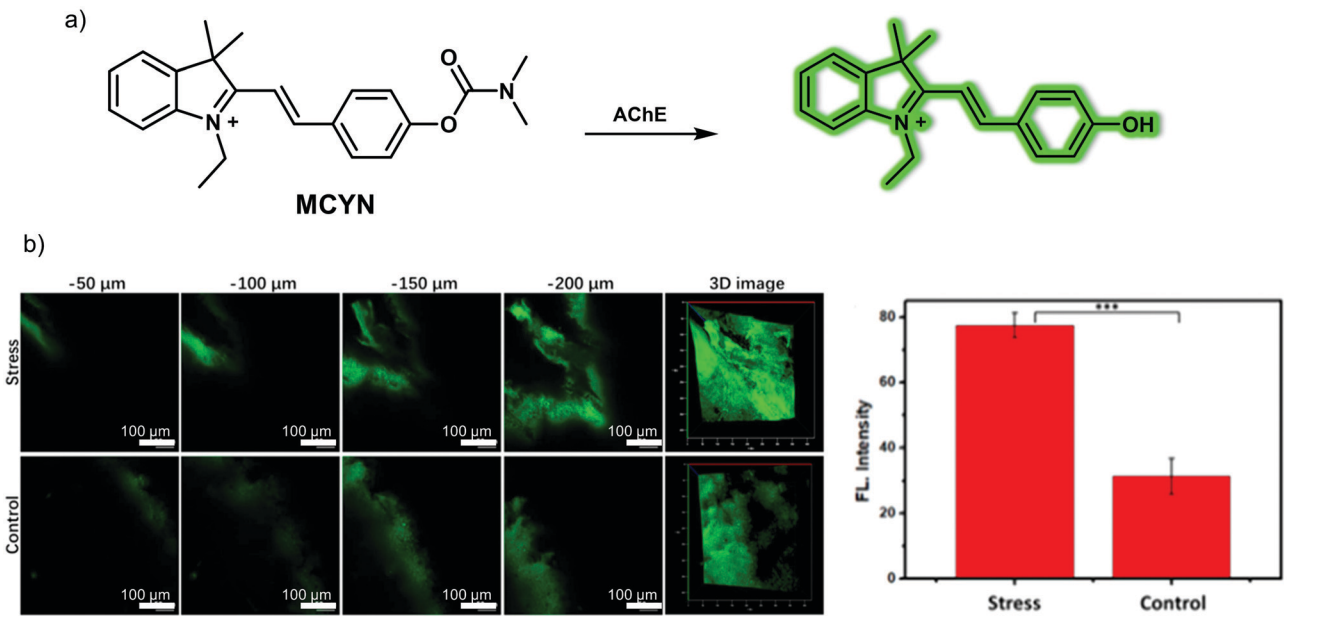

Fig. 13 (a) Small molecule-based two-photon fluorescent probe **MCYN** developed to allow the detection of acetylcholinesterase (AChE). (b) Fluorescence images and quantification of the signals in the brains of normal and chronic stress-induced living depressive mice injected with **MCYN** (0.15 mg kg^{-1}). λ_{ex} = 800 nm, λ_{em} = 480–650 nm. Reproduced with permission from ref. 20. Copyright (2019) American Chemical Society.

of ion channel involvement in depression. In 2020, the Tang group developed a small molecule-based fluorescent probe (**DNP**) for detecting Zn^{2+} and H^+ simultaneously *in situ*.[21] In designing this probe, a Zn^{2+}-responsive DPA (2,2′-dipicolylamine) group attached to a coumarin core was introduced as the Zn^{2+} indicator while a naphthalene fluorescein was used as the H^+ reporter (Fig. 14). The two moieties were connected using a linker to form **DNP**. **DNP** itself displayed a relatively weak fluorescence upon excitation at 390 nm or 610 nm. However, upon the addition of Zn^{2+} a characteristic coumarin signal at 460 nm was seen to grow in, a result ascribed to the blocking of intramolecular photo-induced electron transfer (PeT). In contrast, increasing the pH (low H^+) produced a characteristic naphthalene fluorescein emission at 680 nm due to formation of the open quinone form. Importantly, **DNP** exhibited a high selectivity for Zn^{2+} and H^+ over other ions, reactive oxygen species (ROS), and reactive nitrogen species (RNS). Using this system and a two-photon imaging setup, it proved possible to detect Zn^{2+} and H^+ fluctuations simultaneously in PC12 cells and in the brain of depressive mice.

Inflammatory mediators (*e.g.*, cytokines) secreted as part of the immune inflammatory response are believed to be important contributors to the development of depression. Ozone (O_3) produced in the inflammatory response of the immune system promotes the release of cytokines, such as pro-inflammatory cytokine interleukin-8 (IL-8), which triggers a stronger inflammatory response, ultimately leading to depression. Thus, visualizing O_3 during depression may provide insight into the mechanism of immune inflammation. In 2019, Tang and collaborators designed and synthesized what was reported to be the first near-infrared (NIR) fluorescent probe (**ACy7**) capable of detecting O_3 in the brain of mice during depression.[22] **ACy7** consists of a Cy7-like dye and a 3-butenyl moiety, which serve as the fluorophore and O_3-recognition subunit, respectively (Fig. 15). When **ACy7** is exposed to O_3, a cycloaddition reaction occurs. This extends the degree of conjugation, leading to fluorescence emission. **ACy7** displays excellent selectivity for O_3, exhibits a high signal-to-noise ratio, a low detection limit (10 nM), good photostability and low cytotoxicity. It was thus deemed suitable for use in biological applications. In fact, **ACy7** proved capable of tracking the O_3 produced during cell inflammation in living RAW 264.7 macrophages and PC12 nerve cells. The fact that **ACy7** emits in the NIR spectral region facilitates the monitoring of O_3 in living animals. For instance, **ACy7** allowed endogenous O_3 changes in the brain of depressive mice (chronic unpredictable mild stress mouse model) to be monitored readily.

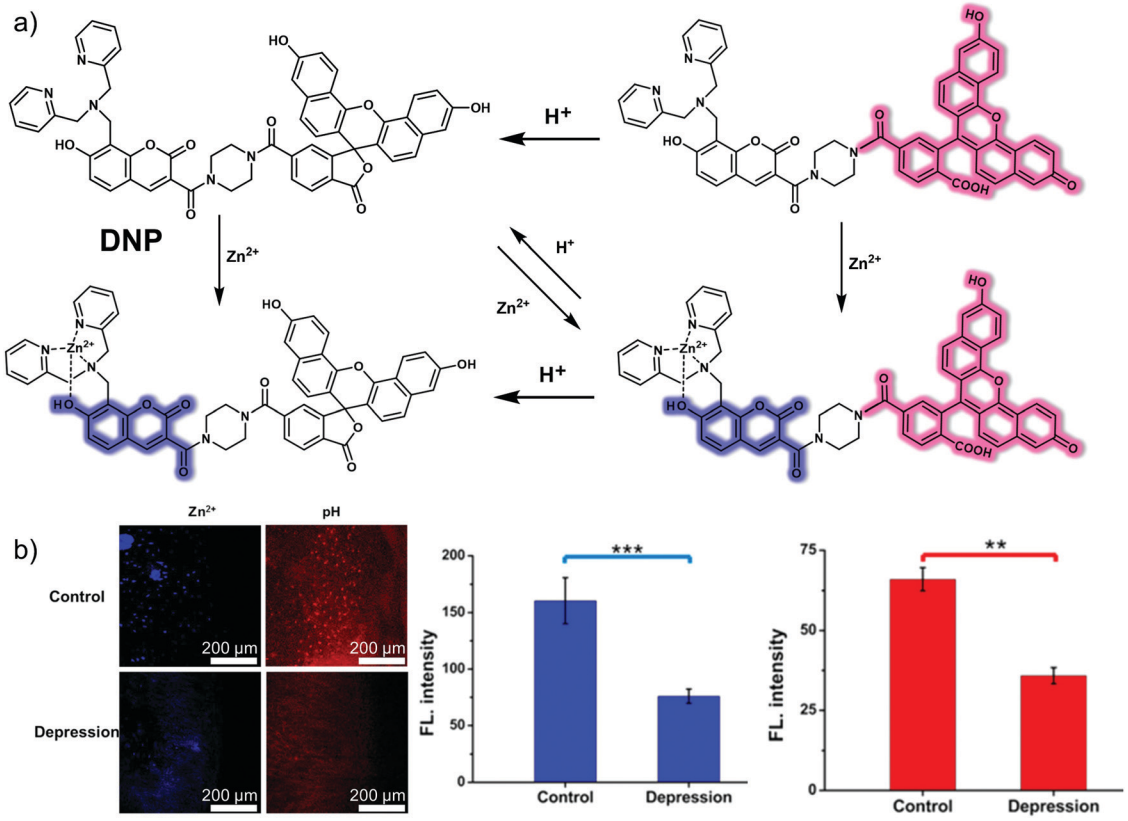

Fig. 14 (a) The chemical structure and working mechanism that is thought to underlie the detection of Zn^{2+} and H^+ achieved by the small molecule two-photon (TP) fluorescent probe **DNP**. (b) *In situ* TP fluorescence imaging and quantification of the brain of normal and depressive mice injected with **DNP** (100 μM). Blue: λ_{ex} = 800 nm, collected 410–560 nm. Red: λ_{ex} = 633 nm, collected 650–750 nm. The values are the mean ± SD for n = 3, $^{**}p < 0.01$, $^{***}p < 0.001$. Reproduced with permission from ref. 21. Copyright (2020) American Chemical Society.

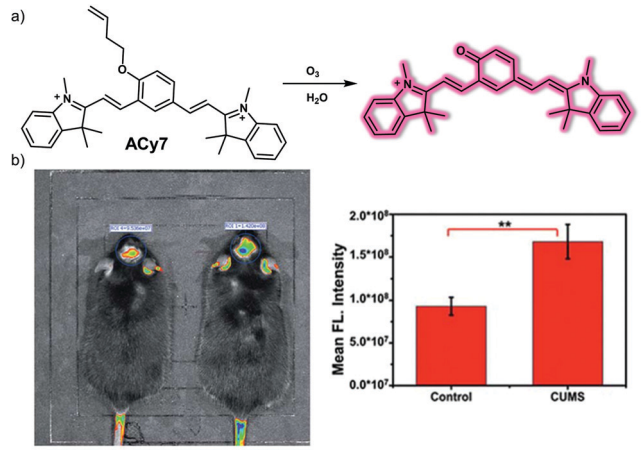

Fig. 15 (a) Chemical structure of the small molecule-based NIR fluorescent probe **ACy7** and working model of the reaction-based transformation that allows for the detection of O_3. (b) *In vivo* fluorescence imaging and quantification of the brains of normal and depressive mice (chronic unpredictable mild stress, CUMS) injected with **ACy7** (0.15 mg kg^{-1}). λ_{ex} = 570 nm, λ_{em} = 690 nm. The values are the mean ± SD for n = 3, $^{**}p < 0.01$. Reproduced with permission from ref. 22. Copyright (2019) The Royal Society of Chemistry.

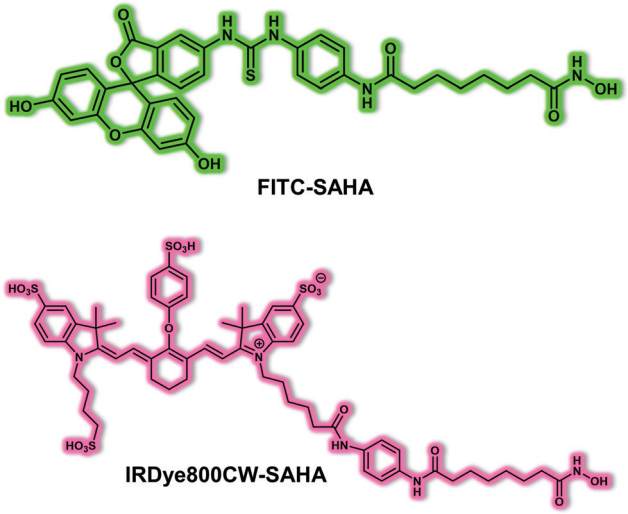

Fig. 16 Chemical structure of the small molecule-based fluorescent probes **FITC-SAHA** and **IRDye800CW-SAHA** designed to allow the targeting of HDAC in HCC models.

4. Small molecule-based fluorescent probes for liver disease

The liver is the largest organ in the human body, located on the right side of the abdomen, below the diaphragm and protected by the lower right ribs. The liver is an important metabolic organ involved in the transformation of xenobiotics, sugar storage and protein secretion. Acting as the body's chemical factory, it produces many important substances, including bile, proteins that aid in blood clotting, and cholesterol. Liver disease can be instigated by a variety of causes, including infections, drugs, poisons, ischemia and autoimmune diseases.[23] This section will include some representative small molecule-based fluorescent probes for imaging common liver diseases (hepatocellular carcinoma, drug-induced liver injury/hepatotoxicity, liver fibrosis, *etc.*). The discussion will focus on the underlying design principles, as well as demonstrated biological applications.

4.1 Small molecule-based fluorescent probes for hepatocellular carcinoma (liver cancer)

Liver cancer is the fourth leading cause of cancer-related deaths worldwide, accounting for nearly 800 000 deaths each year. Of these, hepatocellular carcinoma (HCC) is the most common form of primary liver cancer, and HCC patients account for three quarters of all liver cancer patients. With an increase in risk factors, such as poor lifestyle and metabolic diseases, the incidence and mortality of hepatocellular carcinoma are increasing.

Tian *et al.* noted that the expression of histone deacetylases (HDACs), especially HDAC 6, was elevated in tumour samples from HCC patients. Therefore, they envisioned that targeting HDAC could allow the diagnostic imaging of HCC while improving the precision of intraoperative tumour surgery. To test this hypothesis, Tian and colleagues developed an HDAC-targeting small molecule-based fluorescent probe **FITC-SAHA** that was designed to permit HCC detection and provide a tool for facilitating fluorescent image-guided surgical resection.[24] In terms of design, SAHA, an FDA-approved small molecule inhibitor for HDAC6 was used as an HCC-specific targeting ligand. Using fluorescein isothiocyanate (FITC) labelled SAHA, these researchers were able to assess the targeting and imaging ability of **FITC-SAHA**. It was found that **FITC-SAHA** was specifically taken up by the HCC cell line Bel-7402. For *in vivo* imaging, the NIR fluorescent dye IRDye800CW was used to label SAHA in order to produce **IRDye800CW-SAHA** (Fig. 16). **IRDye800CW-SAHA** displayed rapid tumour accumulation, exhibited a high signal-to-noise ratio and was not toxic to healthy tissues in both subcutaneous and orthotopic HCC mouse tumour models. In addition, Tian and his team successfully guided surgical resection of liver cancer tumours *in situ* using **IRDye800CW-SAHA**. The results were considered to provide support for the suggestion that **IRDye800CW-SAHA** might allow the detection of liver cancer while providing a tool that could improve fluorescence-guided surgery.

The protein glypican-3 (GPC-3) is a key biomarker used clinically for the early diagnosis of primary liver cancer, including HCC.[25] In addition to using small molecules as targeting moieties, peptides have recently been used as recognition ligands for GPC-3 due to their high biocompatibility, non-immunogenicity, rapid clearance, and ease of modification. In 2018, Gu *et al.* developed a small molecule peptide-based fluorescent probe that can target GPC-3 for HCC diagnosis.[26] They developed the key GPC-3-targeting peptide IPA (sequence: DYEMHLWWGTEL) using a structure-based virtual simulation. In solution and at the cellular level, IPA displayed a higher binding capacity compared to other previously reported GPC-3 targeting peptides, such as YP (sequence: DHLASLWWGTEL). The fluorescent probe **IPA-MPA** (Fig. 17) was prepared by covalently linking a NIR dye to IPA. The result was a system that could be used for the *in vivo* tumour imaging of GPC-3-positive (HepG2)

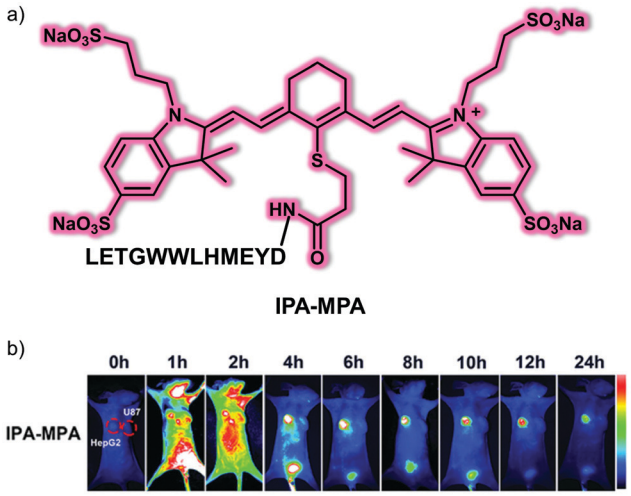

Fig. 17 (a) Chemical structure of small molecule peptide-based NIR fluorescent probe **IPA-MPA** designed to target GPC-3 and permit imaging of HCC. (b) Time-dependent *in vivo* fluorescence imaging of **IPA-MPA** (150 μL, 5 mM) in HepG2 (GPC3-positive HCC cell line) and U87 (GPC3-negative cell line) tumour-bearing mice. Reproduced with permission from ref. 26. Copyright (2019) The Royal Society of Chemistry.

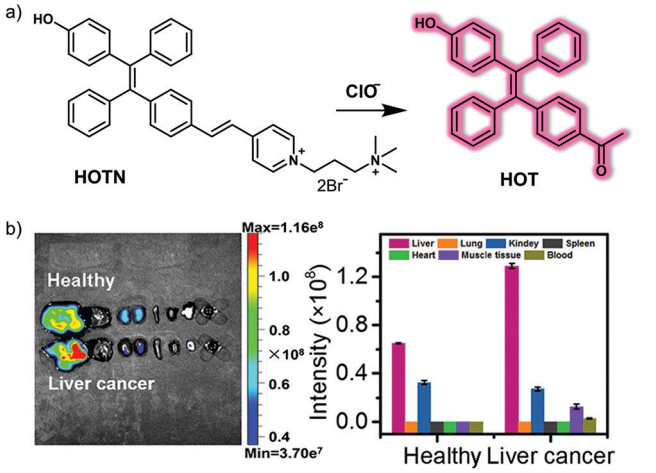

Fig. 18 (a) Chemical structure of the small molecule-based AIE fluorescent probe **HOTN** and working model for the detection of HClO. (b) *In situ* fluorescence imaging and quantification of major organs (From left to right, there are liver, lung, kidney, spleen, heart, muscle tissue, and blood) of the healthy mice and orthotopic liver cancer mice injected with **HOTN** (20 μM, 100 μL in PBS) through the tail vein. λ_{ex} = 430 nm, λ_{em} = 520–620 nm. Reproduced with permission from ref. 27. Copyright (2020) American Chemical Society.

tumour-bearing mice but not GPC-3-negative (U87) tumour-bearing mice. The results led the authors to suggest that **IPA-MPA** could be used for the early diagnosis of HCC.

The abnormal elevation of HClO is strongly correlated with the development of inflammation, and inflammatory damage drives the development of cancer. Several studies have reported an excess of HClO in cancerous tissues and organs. Wang *et al.* have developed a simple, water-soluble AIE-based probe, **HOTN**, for visualizing HClO in an inflammation and a hepatocellular carcinoma model.[27] The hydrophilic group (4-methyl-1-(3-(trimethylammonio)propyl)pyridin-1-ium bromide: Py^+–N^+) and the hydroxyl group were modified at both sides of the AIEgen-tetraphenylethylene (TPE) moiety, which make up the probe **HOTN** (Fig. 18). **HOTN** exhibited good aqueous solubility and was non-fluorescent. However, after reacting with HClO, the double bond of **HOTN** becomes oxidized and cleavage of the Py^+–N^+ group, results in an enhanced aggregation-induced fluorescence emission. It is noteworthy that the strong fluorescence emission on production of **HOT** benefits from enhanced AIE due to intramolecular hydrogen bonding (H-bond) interactions. The turn-on response of **HOTN** to HClO afforded fluorescent enhancements of 1000-fold with addition of HClO (0 to 50 μM). The fluorescence emission increase at 535 nm of **HOTN** displayed good linearity with concentrations of HClO from 0 to 40.0 μM. Moreover, **HOTN** was found to be selective towards HClO over other biological analytes (*e.g.*, biothiols, ROS, RNS and common anions), and the detection limit of **HOTN** towards HClO was determined to be 0.108 μM. Inspired by above results, **HOTN** was used for the fluorescence imaging of both exogenous and lipopolysaccharide (LPS)-/phorbol-12-myristate-13-acetate (PMA)-induced endogenous HClO in RAW 264.7 macrophage cells. Finally, **HOTN** was used to successfully image endogenous HClO in inflammation mouse models (mouse peritonitis and mouse rheumatoid arthritis) and orthotopic liver cancer mice model using an IVIS® Spectrum animal imaging system.

4.2 Small molecule-based fluorescent probes for drug-induced liver injury/hepatotoxicity

Drug-induced liver injury (DILI, also known as drug-induced hepatotoxicity) refers to liver damage caused by direct toxicity or allergic or metabolism-specific reactions to drugs or their metabolites. DILI is a common cause of liver biochemical abnormalities, accounting for about 6% of adverse drug reactions. DILI is also the most common cause for the regulatory withdrawal of a drug after release.

Peroxynitrite ($ONOO^-$) is known to be induced by drug metabolites and has been considered as an excellent biomarker for predicting and detecting DILI. Therefore, the development of appropriate chemical tools to track the dynamic changes of $ONOO^-$ concentrations in liver model systems may help to understand the pathogenesis of hepatotoxicity. In 2019, Tang and colleagues developed a two-photon "turn-on" fluorescent probe **TP-KA** for $ONOO^-$.[28] **TP-KA** was constructed using 1,8-naphthalimide as the fluorophore, while a α-ketoamide group was used as the recognition site for $ONOO^-$ (Fig. 19). In addition, a *tert*-butyl ester group was introduced to enhance the membrane permeability of **TP-KA**. **TP-KA** exhibited a bright fluorescence in the presence of $ONOO^-$, a finding ascribed to oxidation of the α-ketoamide moiety and release of the fluorophore. **TP-KA** was used to evaluate drug-induced hepatotoxicity in living cells using a two-photon microscope. In these studies, HepG2 cells were stained with **TP-KA** and then treated with acetaminophen (APAP, a common pain reliever and fever reducer) or tolcapone (a drug originally was used to treat Parkinson's disease prior to being

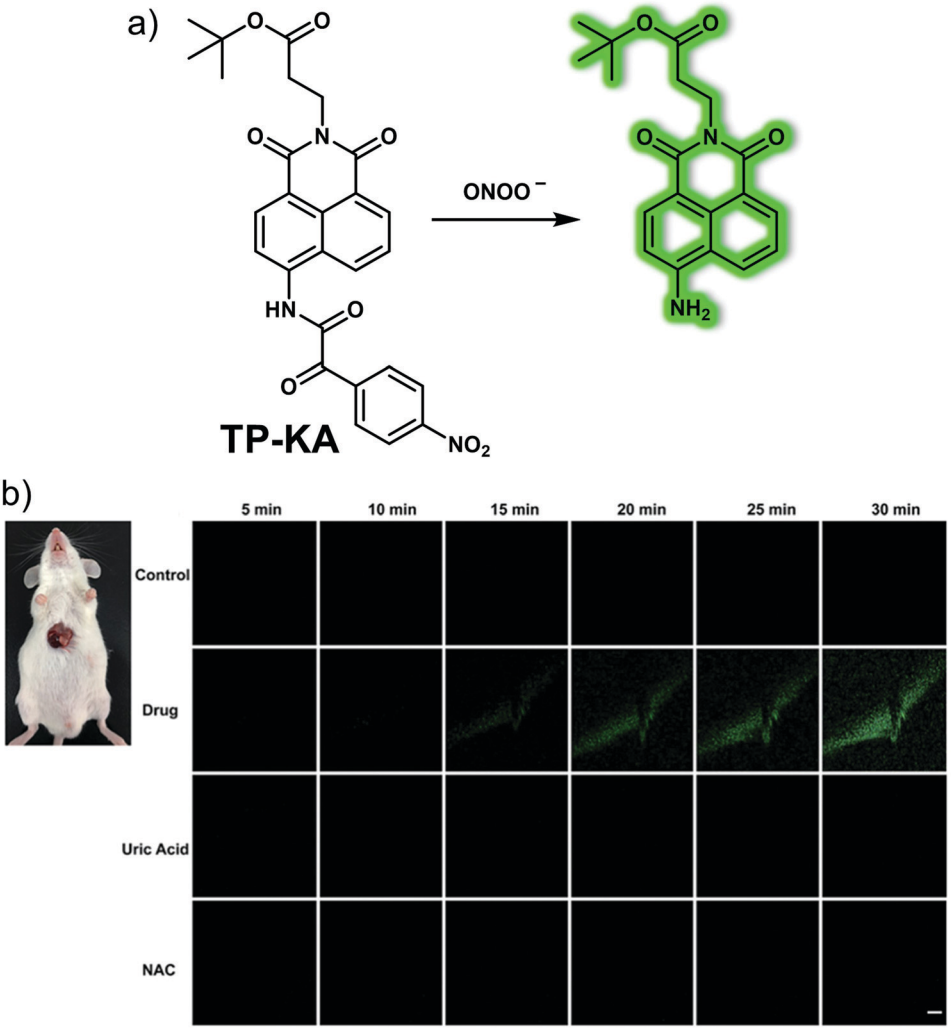

Fig. 19 (a) Chemical structure and working mode for the detection of $ONOO^-$ by means of the small molecule-based two-photon (TP) fluorescent probe **TP-KA**. (b) Real-time TP fluorescence imaging of the livers of normal, tolcapone (300 mg kg^{-1})-induced DILI mice and DILI mice remediated with uric acid (300 mg kg^{-1}) or NAC (300 mg kg^{-1}) following injection with **TP-KA** (50 μM, 100 μL). λ_{ex} = 800 nm, λ_{em} = 500–600 nm. Scale bar = 50 μm. Reproduced with permission from ref. 28. Copyright (2017) The Royal Society of Chemistry.

withdrawn due to serious hepatotoxicity) to induce cell damage. Bright fluorescence was observed in the APAP treated group, while no fluorescence was observed for the control group and only a low fluorescence was observed in the *N*-acetyl cysteine (NAC, a precursor of GSH biosynthesis) treated group. These results provided support for the contention that **TP-KA** could be used to visualize drug-induced hepatotoxicity *via* the imaging of $ONOO^-$ at the cellular level. The two-photon nature of **TP-KA** allowed for the imaging of mouse tissue and the real-time imaging of mice livers. As such, the authors suggested the **TP-KA** could represent a powerful tool for evaluating $ONOO^-$-related DILI.

To follow effectively the production of $ONOO^-$ in the liver, the Li group developed a hepatocyte targeting near-infrared $ONOO^-$-responsive ratiometric fluorescent probe, **Gal-NIR** (Fig. 20).[29] This probe contains a galactose moiety and can achieve hepatocyte-specific targeting due to galactose uptake by the asialoglycoprotein receptor (ASGPR) that is overexpressed on the surface of hepatocytes. **Gal-NIR** exhibits NIR wavelength emission at *ca.* 720 nm due to its extended π-conjugation. However, after reacting with $ONOO^-$, the coumarin 343 group of **Gal-NIR** is released, and the π-conjugated system becomes smaller, producing a higher energy emission with a maximum at *ca.* 500 nm. Reaction with $ONOO^-$, resulted in a 72-fold fluorescence enhancement (F_{500}/F_{720}) in PBS buffer solution. **Gal-NIR** was then used to target HepG2 cells over ASGPR-negative HCT116, HeLa and MCF-7 cells. The probe was used as an effective hepatocyte-targeting $ONOO^-$-tracing reagent in an APAP-induced DILI cell model. *Ex vivo* studies further demonstrated the ability of **Gal-NIR** to target the liver. Specifically, **Gal-NIR** was shown to be successful in monitoring changes in $ONOO^-$ levels in an APAP-induced DILI mice model and the efficacy of hepatoprotective agents (glutathione, *N*-acetylcysteine, biphenyldicarboxylate). These observed results were found to correlate with conventional hematoxylin and eosin (H&E) staining and augur well for the use of this probe in studying DILI *in vivo*.

Yoon *et al.* developed an AIE fluorescent probe, **DQM-ALP**, based on a paired amphiphilic structure design strategy for

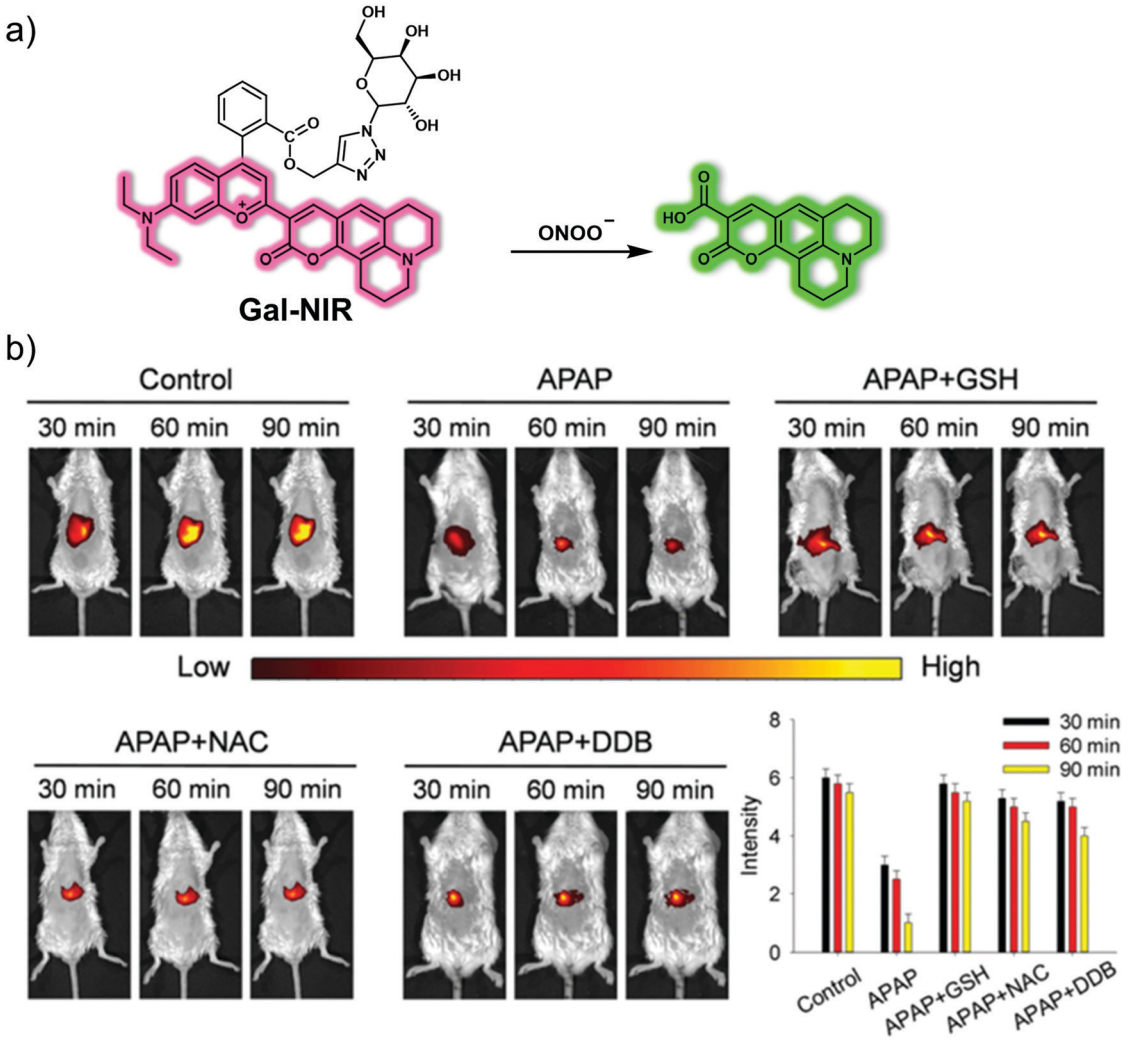

Fig. 20 (a) Chemical structure and working mechanistic model underlying the use of the small molecule-based NIR fluorescent liver-targeting probe, **Gal-NIR**, for the ratiometric detection of $ONOO^-$. (b) Real-time fluorescence imaging and quantification of livers of normal, APAP (500 mg kg^{-1})-induced DILI mice and glutathione (GSH, 400 mg kg^{-1})-, *N*-acetylcysteine (NAC, 400 mg kg^{-1})-, or biphenyldicarboxylate (DDB, 400 mg kg^{-1})-remediated DILI mice injected with **Gal-NIR** (100 μL, 200 μM). λ_{ex} = 640 nm, λ_{em} = 680–780 nm. Reproduced with permission from ref. 29. Copyright (2019) The Royal Society of Chemistry.

monitoring alkaline phosphatase (ALP) activity in DILI (Fig. 21).[30] **DQM-ALP** was constructed using an AIE quinolone-malononitrile (QM) fluorophore and a hydrophilic phosphate group as the ALP recognition unit.[31] In Tris-buffer solution (TBS, 10 mM, pH = 8.0, 1% DMSO), **DQM-ALP** produced a turn on response at λ_{em} = 550 nm in the presence of ALP. It was proposed that the phosphate group of **DQM-ALP** increased the hydrophilicity of the probe; and upon cleavage by ALP, the resulting **DQM-OH** was insoluble in solution and aggregated to give an AIE response. A linear increase in emission at 550 nm was observed, with increasing concentrations of ALP (0–60 mU mL^{-1}). Furthermore, **DQM-ALP** was found to be highly selective (over other assayed enzymes, biothiols, ROS, RNS and common anions) and was stable over a pH range from 4.54 to 10.02 and exhibited greater photostability over commercial dye indocyanine green (ICG, a dye approved by the FDA for clinical use). Moreover, the low cytotoxicity of **DQM-ALP** facilitated the monitoring of endogenous and sodium butyrate or cortisol-induced upregulated ALP activity in HeLa cells. Inhibition studies confirmed that the AIE fluorescent response in living cells was triggered by ALP activity. Inspired by these results, **DQM-ALP** was used to monitor endogenous ALP activity in liver tissue slices of APAP-induced DILI mice and was able to distinguish hepatocellular carcinoma tissue from normal liver tissue in HepG2 tumour-bearing mice.

A dual-responsive chemo-fluoro-luminescent system, **CFR**, was developed by Pu *et al.* to facilitate the monitoring of superoxide anion ($O_2^{\bullet -}$) and caspase-3 (casp3).[32] According to the authors, this probe constituted the first optical small molecule system with two independent activation channels, namely near-infrared fluorescence and chemiluminescence. The proposed duplex sensing mechanism is depicted in Fig. 22. Addition of casp3 cleaves the amide linkage between the casp3-cleavable peptide (Asp-Glu-Val-Asp) and the self-immolative linker present in **CFR**. This results in the release the hemicyanine unit, which

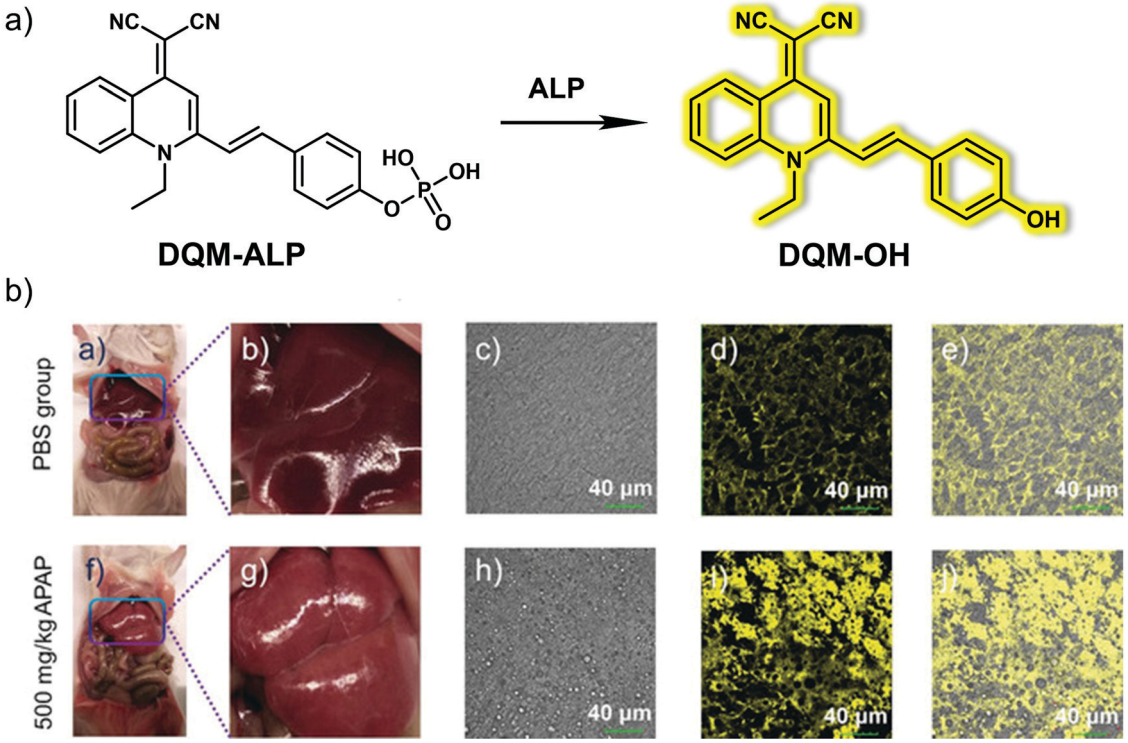

Fig. 21 (a) Chemical structure of the small molecule-based AIE fluorescent probe **DQM-ALP** designed to facilitate the detection of ALP. (b) Fluorescent imaging of the liver tissues of normal (PBS group) and APAP (500 mg kg^{-1}, 12 h)-induced DILI mice followed by incubation with **DQM-ALP** (10 μM). λ_{ex} = 488 nm, λ_{em} = 520–620 nm. Scale bar = 40 μm. Reproduced with permission from ref. 30. Copyright (2020) Wiley-VCH Verlag GmbH & Co. KGaA, Weinheim.

emits at 710 nm. The addition of $O_2^{\bullet-}$ induced chemiluminescence since $O_2^{\bullet-}$ serves to remove the sulfonate ester of **CFR**, resulting in luminescence activation. A 12-fold enhancement in near-infrared fluorescence intensity at 710 nm after treatment of **CFR** with casp3 while a ~40 000-fold enhancement in chemiluminescence was seen when **CFR** was exposed to $O_2^{\bullet-}$. Owing to its high specificity for $O_2^{\bullet-}$ and casp3, **CFR** was successfully applied to the detection of endogenous $O_2^{\bullet-}$ levels and casp3 activity in valproic acid (VPA)-induced DILI cells and mice. **CFR** was also used to obtain insights into the presumed determinants of DILI, namely elevated ROS levels during oxidative stress that causes DNA damage and mitochondrial permeability, triggers that lead to the activation of casp3 and ultimately apoptosis.

4.3 Small molecule-based fluorescent probes for liver fibrosis

Liver fibrosis occurs when inflammation leads to the accumulation of excess scar tissue in the liver. Liver fibrosis is a healing response to liver injury, which is characterized by excessive deposition of extracellular matrix (ECM) proteins. Liver fibrosis is beneficial at first because it can enclose the damage and is considered reversible at an early stage. However, if left uncontrolled, it can eventually develop into advanced fibrosis or cirrhosis, or even liver cancer, which is irreversible. Therefore, the development of strategies for the early diagnosis of liver fibrosis could help prevent progression toward HCC.

Hypoxia refers to an insufficient supply of oxygen to tissues or organs. While there are a number of factors that can lead to hypoxia, it is often associated with inflammatory disease, including liver fibrosis. Li *et al.* designed a small molecule-based fluorescent probe, **Cy-AP**, for the real-time imaging of hypoxia in a mouse liver fibrosis model.[33] To create **Cy-AP**, a NIR fluorescent hemicyanine was linked to an azo group, which served as a reporter for hypoxia (Fig. 23). The azo group was chosen since other hypoxia sensitive groups, such as nitroaryl or quinone, are susceptible to changes in the environmental conditions (such as pH or polarity). Per the design expectations of the authors, in hypoxic cellular microenvironments, the azo group present in **Cy-AP** was readily reduced to the corresponding amino group; this gives **Cy-NH_2** and results in an increase in the fluorescence emission at 725 nm. **Cy-AP** was used to monitor hypoxia in living HepG2, HCT116, HeLa, and MCF-7 cells. Due to its NIR emission, high selectivity, and excellent fluorescence response, **Cy-AP** was used to monitor the state of hypoxia in CCl_4-induced liver fibrosis mice.

During the course of liver fibrosis, lysine oxidase (LOX) oxidizes lysine to produce allsysine, a metabolite regarded as a reliable pathological indicator of liver fibrosis. In 2019, Wang *et al.* developed a NIR fluorescent probe, **BNLBN**, based on a NIR dye (**BNLB**, modified from Nile blue) designed to monitor allysine and hence permit visualisation of liver fibrosis (Fig. 24).[34] **BNLBN** contained a hydrazine unit that was introduced into the probe as an allysine-responsive moiety. The initial fluorescence of **BNLBN** was weak, presumably due to an acceptor-photoinduced electron transfer (a-PeT) effect; however, addition of allysine negates this

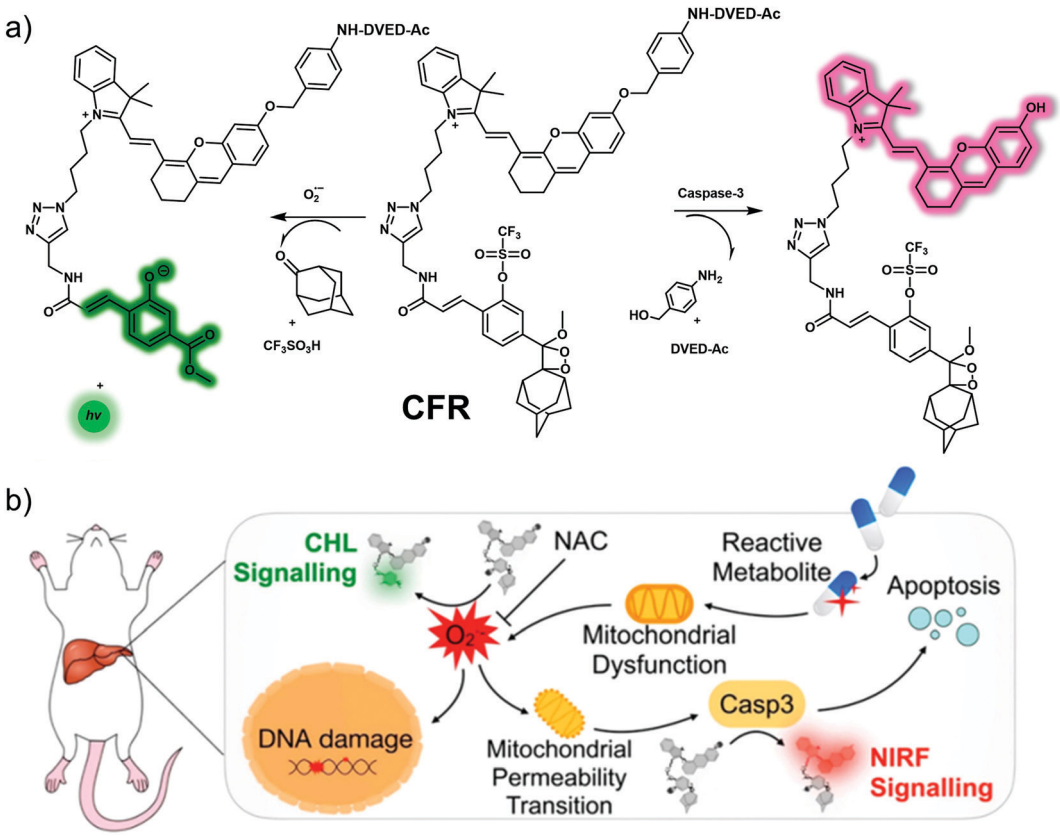

Fig. 22 (a) Chemical structure of small molecule-based chemo-fluoro-luminescent probe, **CFR**, and a working model showing how it may be used to effect the dual detection of superoxide anion ($O_2^{\bullet-}$) and caspase-3 (casp3). (b) Schematic illustration of how **CFR** sequentially detects upregulated $O_2^{\bullet-}$ and casp3, species that are thought critical to the progression of DILI. Reproduced with permission from ref. 32. Copyright (2019) American Chemical Society.

a-PeT effect resulting in enhanced fluorescence. **NLBN**, also based on Nile blue, was prepared as a control that was expected to interact with serum albumin. Many fluorescent imaging probes are bound to albumin in the bloodstream. This can result in false positive signals. In contrast to **NLBN**, **BNLBN** was designed to be relatively inert with regard to albumin binding thereby providing a higher level of accuracy and resolution in terms of fibrotic disease. In fact, **BNLBN** proved useful in identifying oxidized albumin (O-SA, which has allysine) in a PBS environment. In contrast, a nonselective strong fluorescence signal was seen when **NLBN** was allowed to interact with either albumin (SA) or O-SA. Further highlighting the difference between these ostensibly similar systems was the fact that **NLBN** proved to be non-selective in living mice presenting with either normal, mild or severe fibrosis, whereas, **BNLBN** could be used to monitor allysine in living mice with different levels of CCl_4-induced liver fibrosis.

MAO-A can be regarded as a potential biomarker of neurodegenerative disease, including AD. Studies have led to the consensus view that the activity of MAO-A is increased in liver disease, especially during liver fibrosis.[35] Qin and co-workers developed a "turn-on" NIR probe **DHMP2** based on an intramolecular charge transfer (ICT) mechanism and showed it was effective for the detection of MAO-A in a mouse model for liver fibrosis (Fig. 25).[36] In **DHMP2**, a dihydroxanthene (DH) moiety serves as the fluorophore, while a propylamine group acts as the recognition group for MAO-A and a quaternary ammonium salt as the mitochondrial-targeting subunit. **DHMP2** could be used to detect changes in MAO-A activity with high selectivity and sensitivity in PBS buffer solution and in living cells. **DHMP2** was found to act as a turn on NIR fluorescence sensor that allowed detection of MAO-A in zebrafish and in a SH-SY5Y (overexpressing MAO-A) tumour-bearing mouse model. It was also found that **DHMP2** could be used to evaluate the therapeutic effect of a MAO-A inhibitor (clorgyline) in CCl_4-induced hepatic fibrosis rats.

5. Small molecule-based fluorescent probes for kidney disease

The kidney is responsible for filtering impurities in the blood, maintaining the balance of body fluids and electrolytes, and producing urine to be excreted; it also has endocrine functions that serve to regulate blood pressure. When kidney damage occurs, it triggers kidney-based disorders, many of which are slow to manifest and not easily detected.[37] The development of small molecule-based fluorescent probes may allow for the early

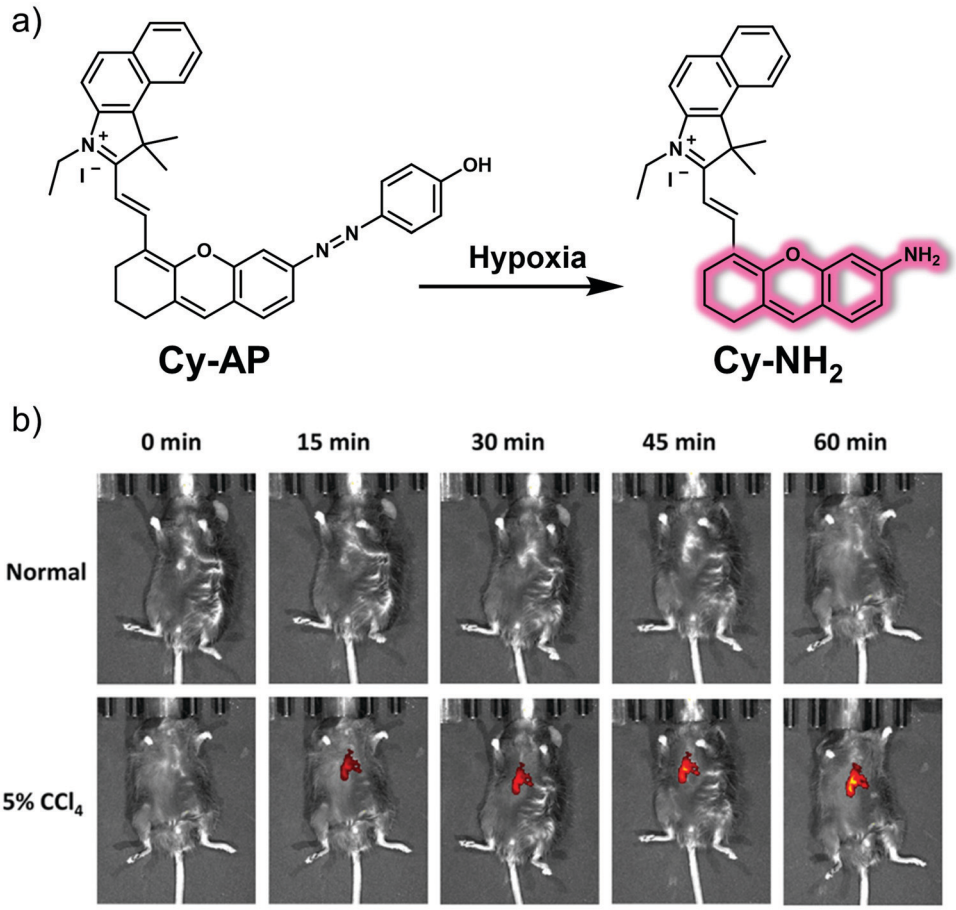

Fig. 23 (a) Chemical structure of the small molecule-based fluorescent probe **Cy-AP** designed to allow detection of hypoxia and its proposed mode of action. (b) Time-dependent *in vivo* fluorescence images of normal mice and those subject to 5% CCl_4; both sets of animals were monitored after tail vein injection of **Cy-AP** (250 μM). λ_{ex} = 640 nm, λ_{em} = 695–770 nm. Reproduced with permission from ref. 33. Copyright (2020) American Chemical Society.

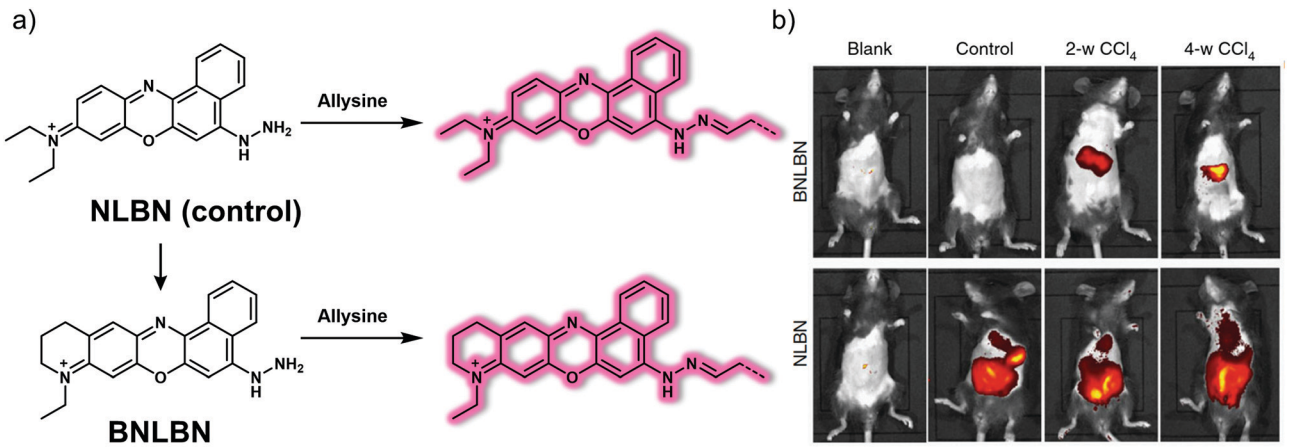

Fig. 24 (a) Chemical structure of the small molecule-based NIR probes **NLBN** (control) and **BNLBN** and working model for how the latter may be used to detect allysine. (b) *In vivo* fluorescence images of mice in the blank, normal, 2-w CCl_4 and 4-w CCl_4 groups recorded after subjecting to **NLBN** (100 μL, 200 μM, i.v. injection) and **BNLBN** (100 μL, 200 μM, i.v. injection). Blank: without any treatment; control: treated with PBS; mild fibrosis: twice a week, intraperitoneal injection of CCl_4 (10% in olive oil; 1 mL kg^{-1}, for 2 weeks); severe fibrosis: the same treatment but for 4 weeks. Reproduced with permission from ref. 34. Copyright (2020) by the authors (P. Xing, Y. Niu, R. Mu, Z. Wang, D. Xie, H. Li, L. Dong and C. Wang). Published by Springer Nature.

diagnosis of kidney disease, permit more effective monitoring of progression, and aid in the selection of optimal treatment protocols. This section will detail some representative small molecule-based fluorescent probes that show potential for

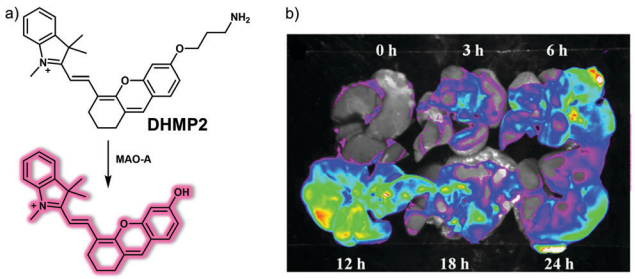

Fig. 25 (a) Chemical structure of small molecule-based NIR probe **DHMP2** and working model for the chemical changes that make it useful in the detection of MAO-A activity. (b) Fluorescence images of MAO-A in liver fibrosis tissue of CCl_4-induced fibrotic rats treated with probe **DHMP2** (50 μM, 1 mL) at different times (0, 3, 6, 12, 18 and 24 h). λ_{ex} = 630 nm, λ_{em} = 700 nm. Reproduced with permission from ref. 36. Copyright (2020) American Chemical Society.

imaging kidney disorders, including kidney dysfunction and acute kidney injury.

5.1 Small molecule-based fluorescent probes for kidney dysfunction

Real-time, and non-invasive monitoring of renal dysfunction is important for assessing drug-induced nephrotoxicity and preventing the progression of kidney disease. Fluorescence imaging for monitoring changes to renal function is a simple and effective method. In 2019, the Pu group reported a renal-clearable fluorescent probe, **CDIR2**. This probe functions in the low energy second near-infrared window (NIR-II; 1000–1700 nm) where tissues are most transparent. It was found effective in imaging kidney dysfunction with a high signal-to-background ratio and good image resolution.[38] In terms of design, **CDIR2** contains a HPβCD (2-hydroxypropyl-β-cyclodextrin) moiety capable of being cleared by the kidney and a NIR-II fluorophore based on a shielding unit–donor–acceptor–donor–shielding unit (S–D–A–D–S) structure (Fig. 26). Good renal-clearance efficiency was seen for **CDIR2**, as well as a bright fluorescence emission centred around 1050 nm. Pharmacokinetic experiments revealed that **CDIR2** possessed good renal clearance efficiency and displayed adequate *in vivo* stability. The renal clearance pathway of **CDIR2** was found to be *via* unidirectional glomerular filtration. Therefore, the fluorescence intensity of **CDIR2** could be used to directly monitor the functional kidney impairment in mice as induced, for instance, by high-dose cisplatin. More importantly, the results of NIR-II fluorescence imaging using **CDIR2** were consistent with those using clinical diagnostic methods (*e.g.*, blood test, immunofluorescence, H&E (hematoxylin-eosin) staining). This study provided what is believed to be the first NIR-II imaging probe that allows for the real-time and non-invasive detection of renal dysfunction. As such, it may

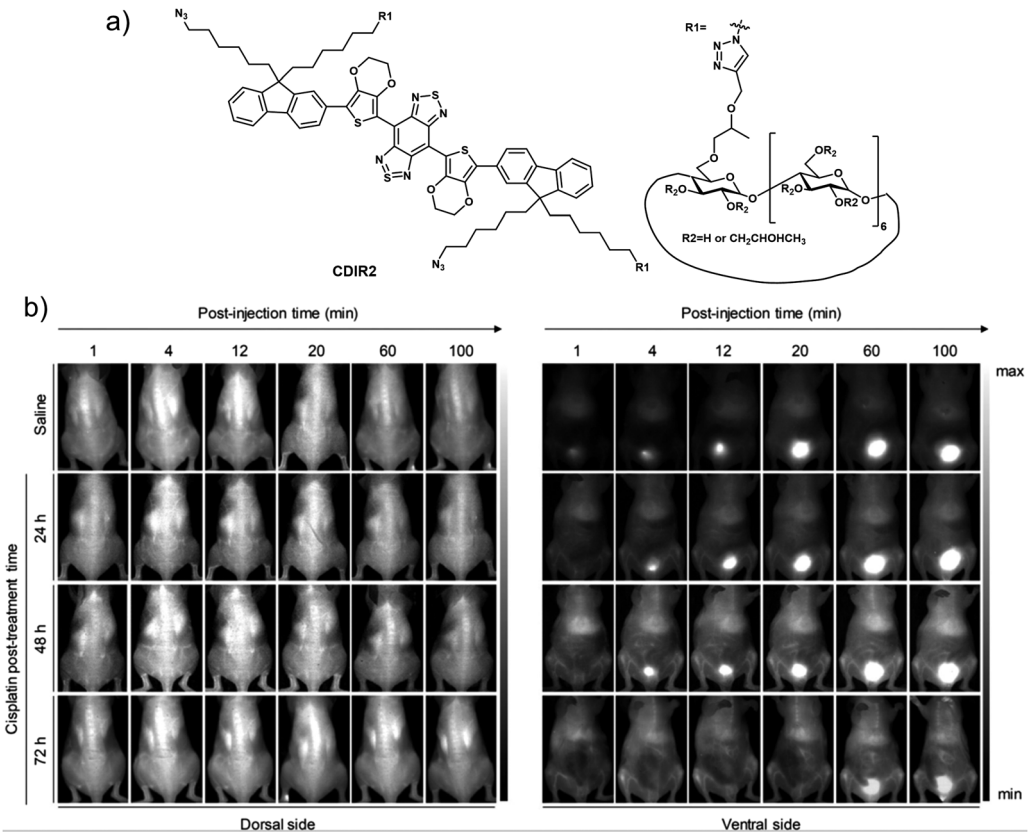

Fig. 26 (a) Chemical structure of small molecule-based NIR-II probe **CDIR2**. (b) NIR-II fluorescence images of normal and cisplatin (20 mg kg^{-1})-treated mice at different post-treatment timepoints after i.v. injection of **CDIR2** (1 μmol kg^{-1} body weight). Reproduced with permission from ref. 38. Copyright (2019) Wiley-VCH Verlag GmbH & Co. KGaA, Weinheim.

see application as an imaging platform for the non-invasive monitoring of other kidney diseases.

5.2 Small molecule-based fluorescent probes for acute kidney injury

Acute kidney injury (AKI), formerly known as acute renal failure (ARF), is a dramatic decline in kidney function that results in a build up of nitrogenous products in the blood with or without a decrease in urinary excretion. AKI results from a variety of traumas, such as decreased renal perfusion, exposure to nephrotoxins, outflow tract obstruction, or parenchymal disease. The clinical diagnosis of AKI relies mainly on blood creatinine and urine volume, but there is a certain lag in the diagnosis of AKI; therefore, developing non-invasive tools that permit effective diagnoses and treatment monitoring could prove beneficial in the clinical management of AKI.

Efficient identification of ROS (*e.g.*, hypochlorous acid, HClO) produced during oxidative stress is considered as a particularly promising strategy for identifying early drug-induced AKI. The groups of Yi and Wei recently developed a dual modal NIR probe, **FDOCl-22**, that permits the detection of HClO *in vitro* and in drug-induced AKI mice (Fig. 27).[39] This near-infrared 'turn-on' probe undergoes a de-formylation reaction upon exposure to HClO leading to its activation. In addition, **FDOCl-22** contains an ethylene glycol chain that serves to enhance its water solubility and kidney-targeting. Fluorescence-response experiments in PBS buffer solution revealed that **FDOCl-22** displays good selectivity towards HClO. The limit of detection for HClO was 20.7 nM. A change in the absorption features of **FDOCl-22** is seen upon reaction with HClO allowing it to serve as functional photoacoustic (PA) agent. Confocal microscopic imaging and flow cytometry studies served to reveal that **FDOCl-22** can detect endogenous HClO in macrophages. The fluorescence intensity of **FDOCl-22** was found to increase in a dose-dependent manner with increasing cisplatin. On the other hand, it decreased in a dose-dependent manner following the addition of L-carnitine, a small molecule that can inhibit cisplatin-induced oxidative injury. Notably, **FDOCl-22** could be used to monitor the dynamic changes of HClO levels in a mouse model for cisplatin-induced AKI while supporting dual-modal NIR and PA imaging.

In addition to causing oxidative stress, upregulation of ROS in the context of kidney injury-induced lysosomal damage leads to the release of the lysosomal enzyme *N*-acetyl-β-D-glucosaminidase (NAG) from renal tubular cells, which is seen as a diagnostic biomarker for the early diagnosis of kidney injury. Pu *et al.* designed a dual-responsive probe **ADR** for the detection of superoxide anion ($O_2^{\bullet -}$), a marker of oxidative stress, and NAG, a marker of lysosome damage.[40] **ADR** contains a near-infrared fluorescence (NIRF) hemi-cyanine and a chemiluminescent phenoxy-dioxane luminophore, as well as a NAG-reactive *N*-acetyl-β-D-glucosamine moiety and the $O_2^{\bullet -}$-responsive trifluoromethanesulfonate group attached to a sulfonated cyclodextrin HPβCD (Fig. 28). As prepared, **ADR** exhibited no detectable fluorescence emission upon excitation at 600 nm and no chemiluminescence at 520 nm. However, upon the addition of NAG, a 10-fold increase in the fluorescence intensity at 720 nm (excitation wavelength 695 nm) was observed. Subsequent addition of $O_2^{\bullet -}$ led to a 1200-fold chemiluminescence increase at 520 nm but produced no obvious fluorescence change. **ADR** exhibited high specificity for NAG and $O_2^{\bullet -}$ over other potentially interfering analytes. Due to its relatively high renal clearance efficiency and good biocompatibility, **ADR** could be used to image and monitor NAG and $O_2^{\bullet -}$ simultaneously in a diatrizoate (DTZ)-induced AKI mouse model (DTZ is a radioactive contrast agent that can cause nephrotoxicity). Importantly, when compared with the current clinical assays, **ADR** performed better for diagnosing the early stages of acute kidney injury.

6. Small molecule-based fluorescent probes for lung disease

The lungs are the most important organ of the human respiratory system, and perform a variety of important functions, including respiratory regulation, pulmonary circulation and hematopoietic function. Poor pulmonary vascular circulation and damage to the alveolar wall can lead to lung dysfunction, which can allow invasive infections by various pathogenic microorganisms (*e.g.*, bacteria, fungi, viruses, mycoplasma, chlamydia). Such insults generally

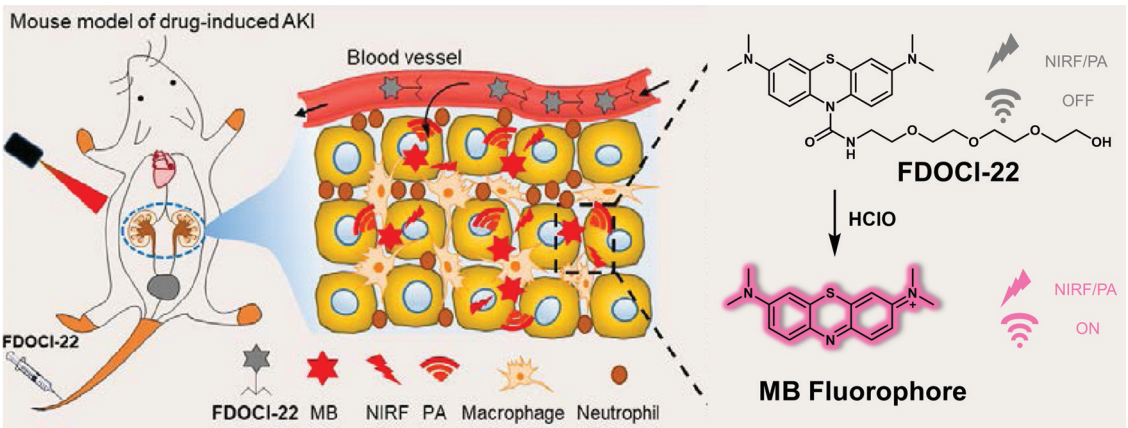

Fig. 27 Diagrammatic sketch of the dual-mode detection of early-stage drug-induced AKI made possible by the small molecule-based NIR-photoacoustic bimodal probe **FDOCl-22**. Reproduced with permission from ref. 39. Copyright (2020) American Chemical Society.

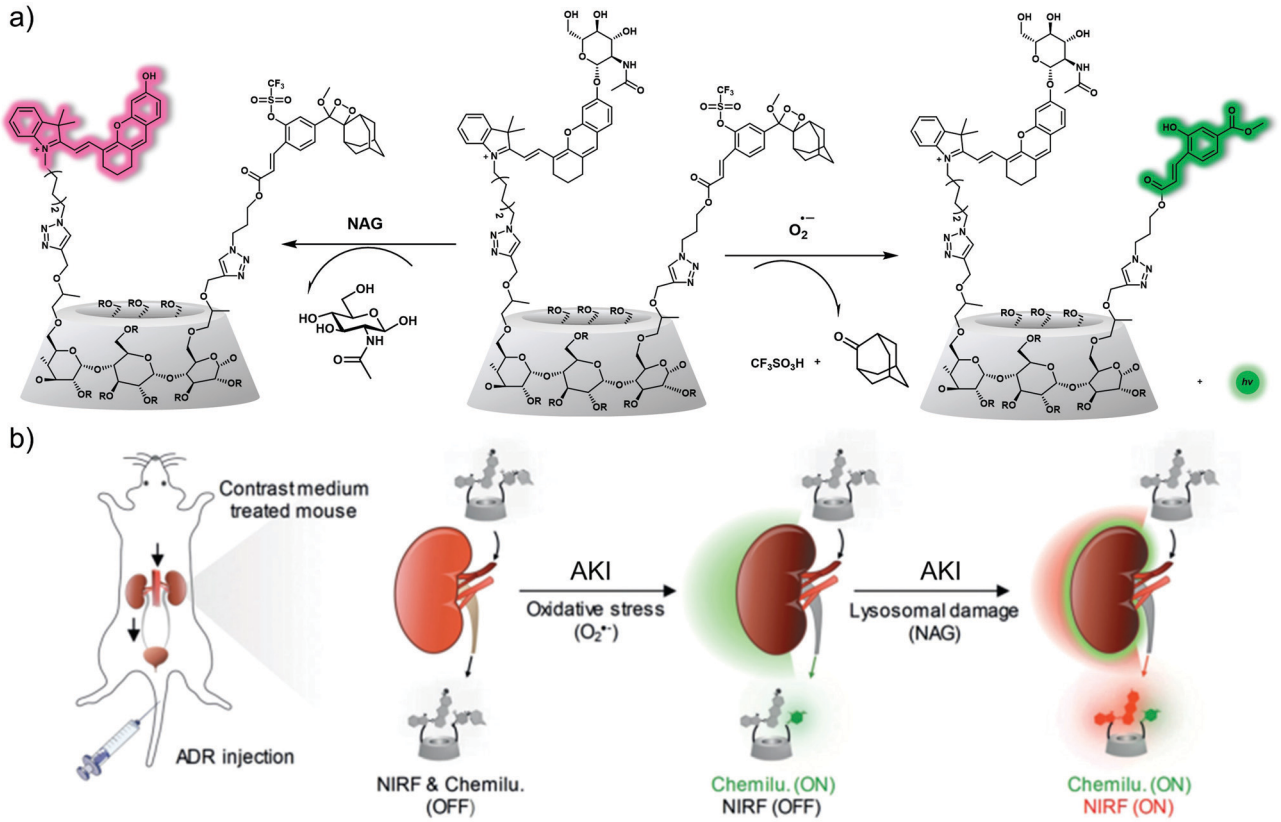

Fig. 28 (a) Chemical structures of **ADR** and its activated forms generated in response to oxidative stress ($O_2^{\bullet-}$) and lysosomal damage (NAG), respectively (R = H, $CH_2CHOHCH_3$ or CH_2CCH). (b) Schematic of real-time duplex imaging and early detection of AKI using **ADR**. NIRF: near-infrared fluorescence. Chemilu: chemiluminescence. Reproduced with permission from ref. 40. Copyright (2019) Wiley-VCH Verlag GmbH & Co. KGaA, Weinheim.

lead to inflammation of the lung parenchyma, which in turn can promote the onset and development of various types of pneumonia. When normal alveolar tissue is damaged and undergoes abnormal repair leading to structural abnormalities, it can trigger lung diseases, such as pulmonary fibrosis, and in severe cases promote other diseases, such as lung cancer.[41] This section will provide an overview of some representative small molecule-based fluorescent probes developed for the purpose of imaging lung disease (lung inflammation, acute lung injury, pulmonary fibrosis, lung cancer *etc.*).

6.1 Small molecule-based fluorescent probes for lung inflammation

Lung inflammation is strongly correlated with oxidative stress. Elevated levels of hypochlorous acid (HClO) expression are associated with the development of inflammatory disease. In 2018, the group of Dong developed a series of heptamethine Cy7 based ratiometric HClO-responsive fluorescent probes **ClO1–ClO6** using different functional groups (*e.g.*, long and short lipid chains; diverse amino group modification) that were characterized by different HClO-detection capabilities and lung targeting abilities (Fig. 29).[42] All probes in the context of this work exhibited NIR fluorescence emission at 768 nm. However, when **ClO1**, **2**, **4**, **6** (5 μM) were allowed to react with HClO (14 μM), an enhanced fluorescence at 605 nm and a decrease in the emission at 768 nm was observed. Cell imaging experiments confirmed that **ClO1**, **6** could be used to visualise exogenous and exogenous HClO in living A549 cells. In particular, **ClO1** with a longer lipid chain (one *n*-octadecane chain) and amino groups (two 2-[[2-(dimethylamino)ethyl]methylamino]-ethyl subunits) exhibited the best comparative lung-targeting ability as inferred from bio-distribution experiments. *In vivo* bio-imaging experiments were carried out and, in combination provided support for the contention that **ClO1** could be used to monitor the *in situ* levels of HClO in tissues characterised by LPS-induced acute lung inflammation.

6.2 Small molecule-based fluorescent probes for acute lung injury (ALI)

Acute lung injury (ALI) is caused by a variety of factors (*e.g.*, severe lung infection, lung contusion, inhalation of toxic gases, drowning, oxygen poisoning, *etc.*) that lead to immune dysfunction in the lungs. The accumulation of leukocytes and release of pro-inflammatory factors causes damage to lung endothelial cells and epithelial cells as well as affecting alveolar membrane integrity.[43] The clinical manifestations of ALI are respiratory distress, refractory hypoxemia, and noncardiogenic pulmonary edema, which can progress to acute respiratory distress syndrome (ARDS) in severe

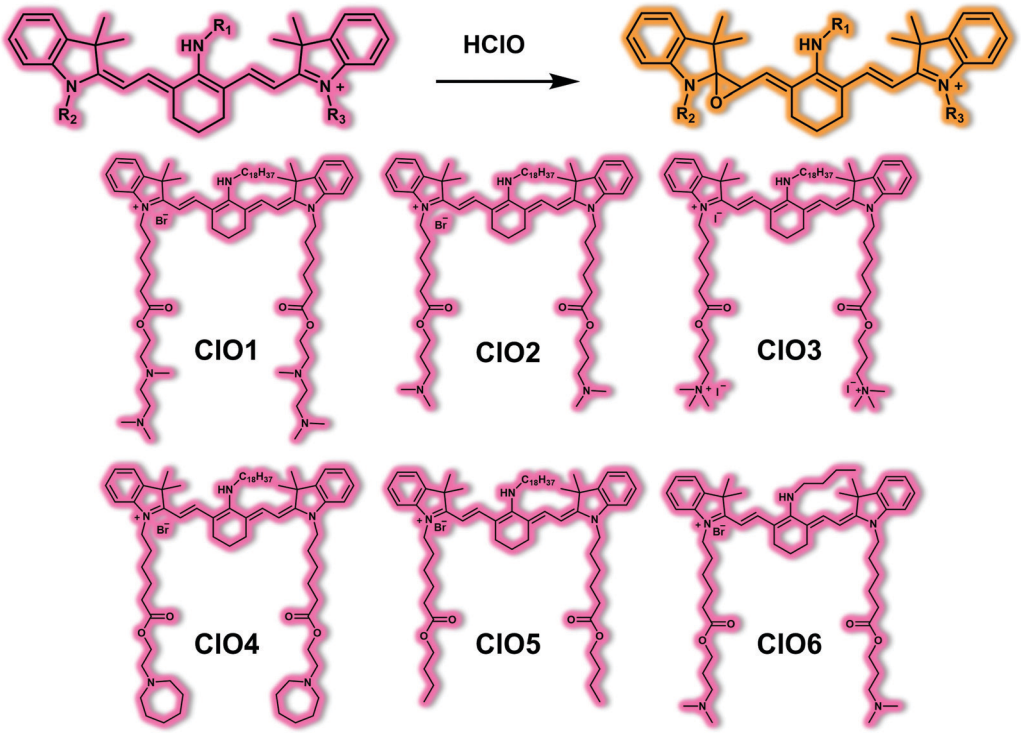

Fig. 29 Chemical structure of small molecule-based ratiometric NIR probes **ClO1–ClO6** and proposed mode of action that allows for HClO detection.

cases. It is now generally accepted that ARDS is caused by an inflammatory response, in which multiple inflammatory mediators are blocked by the pulmonary circulation and then accumulate in the lungs, thus inducing an inflammation of the lung tissue.

Similar to acute injury in other organs (*e.g.*, liver, kidney), oxidative stress plays an important role in the development of acute lung injury (ALI) and especially in its progression towards ARDS. In particular, myeloperoxidase (MPO) activity is found to be elevated in ALI lung tissue. This enzyme modulates the inflammatory response and converts hydrogen peroxide to hypochlorous acid (HClO). Therefore, effective monitoring and tracking of abnormal elevations of pulmonary ROS such as HClO facilitates the ability to study ALI. Lesur *et al.* reported a small molecule-based fluorescent HClO probe (**DSAPF**).[44] As shown in Fig. 30a, **DSAPF** utilizes the fluorescein scaffold and the HClO responsive group 4-aminophenyl moiety. Initially, **DSAPF** is non-fluorescent, but upon addition of HClO, a turn-on fluorescence response was observed (λ_{ex} = 502 nm, λ_{em} = 522 nm) in PBS buffer. **DSAPF** was used for endogenous fluorescence imaging of HClO in LPS-stimulated polymorphonuclear neutrophils (PMNs) and alveolar macrophages (AMs). The HClO response was confirmed using MPO inhibitor, 4-aminobenzoic hydrazide. Moreover, **DSAPF** was used for intravital imaging of endogenous HClO in lung free alveolar cells of hyperoxia (95%, 72 h)-induced ALI rats *via* endoscopic confocal fluorescence microscopy. This study revealed elevated levels of HClO in AMs and PMNs was consistent with *ex vivo* immunohistochemistry studies. Therefore, confirming the reliability of **DSAPF** when compared to known biological methods. Notably, **DSAPF** is the first small molecule-based HClO-responsive fluorescent probe enabling intravital ALI animal imaging at the cellular level.

Yue *et al.* developed the PeT-based fluorescence probe, **BCy-HOCl**, for the detection of HClO *in vitro* and *in vivo* (Fig. 30b and c).[45] **BCy-HOCl** was constructed using a HClO responsive dimethylthiocarbamate unit and a benzoindocyanine moiety as the fluorescent reporter. **BCy-HOCl** was shown to be non-fluorescent in HEPES buffer (10 mM, pH 7.4), However, in the presence of HClO, the dimethylthiocarbamate unit was hydrolysed which inhibited PeT thereby facilitating a fluorescence enhancement at 630 nm under excitation at 500 nm. **BCy-HOCl** exhibited a high sensitivity towards HClO with a limit of detection of 17 nM, and an excellent selectivity over other biologically relevant metal ions, anions, ROS and other RNS species. **BCy-HOCl** proved effective for the fluorescence imaging of exogenous HClO in A549 and RLE-6TN cells and endogenous HClO in LPS-stimulated and H_2O_2-induced ALI cell models. **BCy-HOCl** was successfully deployed for imaging endogenous HClO fluctuations in LPS-induced and hyperoxia-induced ALI mouse models, in which a gradual increase in fluorescence with time was observed post-LPS stimulation. These results indicate that **BCy-HOCl** could be used to monitor the abnormal expression of HClO in ALI.

Neutrophil elastase (NE) is an inflammatory enzyme that promotes an inflammatory response and results in tissue damage and endothelial cell injury. Yang and co-workers developed a turn-on NIR fluorescent probe **NEP** to detect NE *in vitro* and in ALI mice (Fig. 31).[46] **NEP** consists of a hemicyanine dye-based NIR fluorophore and a pentafluoropropionamide unit as the recognition unit

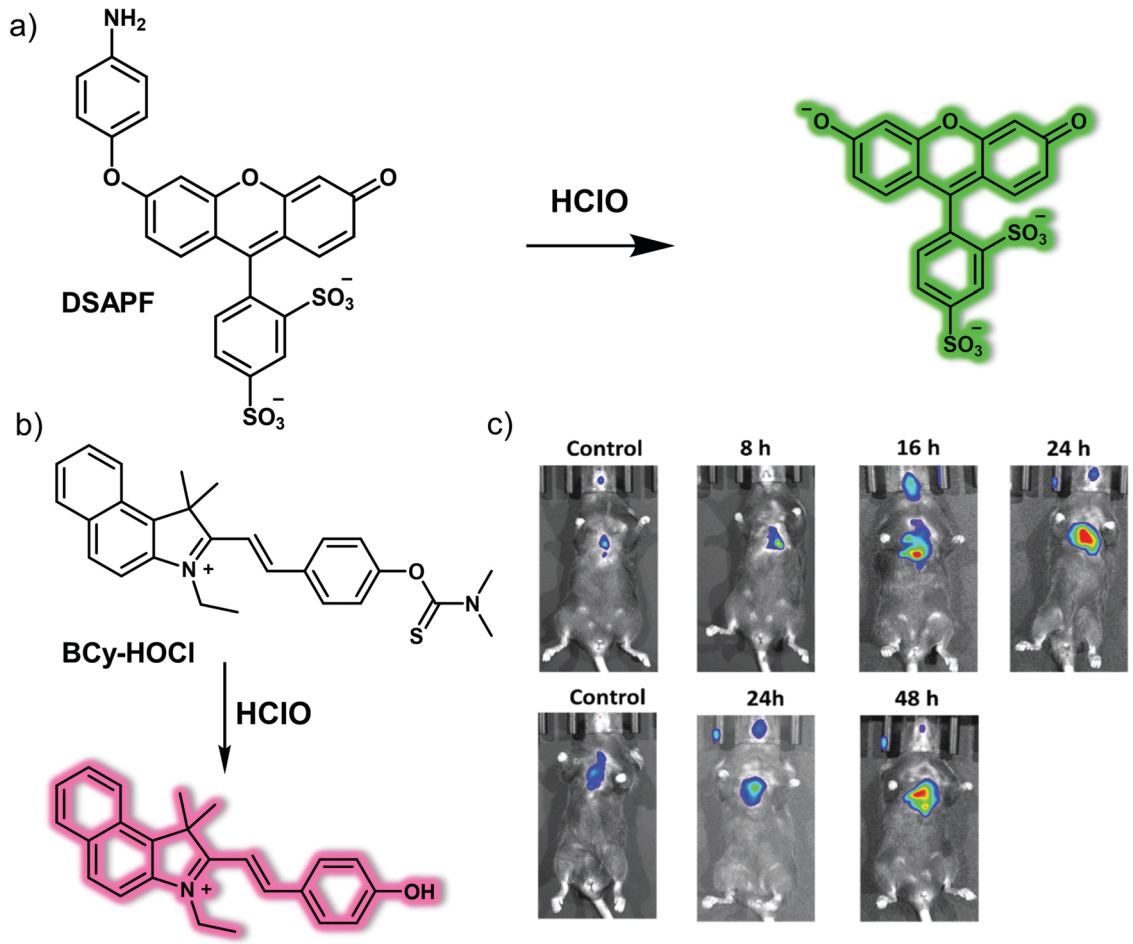

Fig. 30 Chemical structure of small molecule-based fluorescent probes, (a) **DSAPF**, (b) **BCy-HOCl**, and a working model showing how they may be used to detect HClO. (c) Time-dependent fluorescence images of the LPS (top) and hyperoxia (bottom)-induced ALI mice administered intratracheally with **BCy-HOCl**. λ_{ex} = 543 nm, λ_{em} = 600–700 nm. n = 5. Reproduced with permission from ref. 45. Copyright (2020) The Royal Society of Chemistry.

for NE.[47] The addition of NE (0–10 μg mL^{-1}) resulted in a 25-fold fluorescence increase at 700 nm (excitation wavelength 670 nm). The fluorescence emission of **NEP** displayed good linearity with concentrations of NE (0–1.0 μg mL^{-1}) providing a limit of detection (LOD) of 29.42 ng mL^{-1}. **NEP** was shown to be highly selective towards NE over other biologically important enzymes and analytes. **NEP** could be used to visualize induced NE-trafficking and NE upregulation in RBL-2H3 cells and exogenous NE uptake in A549 cancer cells. In addition, **NEP** was used to monitor NE levels in ALI progression, and *in vivo* imaging indicated that LPS-induced ALI mice display up-regulated NE level, suggesting the potential of **NEP** to monitor ALI in real time.

6.3 Small molecule-based fluorescent probes for pulmonary fibrosis

Idiopathic pulmonary fibrosis (IPF) is a rare, chronic, fatal disease that develops gradually over several years and is typically characterized by the formation of scar tissue in the lungs and progressive dyspnoea. It is the most common form of lung disease associated with idiopathic interstitial pneumonia, and its clinical features include shortness of breath, diffuse pulmonary infiltrates on imaging, and varying degrees of inflammation/fibrosis or both on lung biopsy. The development of novel early diagnostic strategies for pulmonary fibrosis may lead to improvements in patient survival and in reduced morbidity.

Chronic inflammation and mitochondrial oxidative stress play an important role in the development of pulmonary fibrosis. Moreover, the level of reactive oxygen species (ROS) or reactive nitrogen species (RNS) is thought to be proportional to the severity of the pulmonary fibrosis. This is providing an incentive to develop fluorescent probes for $ONOO^-$ since in principle they could aid in the diagnosis of pulmonary fibrosis. Appreciating this need, Lv *et al.* designed a ratiometric two-photon fluorescent probe, **rTPONOO-1**, that was designed to allow the transition from lung inflammation to pulmonary fibrosis in living cells and tissue slices to be followed by monitoring the $ONOO^-$ levels.[48] **rTPONOO-1** is based on the acedan fluorophore skeleton and a mitochondria-targeting indolium group; it also contains a carbon–carbon double bond as an $ONOO^-$-responsive moiety (Fig. 32). As prepared **rTPONOO-1** exhibited a NIR emission *ca.* 718 nm. Upon the addition of $ONOO^-$, the C=C bond was oxidized and cleaved, and the fluorophore acedan was released, resulting in a green fluorescence emission centred

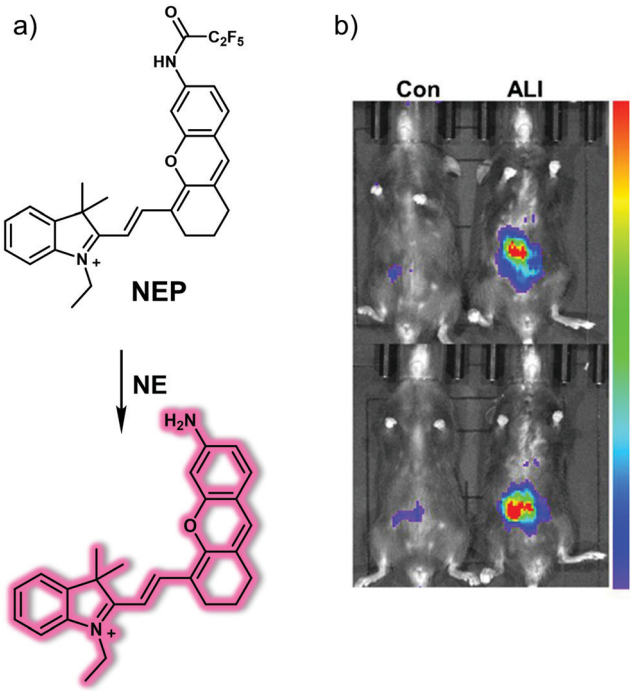

Fig. 31 (a) Chemical structure of small molecule-based NIR probe **NEP** and proposed mode of action that allows for NE detection. (b) *In vivo* fluorescent imaging of healthy (left) and ALI mice (right) intravenously injected with **NEP** (50 μM, 200 μL). λ_{ex} = 660 nm, λ_{em} = 670–730 nm. n = 3. Reproduced with permission from ref. 46. Copyright (2019) American Chemical Society.

around *ca.* 535 nm. Colocalization experiments provided support for the suggestion that **rTPONOO-1** could target mitochondria. Importantly, the cellular $ONOO^-$ levels could be monitored using a ratiometric response, since the ratio of $I_{718\,nm}/I_{535\,nm}$ decreased when the $ONOO^-$ concentration increased while the ratio of $I_{718\,nm}/I_{535\,nm}$ increased when the $ONOO^-$ concentration decreased. **rTPONOO-1** was used to monitor the levels of exogenous and endogenous $ONOO^-$ in live cells with good sensitivity and selectivity. Two-photo excitation of **rTPONOO-1** allowed the visualisation of $ONOO^-$ in bleomycin-induced pulmonary inflammation and pulmonary fibrosis in tissues taken from aminoguanidine hemisulfate (AG)-treated mice. As such, **rTPONOO-1** could have a role to play as a potential screening platform for anti-IPF drug candidates.

Recently, Yu and co-workers developed a mitochondria-targeted NIR fluorescent probe **Mito-Bor** for the study of pulmonary fibrosis (Fig. 33).[49] **Mito-Bor** consists of an aza-BODIPY NIR fluorophore, H_2O_2 responsive 4-phenylboronic acid pinacol ester and the mitochondrial targeting triphenylphosphonium cation unit. **Mito-Bor** was initially non-fluorescent. However, upon addition of H_2O_2, the fluorescence intensity at 730 nm increased with increasing H_2O_2 concentration (0–100 μM) in PBS buffer (10 mM, pH 7.4). Probe **Mito-Bor** exhibited high sensitivity (LOD = 23 nM) and excellent selectivity for H_2O_2 over other ROS, RNS and biologically relevant reactive species. Due to its low cytotoxicity, **Mito-Bor** was suitable for monitoring endogenous H_2O_2 in A549, PC9 lung cancer cells and H_2O_2 fluctuation in transforming growth factor β (TGF-β)-stimulated pulmonary fibrosis cell models.

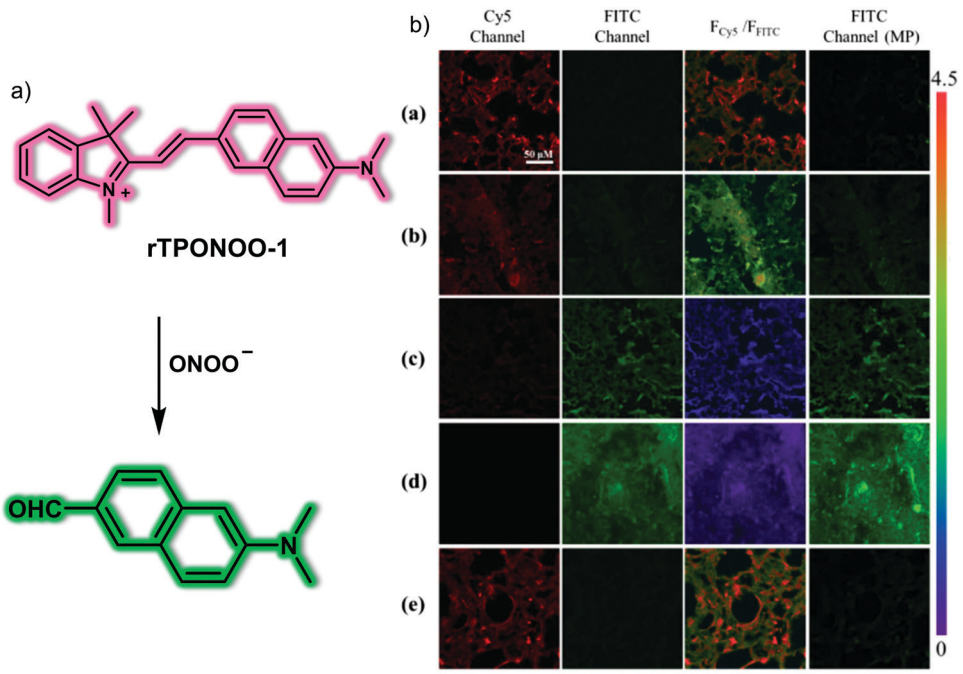

Fig. 32 (a) Chemical structure of the small molecule-based ratiometric two-photon probe **rTPONOO-1** and a schematic view of how it functions as a fluorescent sensor for $ONOO^-$. (b) *Ex vivo* fluorescent imaging of lung slices of healthy (a, sterile normal saline, 0.1 mL), bleomycin (b, bleomycin, 1 mg kg^{-1}, 0.1 mL; c, bleomycin, 2 mg kg^{-1}, 0.1 mL; d, bleomycin, 3 mg kg^{-1}, 0.1 mL)-induced pulmonary fibrosis mice and (e) bleomycin (3 mg kg^{-1}, 0.1 mL) followed by AG (20 mg kg^{-1})-treated mice following incubation of **rTPONOO-1** (50 μM, 0.1 mL). Cy5 channel, λ_{ex} = 488 nm; FITC channel, λ_{ex} = 405 nm; FITC channel (MP), λ_{ex} = 800 nm. Scale bar = 50 μm. Reproduced with permission from ref. 48. Copyright (2019) American Chemical Society.

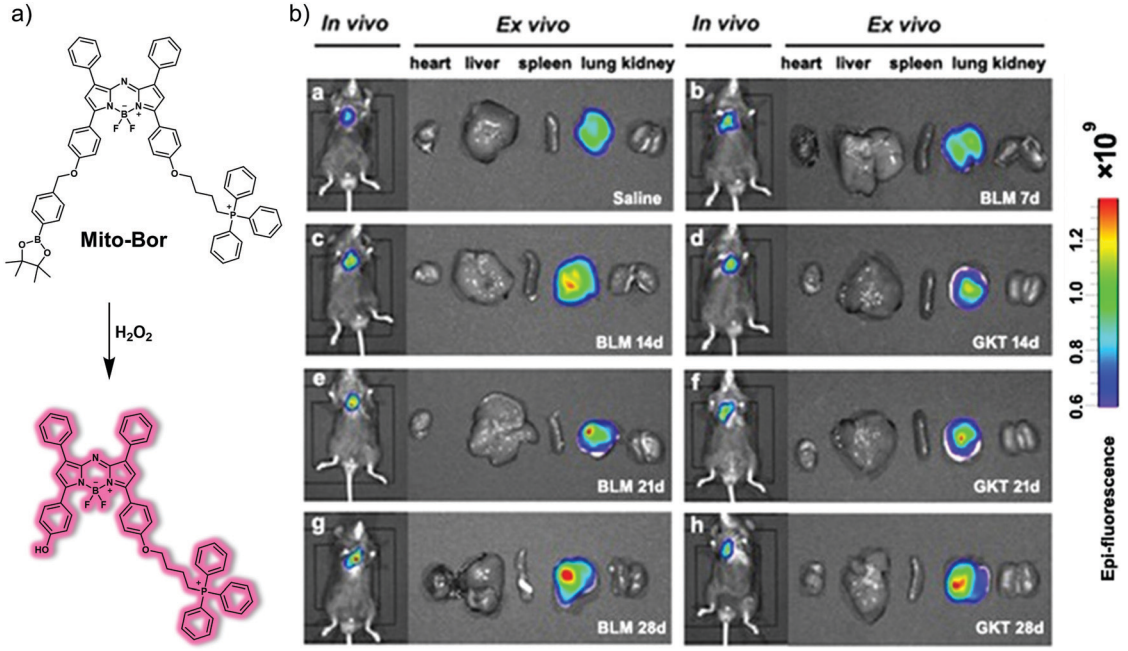

Fig. 33 (a) Chemical structure of small molecule-based NIR probe **Mito-Bor** and working model for the chemical changes that make it useful in the detection of H_2O_2. (b) *In vivo* and *ex vivo* fluorescent imaging of isolated organs of normal (a, saline), bleomycin (BLM, 5 mg kg^{-1}, b: 7 days; c: 14 days; e: 21 days; g: 28 days)-induced pulmonary fibrosis mice and BLM (5 mg kg^{-1}, 7 days) followed by GKT137831 (60 mg kg^{-1}, twice a week) -treated mice *via* gavage for (d) 14 days, (f) 21 days, and (h) 28 days, followed treated with the **Mito-Bor** (10 μM, 200 μL, in DMSO/saline = 1 : 99, v/v) *via* intratracheal spray. λ_{ex} = 710 nm, λ_{em} = 700–800 nm. Reproduced with permission from ref. 49. Copyright (2021) American Chemical Society.

Due to its favourable properties, **Mito-Bor** was used for the detection of H_2O_2 concentrations in bleomycin-induced pulmonary fibrosis mice models. The results indicated that the level of H_2O_2 increased with the degree of fibrosis in the mice; furthermore, **Mito-Bor** was capable of evaluating the therapeutic effects of NADPH oxidase 4 inhibitor (NOX4, results in H_2O_2 production) (GKT137831) in mice.

Glutamyl transpeptidase (GGT) plays an important role in maintaining the level of intracellular GSH in order to resist oxidative stress. As such, it can be considered as a surrogate marker for pathological states associated with oxidative stress. An improved ability to monitor GGT activity may thus lead to improvements in diagnosing pulmonary fibrosis. With such considerations in mind, Lv *et al.* developed a GGT-specific small molecule NIR probe, **Cy-GGT**, that permits the sensitive and rapid tracking of GGT levels.[50] This probe contains a heptamethine cyanine dye as the fluorophore and a γ-glutamyl group as the substrate for GGT (Fig. 34). **Cy-GGT** was shown to be highly selective for GGT with fast reaction kinetics being observed in HEPES buffer solution. It also proved capable of detecting GGT activity in TGF-β1-induced pulmonary fibrosis cell models. More importantly, **Cy-GGT** was able to visualize the changes in activity of GGT in a bleomycin-induced pulmonary fibrosis mouse model, thereby providing evidence for the putative relationship between GGT levels and the occurrence of pulmonary fibrosis.

Intracellular redox plays a key role in the progression of IPF. Glutathione *S*-transferases (GSTs) protect biological macromolecules from oxidative stress by reducing oxidation products. Among them, the Pi isoform of glutathione *S*-transferase (GSTP1) is mainly expressed in the lung and is responsible for *S*-glutathionylation, the conjugation of glutathione to reactive cysteines.[51] Thus, aberrant expression of GSTP1 may positively correlate with the degree of IPF. In addition, visualizing GSTP1 levels during IPF may improve our understanding of the pathogenic mechanisms of IPF. With this in mind, Lv *et al.* developed the first NIR fluorescent probe, **Cy-GST**, for the selective detection of the activity of GSTP1 *via* GST-catalyzed glutathionylation *in vitro* and *in vivo*, as well as in clinical samples (Fig. 35).[52] **Cy-GST** contains a 3,4-dinitrobenzoic acid as GSTP1 specific substrate and a benzo-heptamethine cyanine dye as the NIR fluorogenic reporter. **Cy-GST** was non-fluorescent in HEPES buffer (10 mM, pH 7.4) due to photoinduced electron transfer (PeT). However, upon the addition of GSTP1 and in the presence of GSH, the 3,4-dinitrobenzoic acid group of **Cy-GST** reacted with the sulfhydryl group to form a stable product, **Cy-GST-GSH**, that inhibits PeT and affords a turn-on NIR fluorescence emission at 810 nm. In addition, **Cy-GST** exhibited high selectivity toward GSTP1 over other isozymes of GSTP1 (*e.g.*, GSTA1, GSTM2) and other functional enzymes such as horseradish peroxidase and nitroreductase. **Cy-GST** was suitable for monitoring GSTP1 levels in IMR-90 and RLE-6TN cells, and the fluorescence signal was shown to be suppressed through the addition of the GST inhibitor, TLK117. **Cy-GST** was evaluated in a TGF-β1-induced pulmonary fibrosis cell model to evaluate changes in GSTs concentrations during pulmonary fibrosis. Subsequently, **Cy-GST** was used for the detection of GSTs level in bleomycin-induced pulmonary fibrosis mice models. The results indicated that the expression of GSTs was elevated in response to the degree of fibrosis. **Cy-GST** was shown suitable for *in vivo* therapeutic

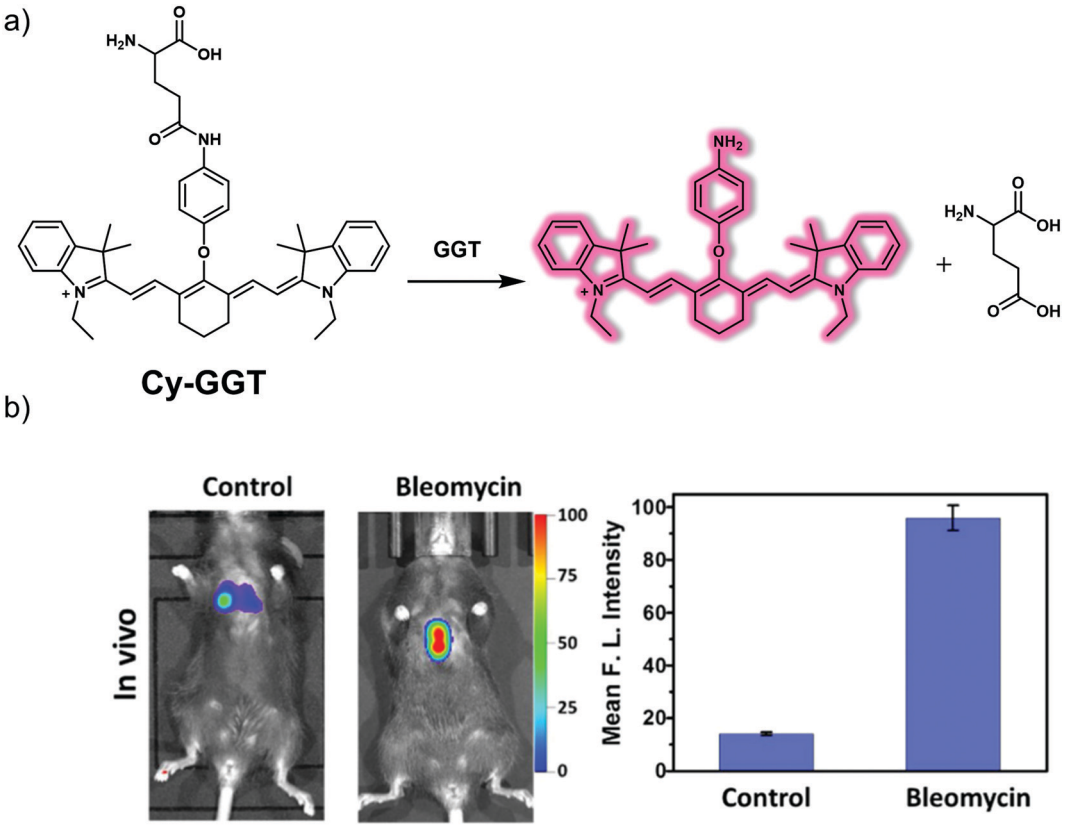

Fig. 34 (a) Chemical structure of the small molecule-based NIR probe **Cy-GGT** and the chemical transformation that is expected to make useful in the detection of glutamyl transpeptidase (GGT) levels. (b) *In vivo* fluorescence imaging and quantification of normal mice (control group) and bleomycin-induced pulmonary fibrosis mice (bleomycin group) recorded 30 min after **Cy-GGT** was intratracheally administered (100 μM, 50 μL in 1 : 99 DMSO/saline, v/v). λ_{ex} = 730 nm, λ_{em} = 750–800 nm. Data are presented as mean ± SD (n = 5). Reproduced with permission from ref. 50. Copyright (2020) Elsevier B.V.

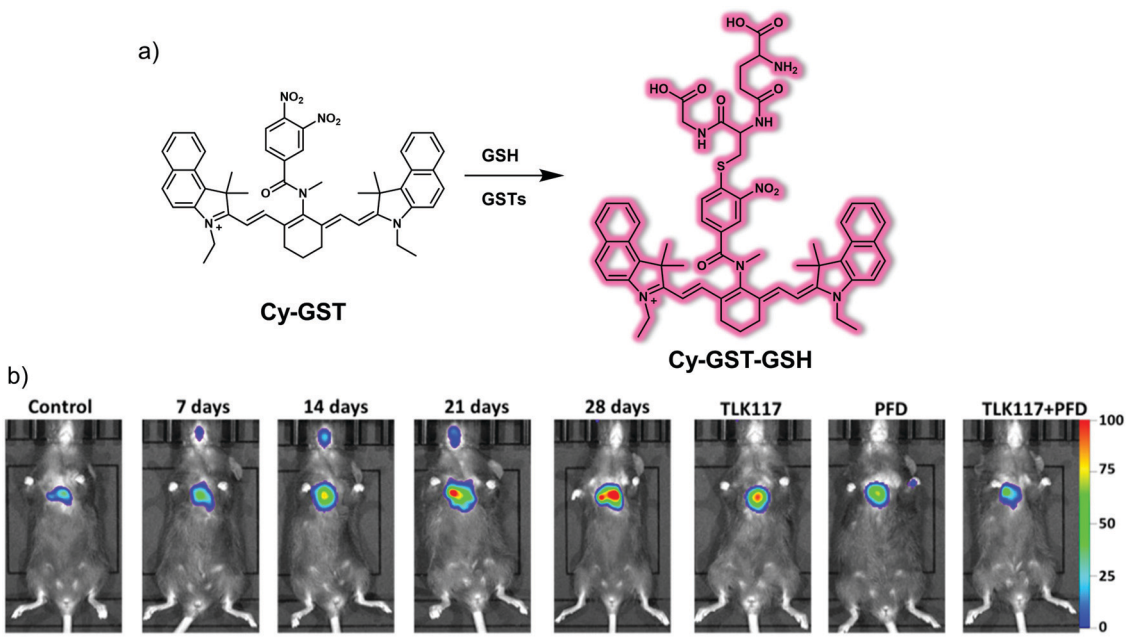

Fig. 35 (a) Chemical structure of the small molecule-based NIR probe **Cy-GST** and the proposed detection mechanism against GSTs. GSH = glutathione. (b) *In vivo* fluorescent imaging of normal (control), bleomycin (BLM, 5 mg kg^{-1}, 7–28 days)-induced pulmonary fibrosis mice and BLM (5 mg kg^{-1}, 28 days) followed by TLK117 (50 mg kg^{-1}, once every 3 days) or PFD (300 mg kg^{-1}, daily) or TLK117 + PFD simultaneously-treated mice *via* oral administration for 28 days, followed by incubation with the **Cy-GST** (100 μM, 50 μL in DMSO/saline = 1 : 99, v/v) *via* intratracheal administration. PFD = pirfenidone. λ_{ex} = 730 nm, λ_{em} = 800–850 nm. Reproduced with permission from ref. 52. Copyright (2019) American Chemical Society.

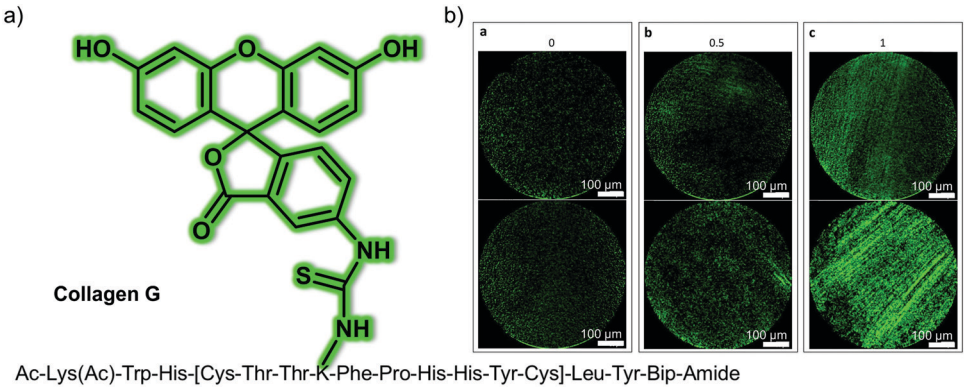

Fig. 36 (a) Chemical structure of small molecule peptide-based fluorescent probe **Collagen G** designed to target collagen and permit the imaging of pulmonary fibrosis. (b) Representative fluorescence endomicroscopic images of (a) 0: no fibers, (b) 0.5: faint appearance of fibers, to (c) 1: presence of fibers with **Collagen G** in the green channel (488 nm). Reproduced with permission from ref. 54. Copyright (2017) by the authors (J. R. Perez, N. Ybarra, F. Chagnon, M. Serban, G. Pare, O. Lesur, J. Seuntjens and I. E. Naqa). Published by Springer Nature.

evaluation of pirfenidone (PFD) and GSTs inhibitor (TLK117) in IPF mice models. In addition, **Cy-GST** was used to image GSTs concentrations in lung tissue samples from IPF patients. Like the fluorescence response *in vivo*, enhanced fluorescence was observed for the samples from IPF patients. This study indicated that **Cy-GST** could serve as a useful tool for assessing the involvement of GSTs in pulmonary fibrosis.

Collagen overexpression is a hallmark of pulmonary fibrosis.[53] Perez *et al.* developed a cyclic peptide-based fluorescent probe **Collagen G** that can selectively target collagen for intravital monitoring of fibrotic damage (Fig. 36).[54] **Collagen G** consisted of a collagen-specific cyclic peptide as the collagen-targeting group and fluorescein isothiocyanate (FITC) as the reporter unit, respectively. **Collagen G** exhibited good binding towards collagen at 1 μM concentrations *in vitro*. Moreover, **Collagen G** was used for the intravital imaging of collagen fibers in radiation-induced pulmonary fibrosis (RIPF) rats using fluorescence endomicroscopy (FE). Interestingly, the results were consistent with the clinically used imaging technique, computed tomography (CT). Both FE and CT imaging could detect distinct differences in lung fibrosis status between normal and RIPF rats. *Ex vivo* lung staining experiments revealed **Collagen G** was less sensitive than collagen binding antibody, and although this does not limit the usefulness of **Collagen G** for intravital imaging of collagen overproduction *in vivo*, the development of more sensitive collagen probes is warranted.

Lysyl oxidase (LOX) is responsible for the cross-linking of collagen found in the extracellular matrix. This enzyme is known to be overexpressed during the development of pulmonary fibrosis and because of this, it is seen as a potential therapeutic target for pulmonary fibrosis. Dhaliwal *et al.* developed a small molecule-based fluorescent probe, **oLOX 1** for monitoring LOX activity and the visualisation of pulmonary fibrosis (Fig. 37).[55] **oLOX 1** consists

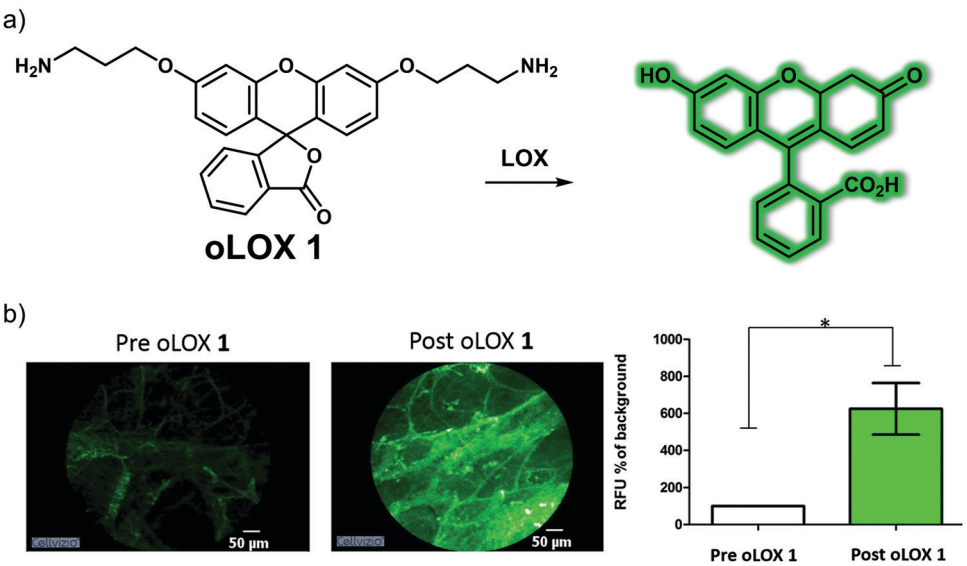

Fig. 37 (a) Chemical structure of the small molecule-based probe **oLOX 1** and the proposed detection mechanism for LOX. (b) Fluorescence imaging of LOX activity and its quantification in fibrotic ventilating *ex vivo* asinine lung treated with **oLOX 1** (200 μM, 1 mL, in PBS buffer). *p = 0.0313, Wilcoxon signed rank test, n = 3. Scale bar = 50 μm. Reproduced with permission from ref. 55. Copyright (2015) The Royal Society of Chemistry.

of a fluorescein scaffold functionalised with LOX-responsive groups. **oLOX 1** displayed a maximum emission peak at 520 nm and responded to LOX in aged human lung tissue homogenate (LOX-positive) with a 300% enhancement in fluorescence intensity. This fluorescence response could be inhibited by pre-incubation with LOX inhibitor, β-Aminopropionitrile (BAPN). **oLOX 1** was then used for imaging LOX activity in *ex vivo* human lung tissue using fibred confocal fluorescence microscopy (FCFM). However, the fluorescence intensity of **oLOX 1** in human lung tissue treated with BAPN did not increase, confirming the specificity of **oLOX 1** for LOX. More importantly, **oLOX 1** could detect LOX activity in a fibrotic ventilating *ex vivo* asinine lung model *via* FCFM.

6.4 Small molecule-based fluorescent probes for lung cancer

Lung cancer is the most fatal malignant tumour in the world. About 85% of the diagnoses are smoking related. Symptoms include cough, chest discomfort or chest pain, weight loss and, less commonly, hemoptysis. However, many patients do not have any clinical symptoms even after suffering from metastases. The prognosis for patients with lung cancer remains poor, with only 15% of patients surviving for more than 5 years from the point of initial diagnosis. In patients with stage IV (metastasis), the 5-year overall survival rate is under 1%. At present, chest X-rays or CT scans are used for initial screening, but a biopsy is needed to confirm the actual diagnosis. Compared with biopsy-based detection, small molecule-based fluorescent probes could offer advantages, including being less invasive and potentially easier to implement in a clinical setting.

Cysteine (Cys) is an important biothiol whose abnormal expression is closely associated with the development of many diseases. For instance, in lung cancer cells Cys levels are much higher than in normal cells. Cys has thus been explored as a biomarker for lung cancer in the context of fluorescent probe development. Chen *et al.* developed a colorimetric and ratiometric mitochondria-targeting NIR fluorescent probe, **Cy-OAcr**, based on a ketone cyanine that was found to permit Cys sensing in living cells and in orthotopic lung cancer murine models (Fig. 38).[56] This probe benefited from a fluorescence selective turn-on mechanism that was ascribed to an intramolecular cyclisation of an α,β-unsaturated acrylate (Acr) with Cys, a transformation that does not occur readily with other biothiols or analytes. **Cy-OAcr** reacts rapidly with Cys to generate the product **Keto-Cy**. This transformation is accompanied by a colour change from green to red. Upon the addition of Cys, the fluorescence intensity at 794 nm is significantly quenched while a strong NIR fluorescence peak at 635 nm appears upon excitation at 505 nm. Cell imaging experiments revealed that **Cy-OAcr** may be used for monitoring endogenously produced mitochondrial Cys in A549, H1650 and PC9 cells. In addition, **Cy-OAcr** was used for monitoring Cys fluctuations in three tumour-bearing mice and urethane-stimulated orthotopic lung cancer mice. The results illustrate the potential of **Cy-OAcr** for monitoring the progression of lung cancer and serve to underscore that this probe could serve as a new tool for the further development and study of lung cancer mouse models.

NAD(P)H quinone oxidoreductase 1 (NQO1) is an intracellular protective reductase, which plays an important role in promoting metabolic detoxification. It can catalyse the reduction of quinones to protect cells from oxidative stress and ensure the normal physiological function at the whole-body level. NQO1 is overexpressed in several solid tumours, including carcinomas. Accordingly, fluorescence imaging of NQO1 can potentially aid in the diagnosis of lung cancer. In 2019, the Srivenugopal group reported a turn-on NIR fluorescent probe (**NIR-ASM**) based on

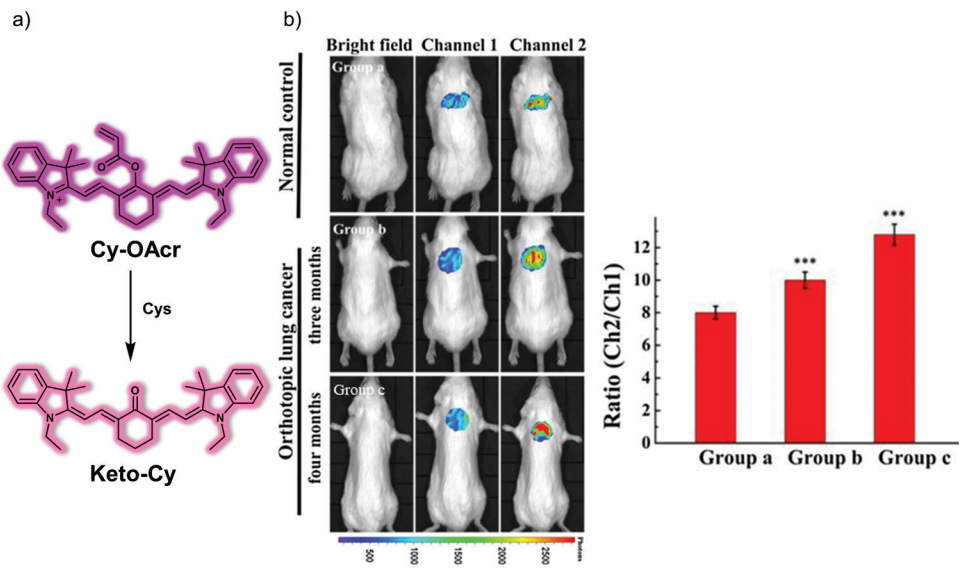

Fig. 38 (a) Chemical structure of the small molecule-based ratiometric NIR probe **Cy-OAcr** and suggested chemical basis for its ability to act as a chemosensor for Cys. (b) *In vivo* fluorescence imaging of Cys and its quantification in normal mice and urethane-stimulated orthotopic lung cancer mice treated with **Cy-OAcr** (10 μM, 200 μL, in DMSO : saline = 1 : 99, v/v) through tracheal spray. Channel 1: λ_{ex} = 740 nm, λ_{em} = 750–830 nm. Channel 2: λ_{ex} = 520 nm, λ_{em} = 580–660 nm. The data are shown as mean (±s.d.) (n = 7). ***$p < 0.001$. Reproduced with permission from ref. 56. Copyright (2019) Elsevier B.V.

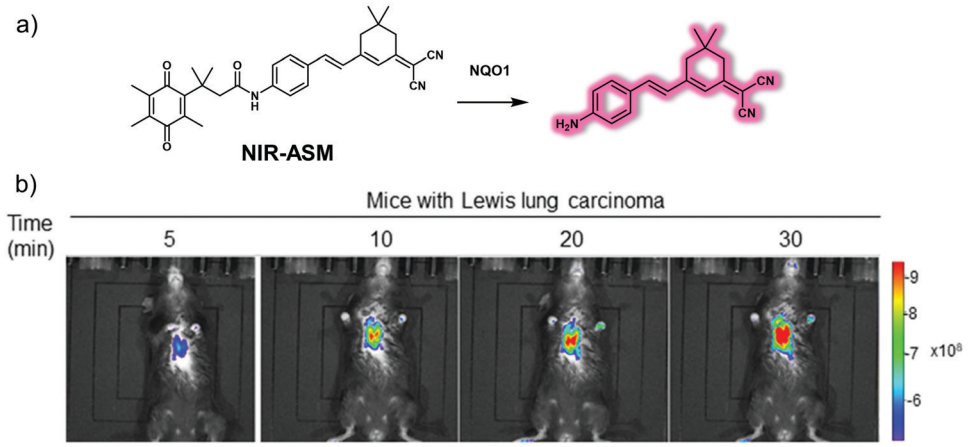

Fig. 39 (a) Chemical structure of the small molecule-based turn-on NIR probe **NIR-ASM** and its proposed mode of action as a chemosensor for NQO1 activity. (b) *In vivo* real-time fluorescence imaging in Lewis lung carcinoma (LLC)-bearing BALB/c57 mice after intravenous administration of **NIR-ASM** (5 mg kg^{-1}, 50 μL). λ_{ex} = 500 nm, λ_{em} = 640 nm. Reproduced with permission from ref. 57. Copyright (2019) by the authors (S. R. Punganuru, H. R. Madala, V. Arutla, R. Zhang and K. S. Srivenugopal). Published by Springer Nature.

the dicyanoisophorone (ASM) fluorophore and quinone propionic acid (QPA) in an effort to monitor the activity of NQO1 and diagnose non-invasively lung cancer (Fig. 39).[57] Reaction with NQO1 in the presence of NADH, results in a significant increase in the fluorescence intensity of **NIR-ASM** in PBS buffer. The proposed mode of action involves cleavage of the amide bond, which triggers the spontaneous release of strong fluorescent dicyanoisophorone (ASM). **NIR-ASM** exhibits excellent selectivity for NQO1 in solution, as well as good biocompatibility in several cell lines and *in vivo*. Accordingly, **NIR-ASM** was used to detect the activity of NQO1 in the presence and absence of an NQO1 inhibitor (ES936). An obvious decrease in the fluorescence of probe **NIR-ASM** was observed when NQO1-positive cells (A549 and H460) were treated with ES936. **NIR-ASM** was able to detect NQO1 activity in tumour-bearing nude mice, as well as in an orthotopic lung cancer model (Lewis lung carcinoma (LLC) bearing mice). This study serves as an excellent demonstration of the potential of ASM-based probes for monitoring changes in NQO1 activity *in vitro* and *in vivo*. Ultimately, probes such as **NIR-ASM** could permit non-invasive diagnoses of lung cancer.

7. Small molecule-based fluorescent probes for gastrointestinal (stomach and intestine) disease

The stomach is a cavernous organ, located in the upper abdomen; it is where ingested food is temporarily stored. It carries out some digestion but provides essentially no absorptive function. The intestines, lying between the stomach and the anus, are responsible for the absorption of nutrients from food and is where most chemical digestion occurs. The intestinal organs are divided into two main parts: the small intestine (duodenum, jejunum and ileum) and the large intestine (cecum, colon and rectum). A large amount of digestion and absorption of almost all digestive products takes place in the small intestine, while the large intestine mainly concentrates food residues and forms faeces, which are then excreted through the rectum *via* the anus. Genetic disorders, unhealthy lifestyles, bacterial or viral infections can lead to gastrointestinal disease.[58,59] This section will summarise some representative small molecule-based fluorescent probes for imaging gastrointestinal disease (*e.g.*, colitis, colorectal/colon cancer, and gastric cancer).

7.1 Small molecule-based fluorescent probes for colitis

Colitis is a chronic inflammatory bowel disease caused by inflammation and ulceration of the colon or rectum. The main symptoms during colitis include abdominal pain, diarrhoea, weight loss, fever, and anaemia. Conventional diagnoses for colitis involve colonoscopy and tissue biopsy. Receptor-targeted fluorescent probes represent an alternative chemical-based strategy that relies on detecting abnormal expression of biomarkers. In 2017, Zhu *et al.* designed and synthesized the first NIR fluorescent probe, **DCM–KPV**, designed to facilitate the *in vivo* visualisation and assessment of ulcerative colitis by targeting the oligopeptide transporter PepT1, which is overexpressed in chronic ulcerative colitis.[60] **DCM–KPV** consisted of a NIR donor–π–acceptor (D–π–A)-based dicyanomethylene-4*H*-pyran (DCM) dye, as well as a tripeptide KPV (Lys-Pro-Val) subunit to serve as a targeting moiety for the PepT1 receptor (Fig. 40). This probe exhibits excellent photophysical properties, such as high brightness, good stability, a low propensity towards photobleaching, emission in the NIR region, and low inherent cytotoxicity. It was thus suggested that **DCM–KPV** could be used for the visualisation of cells or employed *in vivo*. Cell imaging results served to confirm that **DCM–KPV** possesses good cell permeability in the case of PepT1-overexpressed cells. Furthermore, **DCM–KPV** enabled the rapid discrimination between chronic and acute ulcerative colitis *in vivo*, presumably as the result of its ability to serve as a fluorescence marker for PepT1.

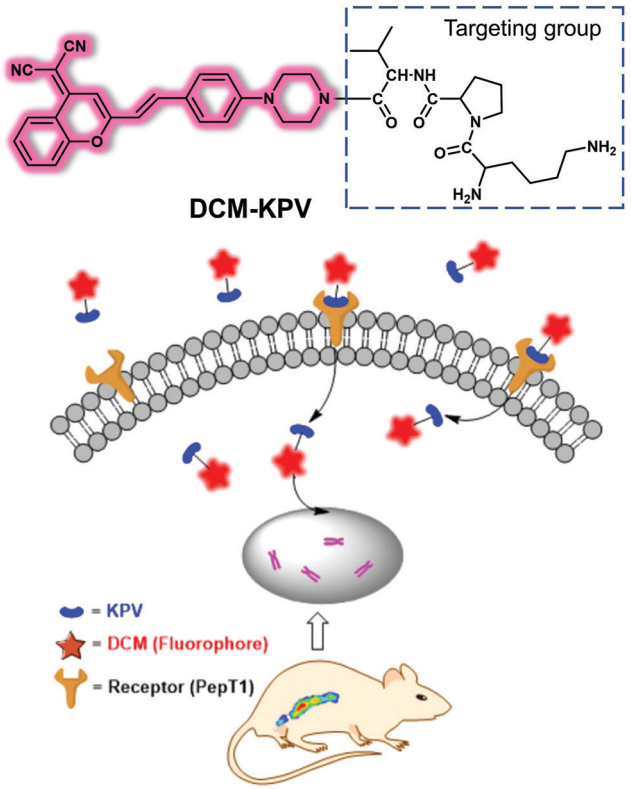

Fig. 40 Diagrammatic sketch showing the mechanism proposed for the receptor-targeted activation of **DCM–KPV**. Reproduced with permission from ref. 60. Copyright (2017) American Chemical Society.

7.2 Small molecule-based fluorescent probes for colorectal/colon cancer

Colorectal/colon cancer is the third most common cancer in men and the second most common cancer in women worldwide, occurring mainly in the mucosa of the large intestine (colon) and rectum. Colon cancer is usually diagnosed by colonoscopy. The development of appropriate small molecule-based fluorescent probes could make routine diagnoses of colon cancer more facile and less invasive. This could translate into improvements in public health.

Ling *et al.* developed a series of fluorescent theranostic probes, **HJTA** and **HJTB**, for the combined fluorescence diagnosis and chemotherapeutic treatment of colon cancer. These systems rely on targeting both pH and GSH within the tumour microenvironment.[61] As shown in Fig. 41, a pH-responsive fluorophore, the natural product 3-amino-β-carboline that exhibits anti-tumor properties, was tethered to one or two GSH-responsive (6-oxocyclohex-1-en-1-yl)methyl (*E*)-but-2-enoate (COMC-6) Michael acceptors to give **HJTA** and **HJTB**. Reaction with GSH catalysed by glutathione *S*-transferase π (GSTπ) that is overexpressed in various tumour cells leads to formation of a covalently bound adduct that can react further with sulfhydryl groups present in a variety of tumour proteins to produce an anti-tumour effect (Fig. 31). Both probes exhibited good fluorescence response to pH (from 3.0 to 7.0); however, the fluorescence intensity and response rate of **HJTA** to GSH was superior to that of **HJTB**. **HJTA** exhibited excellent fluorescence selectivity for GSH and cell imaging results indicated that **HJTA** is rapidly taken up by GSH-rich cancer cells and targets the low pH environment of lysosomes. These cellular localisation features allowed cancer cells to be distinguished from normal cells. **HJTA** exhibited a relatively low IC_{50} against cancer *in vitro* as compared to its formal constituents COMC-6 or 3-amino-β-carboline. More importantly, it was found that **HJTA** could be used as a fluorescent indicator for the image-guided resection of orthotopic HT29/Luc colon cancer lesions and that it exhibited antitumor activity against HT29 tumour-bearing mice *in vivo* by inducing apoptosis and autophagy.

7.3 Small molecule-based fluorescent probes for gastric cancer

Gastric cancer is the second leading cause of cancer-related death and refers to cancer that occurs in the mucous membrane of the stomach. Early gastric cancer is not easily detected because its symptoms are not obvious. Most patients diagnosed with gastric cancer have already deteriorated to an intermediate or advanced stage by the time the disease is detected. Gastroscopy is a common medical diagnosis for gastric cancer, but it is invasive and causes significant pain to the patients. Therefore, it is important to develop a simple, efficient, and non-invasive diagnostic methods for the early diagnosis of gastric cancer.

Chen *et al.* designed a matrix metalloproteinase-2 (MMP-2)-activatable fluorescent probe (**Dab-GPLGVRGY-FITC**), which facilitated the rapid and accurate diagnosis of gastric cancer.[62] MMP-2 is a biomarker whose presence has been correlated with the occurrence, invasion and metastasis of cancer; it is thus considered to be a prognostic indicator of gastric cancer. To prepare **Dab-GPLGVRGY-FITC**, a known peptide substrate (GPLGVRGY) for MMP-2, was labelled with a FITC donor/DABCYL acceptor FRET pair (Fig. 42). As prepared, **Dab-GPLGVRGY-FITC** proved nonfluorescent, a feature ascribed to the proximity between the DABCYL and FITC moieties, which leads to FRET-based of the FITC emission. When the probe interacts with MMP-2, peptide cleavage occurs. This precludes effective FRET and results in an increased FITC donor emission. Using **Dab-GPLGVRGY-FITC**, it was possible to monitor the activity of MMP-2 in gastric carcinoma MGC-803 cells, while the addition of an MMP-2 inhibitor served to quench the fluorescence. **Dab-GPLGVRGY-FITC** proved capable of detecting MMP-2 activity in MGC-803 tumour-bearing mice when administered *via* tail vein injection. Importantly, **Dab-GPLGVRGY-FITC** could be used to distinguish clinical gastric cancer tissues from gastritis tissues and do so rapidly by monitoring the MMP-2 activity.

Another commonly used method for tumour imaging is to target biomarkers on the surface of cancer cells with ligand-modified fluorophores. To improve the binding efficiency of fluorescent probes sensitive to biomarkers and thus the efficacy of tumour detection, Wang *et al.* combined an active targeting approach with bioorthogonal chemical reactions. This strategy was embodied in the form of a small molecule-based copper-free click-type fluorescent system that permitted the prolonged and enhanced targeted bioimaging of gastric cancer cells.[63] Specifically, the NIR fluorophore Cy 5.5 was covalently conjugated to the

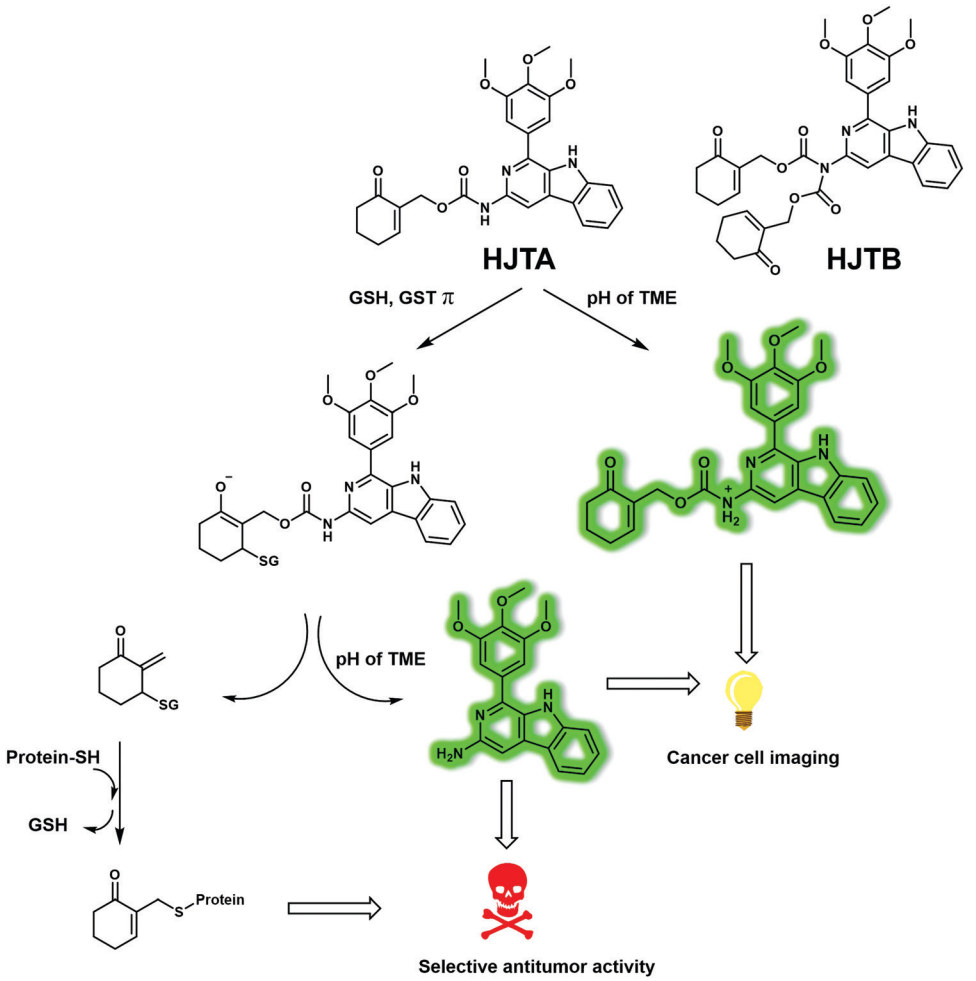

Fig. 41 Schematic illustration of the activation of the orthotopic HT29/Luc colon/HT29 colon xenograft tumour-targeting and pH- and GSH/GSTπ-dependent probes **HJTA** and **HJTB**. TME = tumour microenvironment. GSTπ = glutathione *S*-transferase π.

targeting peptide (GEBP11) by means of a *trans*-cyclooctene (TCO) and tetrazine (Tz) Diels–Alder cycloaddition (Fig. 43). Gastric cancer cells were treated with GEBP11-TCO, followed by Tz conjugated to Cy5.5 (**Cy5.5-Tz**), a sequence that permitted the fluorescent labelling of cells overexpressing the GEBP11 peptide receptor. Compared to the directly conjugated probe **GEBP11-Cy5.5** or a mixture of the unreactive control system **GEBP11** and **Cy5.5-Tz**, the fluorescent probe produced from the reaction of **GEBP11-TCO** with **Cy5.5-Tz** exhibited a higher affinity towards the GEBP11 peptide receptor. It was thus able to target gastric cancer cells and do so rapidly. In addition, *in vivo* experiments involving mouse models revealed that the click fluorescent probe has a high tumour specificity, gives rise to an easily monitored fluorescent response, and displays a prolonged gastric cancer tumour targeting capability.

8. Small molecule-based fluorescent probes for heart disease

The heart is the main organ in the circulatory system and located in the middle left of the mediastinal cavity of the chest. Its sole function is to promote the circulation of blood to allow oxygen and nutrients to reach all parts of body, and help the body remove metabolic waste. Heart disease can be caused by a variety of factors, including high blood pressure, convulsion, diabetes, lack of exercise, obesity, hyperlipidemia, poor diet and genetic abnormalities.[64,65] In this section, some representative small molecule-based fluorescent probes for imaging heart disease (myocardial fibrosis, drug-induced cardiotoxicity) will be summarised.

8.1 Small molecule-based fluorescent probes for myocardial fibrosis

Myocardial fibrosis (MF) is characterized by proliferation of fibroblasts and excessive accumulation of extracellular matrix, as well as a significant increase in the collagen of cardiac tissue. MF is a key indicator for cardiovascular disease. An excessive accumulation of inducible nitric oxide synthase (iNOS) plays a key role in the development of myocardial fibrosis and is known to induce nitric oxide (NO) production in cardiac fibroblasts. As such, the real-time monitoring of NO during MF could lead to an improved understanding of the disease.

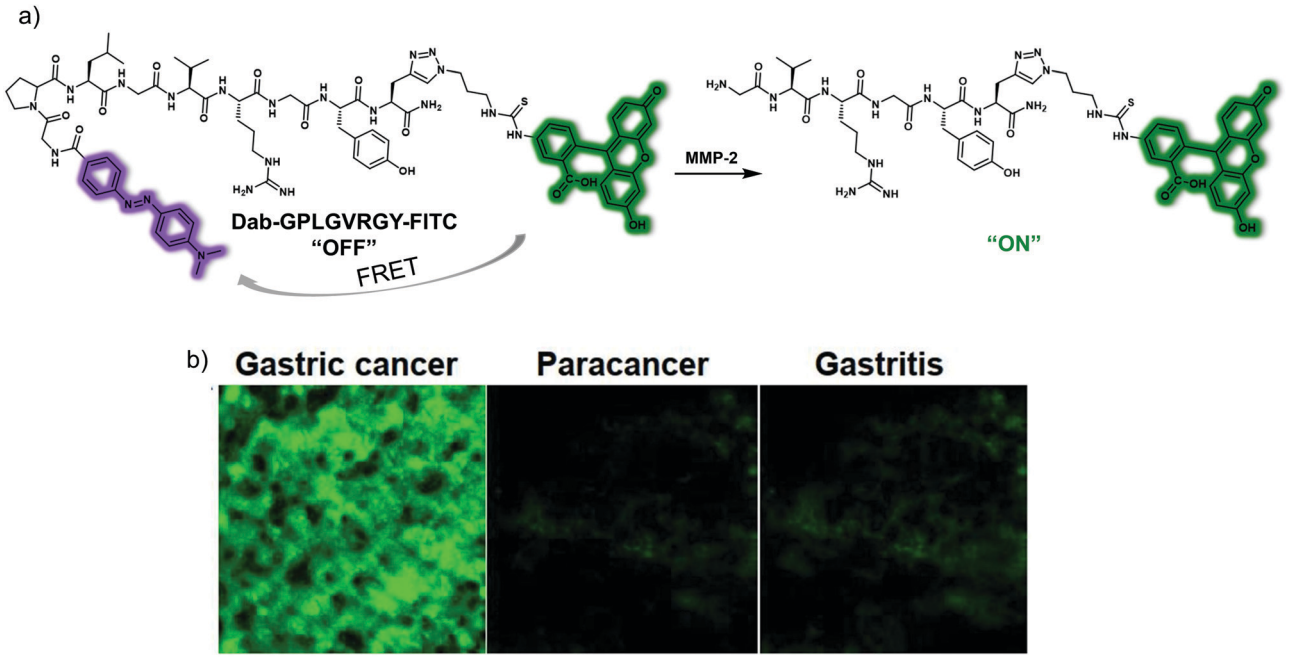

Fig. 42 (a) Schematic illustration of **Dab-GPLGVRGY-FITC**, a probe that permits detection of MMP-2 activity based on the substrate triggered release of an active fluorophore. (b) *Ex vivo* fluorescent imaging of clinical gastritis, paracancer and gastric cancer tissues cryosection after incubated with **Dab-GPLGVRGY-FITC** (2 μM). Reproduced with permission from ref. 62. Copyright (2019) The Royal Society of Chemistry.

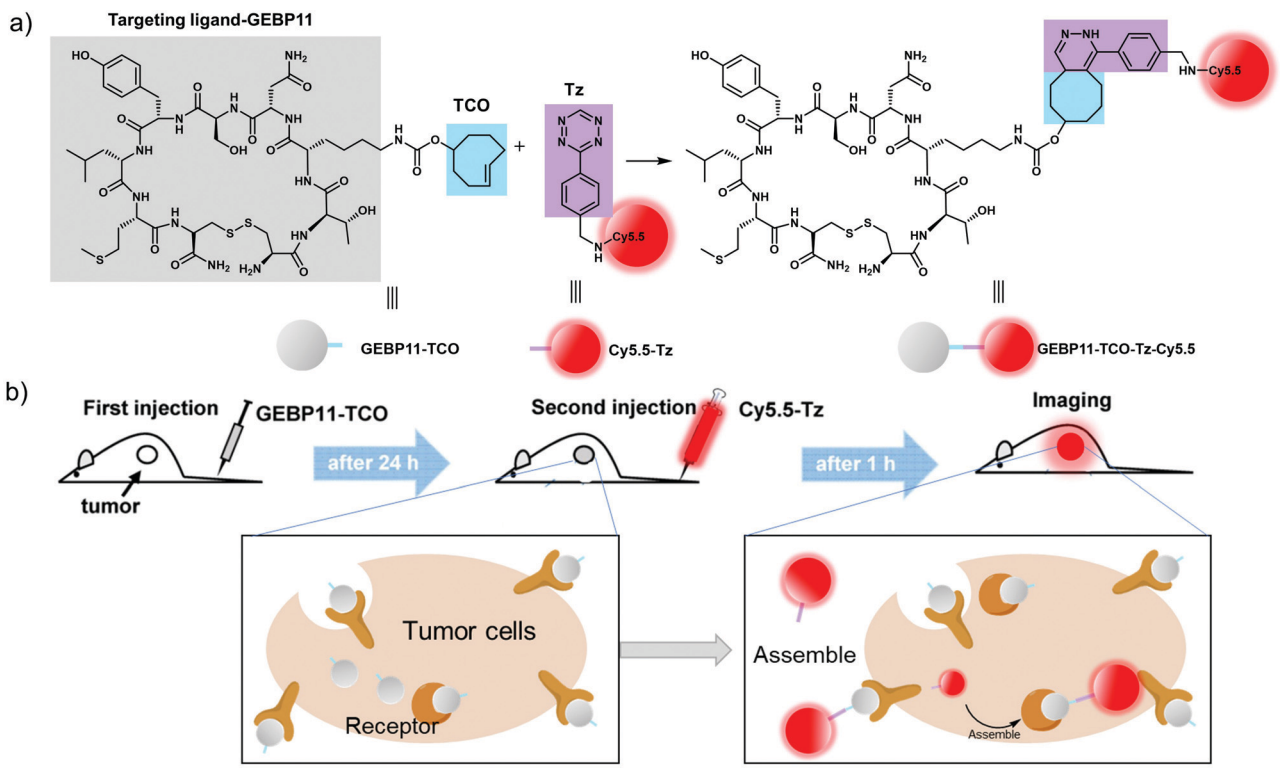

Fig. 43 Schematic illustration of the construction of a fluorescent probe that permits *in vivo* imaging of human tumour xenograft mouse models and which relies on the judicious use of a Click-type coupling strategy (a) Bioorthogonal inverse electron-demand Diels–Alder reaction between GEBP11-TCO and Cy5.5-Tz. Colour code: blue, the trans-cyclooctene group (TCO); purple, the tetrazine group (Tz); grey, the vascular homing targeting peptide GEBP11; red, NIR fluorophore Cy5.5. (b) Mice are treated first with GEBP11-TCO and then with Cy5.5-Tz. Reproduced with permission from ref. 63. Copyright (2017) Published by Ivyspring International Publisher.

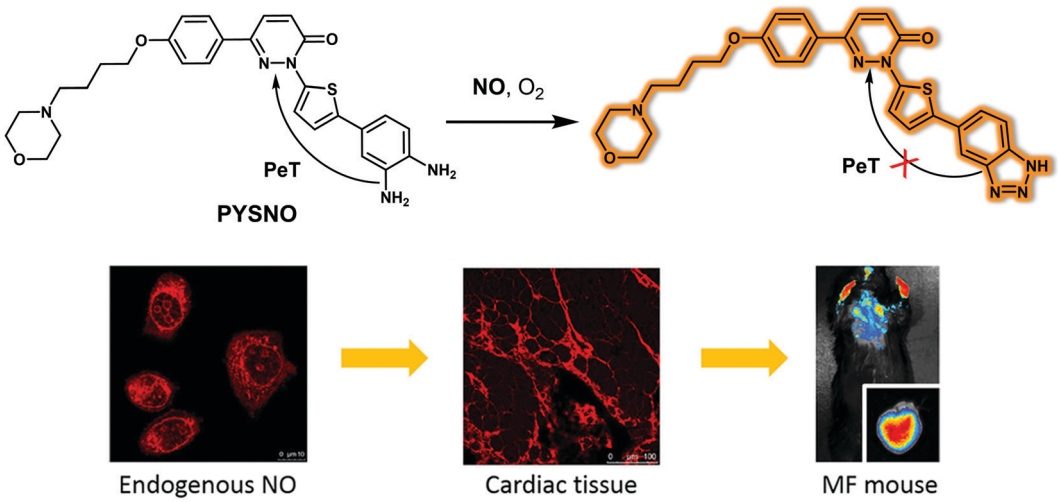

Fig. 44 Chemical structure of small molecule-based fluorescent probe **PYSNO** and the reaction-based conversion that makes it effective as a probe for NO as judged from studies carried out in an isoproterenol (ISO)-induced MF mouse model. Reproduced with permission from ref. 66. Copyright (2020) American Chemical Society.

Xu *et al.* designed a small molecule-based fluorescent probe, **PYSNO**, that permits the selective recognition of NO.[66] They used pyridazinone as a fluorescence unit, *o*-phenylenediamine as the recognition group for NO, and an alkyl morpholine as the lysosome-targeting moiety (Fig. 44). In addition, a thiophene group was used to extend the π-conjugation pathway and shift the optical transitions to the red. The fluorescence intensity of **PYSNO** at 548 nm is weak. However, in the presence of excess NO a strong enhancement in the fluorescence signal centred around 548 nm is seen. This enhancement was ascribed to the reaction between the *o*-phenylenediamine and NO. The limit of detection of **PYSNO** was determined to be approximately 240 nM with good selectivity for NO being observed. Co-localisation experiments with Lyso-Tracker® Red revealed that **PYSNO** was localized in the lysosomes after cells were exposed to with NO for 30 min. **PYSNO** proved effective for the detection of NO in cellular and mouse heart tissues of an isoproterenol (ISO)-induced MF model. *In vivo* fluorescence bioimaging results revealed no appreciable fluorescence response when normal mice were treated with **PYSNO**. On the other hand, a fluorescence response was readily discernible when MF mice were subject to treatment with **PYSNO**. These results provide support for the contention that **PYSNO** could emerge as a useful tool for evaluating the role of NO in cellular environments and *in vivo* during physiological and pathological processes.

8.2 Small molecule-based fluorescent probes for drug-induced cardiotoxicity

The discovery of drugs such as anthracycline antineoplastic drugs has brought hope for the treatment of cancer patients. However, these agents are plagued by side effects, including cardiotoxicity. In the clinic, these side effects are manifested by such symptoms as arrhythmias, blood pressure changes, and myocardial damage. Cardiotoxicity caused by anthracyclines is often progressive and irreversible. Therefore, the early monitoring and prevention of anthracycline-induced cardiotoxicity is important to improve patient outcomes. The mechanism of drug-induced cardiotoxicity is believed to originate with oxidative stress within cardiomyocytes that can be traced to the accumulation of large amounts of ROS. The real-time, non-destructive monitoring of ROS production could thus prove useful in terms of disease management. $ONOO^-$ contributes to oxidative and nitrative stress. Its overexpression induces mitochondrial damage and apoptosis, thus playing an important role in the pathogenesis of anthracycline-induced cardiotoxicity. Using **TPNIR-NH2** as the fluorophore and mitochondria-targeting unit, in 2018 the group of Tang reported the mitochondria-targeting probe **TPNIR-FP** suitable for two-photon imaging and NIR emission. This probe permitted both the *in vitro* and *in vivo* detection of $ONOO^-$ in drug-induced cardiotoxicity mouse models (Fig. 45).[67] The α-ketoamide group of **TPNIR-FP** acts as the $ONOO^-$-recognition site. Imaging results obtained using live cardiomyocytes and mouse heart slices served to confirm that $ONOO^-$ is overexpressed in anthracycline (doxorubicin or epirubicin)-treated cardiomyocytes and cardiotoxicity mouse heart slices. These results provide support for the notion that increased levels of $ONOO^-$ correlate with the progression of anthracycline-induced cardiotoxicity. This work could provide a new chemical tool that in due course could allow for the early diagnosis and efficient treatment of drug-induced cardiotoxicity.

9. Conclusion and outlook

Various organs within the human body work in synergy to ensure the normal and efficient functioning of the body, and when they are damaged or diseased reduction in function and even death can result. Therefore, monitoring the onset and progression of diseases related to major organs, as well as differentiating acute and chronic forms of the same diseases, is beneficial. This is true not only in terms of fundamental biological research, but also

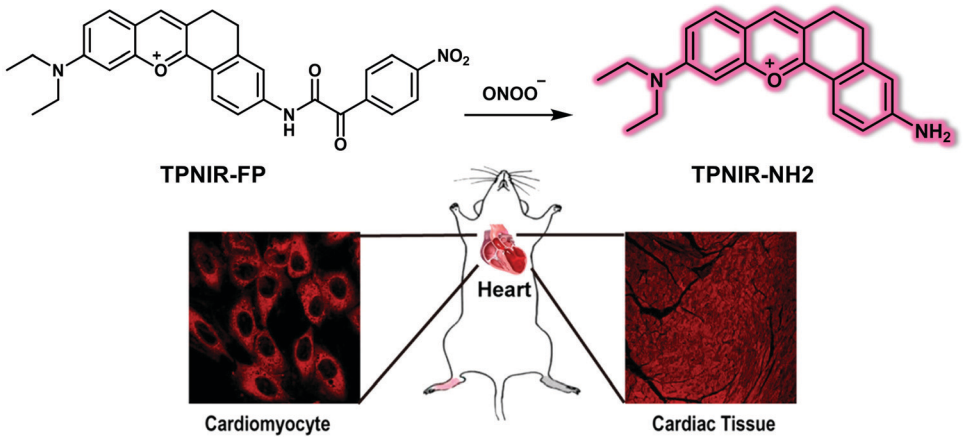

Fig. 45 Chemical structure of the small molecule-based two-photon fluorescent probe **TPNIR-FP** and the chemical conversion that is proposed as making it useful for the detection of $ONOO^-$ in anthracycline-induced cardiotoxicity mouse models. Reproduced with permission from ref. 67. Copyright (2018) American Chemical Society.

potentially in the context of clinical diagnosis and treatment of organ diseases. To date, significant progress has been made in the development of small molecule-based fluorescent probes that permit real-time detection and study of organ disease. These small-molecule fluorescent probes have been designed to target or respond to biomarkers that are abnormally expressed in specific organ diseases. Many probes target organs according to the specific characteristics of the different organs and are activated by specific pathogenic biomarkers. This specificity aids accurate disease monitoring within the organs of interest. Some probes have dual response properties, meaning that different fluorescence signals or optical signals are produced in response to specific bioanalytes that are often uniquely correlated at different stages of disease progression. This has allowed the monitoring and tracing of different disease stages using a single probe. Moreover, due to the deep seated nature of organ disease, most small molecule-based fluorescent probes have been designed to exhibit near-infrared fluorescence emission or possess two-photon absorption and imaging properties, features that can reduce the interference from the background and provide high-precision imaging of deep tissues or organs. More broadly, work in the area is advancing the development of small molecule-based fluorescent probes for clinical diagnosis.

Despite the exciting progress made in the development of small molecule-based fluorescent probes for the study of organ disease, there are still some unresolved challenges to overcome. Firstly, most fluorescent probes are essentially monochromatic, and such probes are susceptible to interference from external factors. Moreover, most of the fluorescent probes reported to date lack organ-targeting components and reach the diseased organs through nonspecific blood transport in response to abnormally expressed bioactive components; this reduces potentially the benefit associated with monitoring the diseased organs. On the other hand, because of the deep tissue depth of some organs, fluorescent probes that exhibit good tissue penetration and high spatial resolution are likely to see the greatest application. Most of the fluorescent probes reported to date rely on fluorescent reporter groups that absorb and emit in the NIR I region or visible light range.[68] This limits their utility in terms of studying organ diseases. On the other hand, the development of small molecule-based fluorescent probes with higher emission wavelengths (near-infrared region II band) are expected to facilitate the development of systems suitable for monitoring deep-set organ-related diseases. However, obtaining such systems remains a challenge. It is thus a truism that the dream of creating small molecule-based fluorescent probes that can be used routinely to diagnose and monitor clinical diseases remains largely unfulfilled. As such, it is hoped that the current summary of the design and response mechanisms being used to create new probes will set the stage for future advances.

Abbreviations

AβOs	Aβ oligomers
AChE	Acetylcholinesterase
AD	Alzheimer's disease
AG	Aminoguanidine hemisulfate
AIE	Aggregation-induced emission
AKI	Acute kidney injury
ALI	Acute lung injury
ALP	Alkaline phosphatase
AMs	Alveolar macrophages
a-PeT	Acceptor-photoinduced electron transfer
ARDS	Acute respiratory distress syndrome
ARF	Acute renal failure
ASGPR	Asialoglycoprotein receptor
ASM	Dicyanoisophorone
BAPN	β-Aminopropionitrile
BBB	Blood–brain barrier
casp3	Caspase-3
CT	Computed tomography
Cys	Cysteine

DCM	Dicyanomethylene-4*H*-pyran
DH	Dihydroxanthene
DILI	Drug-induced liver injury
DTT	dithiothreitol
DTZ	Diatrizoate
D–π–A	Donor–π–acceptor
ECM	Extracellular matrix
ELISA	Enzyme-linked immunosorbent assay
ESIPT	Excited-state intramolecular proton transfer
FAD	Flavin adenine dinucleotide
FCFM	Fibred confocal fluorescence microscopy
FE	Fluorescence endomicroscopy
FITC	Fluorescein isothiocyanate
GGT	Glutamyl transpeptidase
GPC-3	Glypican-3
GSTP1	The Pi isoform of glutathione *S*-transferase
GSTs	Glutathione *S*-transferases
GSTπ	Glutathione *S*-transferase π
H&E	Hematoxylin and eosin
H_2O_2	Hydrogen peroxide
H_2S	Hydrogen sulphide
HCC	Hepatocellular carcinoma
HClO	Hypochlorous acid
HDACs	Histone deacetylases
HEWL	Hen egg white lysozyme
ICT	Intramolecular charge transfer
IF	Immunofluorescence
IHC	Immunohistochemistry
IL-8	Interleukin-8
iNOS	Inducible nitric oxide synthase
IPF	Idiopathic pulmonary fibrosis
IPF	Idiopathic pulmonary fibrosis
ISO	Isoproterenol
KA	Kainate
LLC	Lewis lung carcinoma
LOD	Limit of detection
LOX	Lysine oxidase
LOX	Lysyl oxidase
LPS	Lipopolysaccharide
MAO	Monoamine oxidases
MB	Methylene blue
MF	Myocardial fibrosis
MMP-2	Matrix metalloproteinase-2
MPO	Myeloperoxidase
NAC	*N*-Acetyl cysteine
NE	Neutrophil elastase
NFTs	Neurofibrillary tangles
NIR	Near-infrared
NIRF	Near-infrared fluorescence
NMDA	*N*-Methyl-D-aspartic acid
NO	Nitric oxide
$NO^{\bullet}$	Nitric oxide
NQO1	NADPH quinone oxidoreductase 1
$O_2^{\bullet -}$	Superoxide radical anion
O_3	Ozone
$^{\bullet}OH$	hydroxyl radical $^{\bullet}$
$ONOO^-$	Peroxynitrite
PA	Photoacoustic
PAG	Propargylglycine
PD	Parkinson's disease
PeT	Photoinduced electron transfer
PMA	Phorbol-12-myristate-13-acetate
PMNs	Polymorphonuclear neutrophils
PTZ	Pentylenetetrazole
QM	Quinoline-malononitrile
QPA	Quinone propionic acid
RIPF	Radiation-induced pulmonary fibrosis
RIR	Restriction of intramolecular rotation
RO	Rotenone
ROS/RNS	Reactive oxygen/nitrogen species
ROT	Rotenone
S–D–A–D–S	Shielding unit–donor–acceptor–donor–shielding unit
TCO	*trans*-Cyclooctene
Tg	Transgenic
TGF-β	Transforming growth factor β
ThS	Thioflavin S
ThT	Thioflavin T
TICT	Twisted intramolecular charge transfer
TME	Tumour microenvironment
TP	Two-photon
TPACS	Two-photon absorption cross section
TPE	Tetraphenylethylene
TPFM	Two-photon fluorescence microscope
Tz	Tetrazine
VB3	Brillian-VB3
VPA	Valproic acid

Conflicts of interest

There are no conflicts to declare.

Acknowledgements

X.-P. H. thanks the National Natural Science Foundation of China (No. 21788102, 91853201), the National Key Sci-Tech Special Projects of Infection Diseases of China (2018ZX10732202), the Shanghai Municipal Science and Technology Major Project (No. 2018SHZDZX03), the International Cooperation Program of Shanghai Science and Technology Committee (No. 17520750100), the Fundamental Research Funds for the Central Universities (222201717003) and the Programme of Introducing Talents of Discipline to Universities (B16017) for financial support. H.-H. H. would like to thank the Project funded by China Postdoctoral Science Foundation (No. 2020M681196). T. D. J. wishes to thank the Royal Society for a Wolfson Research Merit Award and the Open Research Fund of the School of Chemistry and Chemical Engineering, Henan Normal University for support (2020ZD01). Support from the Robert A. Welch Foundation (F-0018 to J. L. S.) is also gratefully acknowledged.

References

1 X.-P. He, X.-L. Hu, T. D. James, J. Yoon and H. Tian, *Chem. Soc. Rev.*, 2017, **46**, 6687–6696.
2 M. Gao, F. Yu, C. Lv, J. Choo and L. Chen, *Chem. Soc. Rev.*, 2017, **46**, 2237–2271.
3 Q. T. Nguyen and R. Y. Tsien, *Nat. Rev. Cancer*, 2013, **13**, 653–662.
4 G. Hong, A. L. Antaris and H. Dai, *Nat. Biomed. Eng.*, 2017, **1**, 0010.
5 L. Wu, J. Liu, P. Li, B. Tang and T. D. James, *Chem. Soc. Rev.*, 2021, **50**, 702–734.
6 Y. W. Choo, J. Jeong and K. Jung, *BMB Rep.*, 2020, **53**, 357–366.
7 S. Ma, G. Chen, J. Xu, Y. Liu, G. Li, T. Chen, Y. Li and T. D. James, *Coord. Chem. Rev.*, 2021, **427**, 213553.
8 W. Fu, C. Yan, Z. Guo, J. Zhang, H. Zhang, H. Tian and W.-H. Zhu, *J. Am. Chem. Soc.*, 2019, **141**, 3171–3177.
9 Y.-L. Wang, C. Fan, B. Xin, J.-P. Zhang, T. Luo, Z.-Q. Chen, Q.-Y. Zhou, Q. Yu, X.-N. Li, Z.-L. Huang, C. Li, M.-Q. Zhu and B. Z. Tang, *Mater. Chem. Front.*, 2018, **2**, 1554–1562.
10 Y. Wang, Y. Qiu, A. Sun, Y. Xiong, H. Tan, Y. Shi, P. Yu, G. Roy, L. Zhang and J. Yan, *Anal. Chim. Acta*, 2020, **1133**, 109–118.
11 F. Zeng, J. Yang, X. Li, K. Peng, C. Ran, Y. Xu and Y. Li, *Biorg. Med. Chem.*, 2020, **28**, 115559.
12 D. Kim, S. H. Baik, S. Kang, S. W. Cho, J. Bae, M.-Y. Cha, M. J. Sailor, I. Mook-Jung and K. H. Ahn, *ACS Cent. Sci.*, 2016, **2**, 967–975.
13 Q. Sun, J. Xu, C. Ji, M. S. S. Shaibani, Z. Li, K. Lim, C. Zhang, L. Li and Z. Liu, *Anal. Chem.*, 2020, **92**, 4038–4045.
14 Y. Liu, L. Bai, Y. Li, Y. Ni, C. Xin, C. Zhang, J. Liu, Z. Liu, L. Li and W. Huang, *Sens., Actuators B*, 2019, **279**, 38–43.
15 Z. Fang, Z. Su, W. Qin, H. Li, B. Fang, W. Du, Q. Wu, B. Peng, P. Li, H. Yu, L. Li and W. Huang, *Chin. Chem. Lett.*, 2020, **31**, 2903–2908.
16 J. S. Hu, C. Shao, X. Wang, X. Di, X. Xue, Z. Su, J. Zhao, H. L. Zhu, H. K. Liu and Y. Qian, *Adv. Sci.*, 2019, **6**, 1900341.
17 C. Shao, J. Yuan, Y. Liu, Y. Qin, X. Wang, J. Gu, G. Chen, B. Zhang, H.-K. Liu, J. Zhao, H. L. Zhu and Y. Qian, *Proc. Natl. Acad. Sci. U. S. A.*, 2020, **117**, 10155–10164.
18 S. Li, D. Song, W. Huang, Z. Li and Z. Liu, *Anal. Chem.*, 2020, **92**, 2802–2808.
19 X. Wang, P. Li, Q. Ding, C. Wu, W. Zhang and B. Tang, *Angew. Chem., Int. Ed.*, 2019, **131**, 4722–4726.
20 X. Wang, P. Li, Q. Ding, C. Wu, W. Zhang and B. Tang, *J. Am. Chem. Soc.*, 2019, **141**, 2061–2068.
21 X. Wang, X. Bai, D. Su, Y. Zhang, P. Li, S. Lu, Y. Gong, W. Zhang and B. Tang, *Anal. Chem.*, 2020, **92**, 4101–4107.
22 P. Li, J. Wang, X. Wang, Q. Ding, X. Bai, Y. Zhang, D. Su, W. Zhang, W. Zhang and B. Tang, *Chem. Sci.*, 2019, **10**, 2805–2810.
23 S. K. Asrani, H. Devarbhavi, J. Eaton and P. S. Kamath, *J. Hepatol.*, 2019, **70**, 151–171.
24 C. Tang, Y. Du, Q. Liang, Z. Cheng and J. Tian, *Mol. Imaging Biol.*, 2020, **22**, 476–485.
25 F. Zhou, W. Shang, X. Yu and J. Tian, *Med. Res. Rev.*, 2018, **38**, 741–767.
26 Q. Zhang, Z. Han, J. Tao, M. Zhao, W. Zhang, P. Li, L. Tang and Y. Gu, *Biomater. Sci.*, 2019, **7**, 159–167.
27 X. Han, Y. Ma, Y. Chen, X. Wang and Z. Wang, *Anal. Chem.*, 2020, **92**, 2830–2838.
28 Y. Li, X. Xie, X. E. Yang, M. Li, X. Jiao, Y. Sun, X. Wang and B. Tang, *Chem. Sci.*, 2017, **8**, 4006–4011.
29 W.-L. Jiang, Y. Li, W.-X. Wang, Y.-T. Zhao, J. Fei and C.-Y. Li, *Chem. Commun.*, 2019, **55**, 14307–14310.
30 H. Li, Q. Yao, F. Xu, Y. Li, D. Kim, J. Chung, G. Baek, X. Wu, P. F. Hillman, E. Y. Lee, H. Ge, J. Fan, J. Wang, S.-J. Nam, X. Peng and J. Yoon, *Angew. Chem., Int. Ed.*, 2020, **59**, 10186–10195.
31 A. C. Sedgwick, K.-C. Yan, D. N. Mangel, Y. Shang, A. Steinbrueck, H.-H. Han, J. T. Brewster, X.-L. Hu, D. W. Snelson, V. M. Lynch, H. Tian, X.-P. He and J. L. Sessler, *J. Am. Chem. Soc.*, 2021, **143**, 1278–1283.
32 P. Cheng, Q. Miao, J. Li, J. Huang, C. Xie and K. Pu, *J. Am. Chem. Soc.*, 2019, **141**, 10581–10584.
33 Y. Tian, Y. Li, W.-X. Wang, W.-L. Jiang, J. Fei and C.-Y. Li, *Anal. Chem.*, 2020, **92**, 4244–4250.
34 P. Xing, Y. Niu, R. Mu, Z. Wang, D. Xie, H. Li, L. Dong and C. Wang, *Nat. Commun.*, 2020, **11**, 1–9.
35 L. Huang, G. Frampton, A. Rao, K.-S. Zhang, W. Chen, J.-M. Lai, X.-Y. Yin, K. Walker, B. Culbreath, D. Leyva-Illades, M. Quinn, M. McMillin, M. Bradley, L.-J. Liang and S. DeMorrow, *Lab. Invest.*, 2012, **92**, 1451–1460.
36 Z.-M. Yang, Q.-Y. Mo, J.-M. He, D.-L. Mo, J. Li, H. Chen, S.-L. Zhao and J.-K. Qin, *ACS Sens.*, 2020, **5**, 943–951.
37 B. Bikbov, C. A. Purcell, A. S. Levey, M. Smith, A. Abdoli, M. Abebe, O. M. Adebayo, M. Afarideh, S. K. Agarwal, M. Agudelo-Botero, E. Ahmadian, Z. Al-Aly, V. Alipour, A. Almasi-Hashiani, R. M. Al-Raddadi, N. Alvis-Guzman, S. Amini, T. Andrei, C. L. Andrei, Z. Andualem, M. Anjomshoa, J. Arabloo, A. F. Ashagre, D. Asmelash, Z. Ataro, M. M. D. W. Atout, M. A. Ayanore, A. Badawi, A. Bakhtiari, S. H. Ballew, A. Balouchi, M. Banach, S. Barquera, S. Basu, M. T. Bayih, N. Bedi, A. K. Bello, I. M. Bensenor, A. Bijani, A. Boloor, A. M. Borzì, L. A. Cámera, J. J. Carrero, F. Carvalho, F. Castro, F. Catalá-López, A. R. Chang, K. L. Chin, S.-C. Chung, M. Cirillo, E. Cousin, L. Dandona, R. Dandona, A. Daryani, R. Das-Gupta, F. M. Demeke, G. T. Demoz, D. M. Desta, H. P. Do, B. B. Duncan, A. Eftekhari, A. Esteghamati, S. S. Fatima, J. C. Fernandes, E. Fernandes, F. Fischer, M. Freitas, M. M. Gad, G. G. Gebremeskel, B. M. Gebresillassie, B. Geta, M. Ghafourifard, A. Ghajar, N. Ghith, P. S. Gill, I. A. Ginawi, R. Gupta, N. Hafezi-Nejad, A. Haj-Mirzaian, A. Haj-Mirzaian, N. Hariyani, M. Hasan, M. Hasankhani, A. Hasanzadeh, H. Y. Hassen, S. I. Hay, B. Heidari, C. Herteliu, C. L. Hoang, M. Hosseini, M. Hostiuc, S. S. N. Irvani, S. M. S. Islam, N. Jafari-Balalami, S. L. James, S. K. Jassal, V. Jha, J. B. Jonas, F. Joukar, J. J. Jozwiak, A. Kabir, A. Kahsay, A. Kasaeian, T. D. Kassa, H. G. Kassaye, Y. S. Khader, R. Khalilov, E. A. Khan, M. S. Khan, Y.-H. Khang, A. Kisa, C. P. Kovesdy, B. Kuate-Defo, G. A. Kumar, A. O. Larsson, L.-L. Lim, A. D. Lopez, P. A. Lotufo, A. Majeed, R. Malekzadeh,

W. März, A. Masaka, H. A. A. Meheretu, T. Miazgowski, A. Mirica, E. M. Mirrakhimov, P. Mithra, B. Moazen, D. K. Mohammad, R. Mohammadpourhodki, S. Mohammed, A. H. Mokdad, L. Morales, I. Moreno-Velasquez, S. M. Mousavi, S. Mukhopadhyay, J. B. Nachega, G. N. Nadkarni, J. R. Nansseu, G. Natarajan, J. Nazari, B. Neal, R. I. Negoi, C. T. Nguyen, R. Nikbakhsh, J. J. Noubiap, C. Nowak, A. T. Olagunju, A. Ortiz, M. O. Owolabi, R. Palladino, M. Pathak, H. Poustchi, S. Prakash, N. Prasad, A. Rafiei, S. B. Raju, K. Ramezanzadeh, S. Rawaf, D. L. Rawaf, L. Rawal, R. C. Reiner Jr, A. Rezapour, D. C. Ribeiro, L. Roever, D. Rothenbacher, G. M. Rwegerera, S. Saadatagah, S. Safari, B. W. Sahle, H. Salem, J. Sanabria, I. S. Santos, A. Sarveazad, M. Sawhney, E. Schaeffner, M. I. Schmidt, A. E. Schutte, S. G. Sepanlou, M. A. Shaikh, Z. Sharafi, M. Sharif, A. Sharifi, D. A. S. Silva, J. A. Singh, N. P. Singh, M. M. M. Sisay, A. Soheili, I. Sutradhar, B. F. Teklehaimanot, B. E. Tesfay, G. F. Teshome, J. S. Thakur, M. Tonelli, K. B. Tran, B. X. Tran, C. Tran-Ngoc, I. Ullah, P. R. Valdez, S. Varughese, T. Vos, L. G. Vu, Y. Waheed, A. Werdecker, H. F. Wolde, A. B. Wondmieneh, S. Wulf Hanson, T. Yamada, Y. Yeshaw, N. Yonemoto, H. Yusefzadeh, Z. Zaidi, L. Zaki, S. B. Zaman, N. Zamora, A. Zarghi, K. A. Zewdie, J. Ärnlöv, J. Coresh, N. Perico, G. Remuzzi, C. J. L. Murray and T. Vos, *Lancet*, 2020, **395**, 709–733.

38 J. Huang, C. Xie, X. Zhang, Y. Jiang, J. Li, Q. Fan and K. Pu, *Angew. Chem., Int. Ed.*, 2019, **58**, 15120–15127.

39 L. Liu, L. Jiang, W. Yuan, Z. Liu, D. Liu, P. Wei, X. Zhang and T. Yi, *ACS Sens.*, 2020, **5**, 2457–2466.

40 J. Huang, Y. Lyu, J. Li, P. Cheng, Y. Jiang and K. Pu, *Angew. Chem., Int. Ed.*, 2019, **131**, 17960–17968.

41 N. W. Schluger and R. Koppaka, *Ann. Am. Thorac. Soc.*, 2014, **11**, 407–416.

42 X. Zhang, W. Zhao, B. Li, W. Li, C. Zhang, X. Hou, J. Jiang and Y. Dong, *Chem. Sci.*, 2018, **9**, 8207–8212.

43 A. M. Manicone, *Expert Rev. Clin. Immunol.*, 2009, **5**, 63–75.

44 F. Chagnon, A. Bourgouin, R. Lebel, M.-A. Bonin, E. Marsault, M. Lepage and O. Lesur, *Am. J. Physiol.: Lung Cell. Mol. Physiol.*, 2015, **309**, L543–L551.

45 N. He, Y. Wang, Y. Huang, L. Chen, X. Wang, C. Lv and S. Yue, *J. Mater. Chem. B*, 2020, **8**, 9899–9905.

46 S.-Y. Liu, H. Xiong, R.-R. Li, W.-C. Yang and G.-F. Yang, *Anal. Chem.*, 2019, **91**, 3877–3884.

47 Z. Jia, H.-H. Han, A. C. Sedgwick, G. T. Williams, L. Gwynne, J. T. Brewster, S. D. Bull, A. T. A. Jenkins, X.-P. He, H. Schönherr, J. L. Sessler and T. D. James, *Front. Chem.*, 2020, **8**, 389.

48 Z. Zhan, R. Liu, L. Chai, Y. Dai and Y. Lv, *Anal. Chem.*, 2019, **91**, 11461–11466.

49 X. Song, S. Bai, N. He, R. Wang, Y. Xing, C. Lv and F. Yu, *ACS Sens.*, 2021, **6**, 1228–1239.

50 N. He, Y. Wang, Y. Huang, X. Wang, L. Chen and C. Lv, *Sens. Actuators, B*, 2020, **322**, 128565.

51 D. H. McMillan, J. L. J. van der Velden, K. G. Lahue, X. Qian, R. W. Schneider, M. S. Iberg, J. D. Nolin, S. Abdalla, D. T. Casey, K. D. Tew, D. M. Townsend, C. J. Henderson, C. R. Wolf, K. J. Butnor, D. J. Taatjes, R. C. Budd, C. G. Irvin, A. van der Vliet, S. Flemer, V. Anathy and Y. M. W. Janssen-Heininger, *JCI Insight*, 2016, **1**, 85717.

52 N. He, S. Bai, Y. Huang, Y. Xing, L. Chen, F. Yu and C. Lv, *Anal. Chem.*, 2019, **91**, 5424–5432.

53 P. Désogère, L. F. Tapias, L. P. Hariri, N. J. Rotile, T. A. Rietz, C. K. Probst, F. Blasi, H. Day, M. Mino-Kenudson, P. Weinreb, S. M. Violette, B. C. Fuchs, A. M. Tager, M. Lanuti and P. Caravan, *Sci. Transl. Med.*, 2017, **9**, eaaf4696.

54 J. R. Perez, N. Ybarra, F. Chagnon, M. Serban, G. Pare, O. Lesur, J. Seuntjens and I. E. Naqa, *Sci. Rep.*, 2017, **7**, 17829.

55 T. Aslam, A. Miele, S. V. Chankeshwara, A. Megia-Fernandez, C. Michels, A. R. Akram, N. McDonald, N. Hirani, C. Haslett, M. Bradley and K. Dhaliwal, *Chem. Sci.*, 2015, **6**, 4946–4953.

56 X. Zhang, N. He, Y. Huang, F. Yu, B. Li, C. Lv and L. Chen, *Sens. Actuators, B*, 2019, **282**, 69–77.

57 S. R. Punganuru, H. R. Madala, V. Arutla, R. Zhang and K. S. Srivenugopal, *Sci. Rep.*, 2019, **9**, 8577.

58 R. H. Hunt, M. Camilleri, S. E. Crowe, E. M. El-Omar, J. G. Fox, E. J. Kuipers, P. Malfertheiner, K. E. L. McColl, D. M. Pritchard, M. Rugge, A. Sonnenberg, K. Sugano and J. Tack, *Gut*, 2015, **64**, 1650.

59 G. F. Longstreth, W. G. Thompson, W. D. Chey, L. A. Houghton, F. Mearin and R. C. Spiller, *Gastroenterology*, 2006, **130**, 1480–1491.

60 M. Zeng, A. Shao, H. Li, Y. Tang, Q. Li, Z. Guo, C. Wu, Y. Cheng, H. Tian and W.-H. Zhu, *ACS Appl. Mater. Interfaces*, 2017, **9**, 13029–13036.

61 J. Liu, X. Liu, J. Qian, C. Meng, P. Zhu, J. Hang, Y. Wang, B. Xiong, X. Qiu, W. Zhu, Y. Yang, Y. Zhang and Y. Ling, *J. Med. Chem.*, 2020, **63**, 9271–9283.

62 F. Luan, Z. Yu, L. Yin, X. Leng, Y. Shi, J. Wang, H. Shi and W. Chen, *Anal. Methods*, 2019, **11**, 1516–1521.

63 X. Zhang, B. Wang, N. Zhao, Z. Tian, Y. Dai, Y. Nie, J. Tian, Z. Wang and X. Chen, *Theranostics*, 2017, **7**, 3794–3802.

64 G. Curigliano, D. Cardinale, S. Dent, C. Criscitiello, O. Aseyev, D. Lenihan and C. M. Cipolla, *Ca-Cancer J. Clin.*, 2016, **66**, 309–325.

65 S. Hinderer and K. Schenke-Layland, *Adv. Drug Delivery Rev.*, 2019, **146**, 77–82.

66 T. Zhou, J. Wang, J. Xu, C. Zheng, Y. Niu, C. Wang, F. Xu, L. Yuan, X. Zhao, L. Liang and P. Xu, *Anal. Chem.*, 2020, **92**, 5064–5072.

67 X. Xie, F. Tang, G. Liu, Y. Li, X. Su, X. Jiao, X. Wang and B. Tang, *Anal. Chem.*, 2018, **90**, 11629–11635.

68 W.-T. Dou, Z.-Y. Qin, J. Li, D.-M. Zhou and X.-P. He, *Sci. Bull.*, 2019, **64**, 1902–1909.